Chapter 1

Ion Channels

1.1 Ion channels

The cells in living organisms are separated from their environment by membranes which form a wall or barrier between the interior of the cell and the outside world. These membranes are formed from molecules known as phospholipids that orient to form thin sheets. These lipids have a long oily tail and a charged or polar headgroup. When placed in water the hydrophyllic heads are attracted to the water molecules whilst the hydrophobic tails try to move away from them. This causes the phospholipds to arrange themselves into a double layer, with the head groups facing the water molecules on each side and the tails in the middle. The lipid molecules are not bound to each other, and so can move past each other, but the hydrophobic forces hold the molecules in their double layer conformation, preventing individual molecules from popping out of the sheet. These membranes may be formed from a wide range of different phospholipids, and their dimensions will vary with their composition, but typically their thickness lies in the range 30 – 70 Å.

Cells in complex organisms must be able to interact with their environment, and so there must be a mechanism for particles to move across the membrane. Because the membrane is a more like a two dimensional fluid than a rigid wall, some neutral molecules are able to do this by simply diffusing or squeezing their way through the membrane. However, the majority of cellular signaling takes place with the movement of ions across cell membranes, and charged particles cannot easily squeeze through a membrane.

The reason for this is that ions try to keep away from the hydrophobic centre of the bilayer, in the same way, but even more strongly so, than water molecules. Bulk water, is comprised of polar molecules which present a much more favourable environment for ions than the lipid. Indeed, an ion attracts a layer of surrounding water molecules (known as the 'hydration shell') which have to be stripped away

if the ion is to squeeze through the membrane. This requires a great amount of energy that cannot be balanced by electrostatic interactions with the non-polar hydrophobic lipid tails.

The amount of energy required to move an ion through the membrane can be quantified by representing the membrane as a region of low dielectric constant, and bulk water as a region with a high dielectric constant. A system with such a sharp change in dielectric properties presents an enormous energy barrier to the permeation of charged particles. The energy required to move an ion, radius r, from bulk water, $\epsilon_{water} = 80$, into an infinitely thick bilayer, $\epsilon_{membrane} = 2$, is given by [117]:

$$E = \frac{z^2 q^2}{8\pi\epsilon_0 r}\left(\frac{1}{\epsilon_{membrane}} - \frac{1}{\epsilon_{water}}\right) \tag{1.1}$$

For a sodium ion at room temperature this energy barrier is about 100 kT. Introducing a correction factor for the finite thickness of the membrane, only reduces the barrier to about 96 kT for a 50 Å thick membrane [45]. As the amount of energy required to pass through the membrane is much greater than the average thermal energy of an ion ($\backsim 3/2\ kT$) the membrane is effectively impermeable to small ions or polar molecules.

Cell membranes are not homogeneous but are full of impurities: other molecules with hydrophobic regions try to take refuge in the bilayer. Thus, membranes do not just differentiate the inside from the outside of the cell, but also provide homes for a large number of protein molecules. Indeed, it is these protein molecules that enable the movement of ions across the membrane.

There are two main mechanisms by which this ion permeation through membranes takes place, both of which involve protein molecules in the membrane. One mechanism involves 'carrier proteins' which bind to the ions and then help them through the membrane. The other involves 'protein pores' which create a small water filled hole or channel through the membrane through which ions can pass. Because pores transport ions passively they can move ions at a great rate, transporting them at the order of 10^7 ions per second. Carrier proteins on the other hand are much slower, moving only 300 or so ions per second [85].

Protein pores, or *ion channels* as they are better known, are simply a protein that spans across the membrane with a hole down its centre. An artists depiction of what they may look like is shown in figure 1.1. This diagram shows the bilayer membrane formed from phospholipids with circular polar heads and wiggly hydrophobic tails. Sitting in this bilayer are two ion channels, the closest shown in cross section to display the central water filled pore that provides a path for ions from one side of the membrane to the other. These channels enable the passive diffusion of ions

across the membrane.

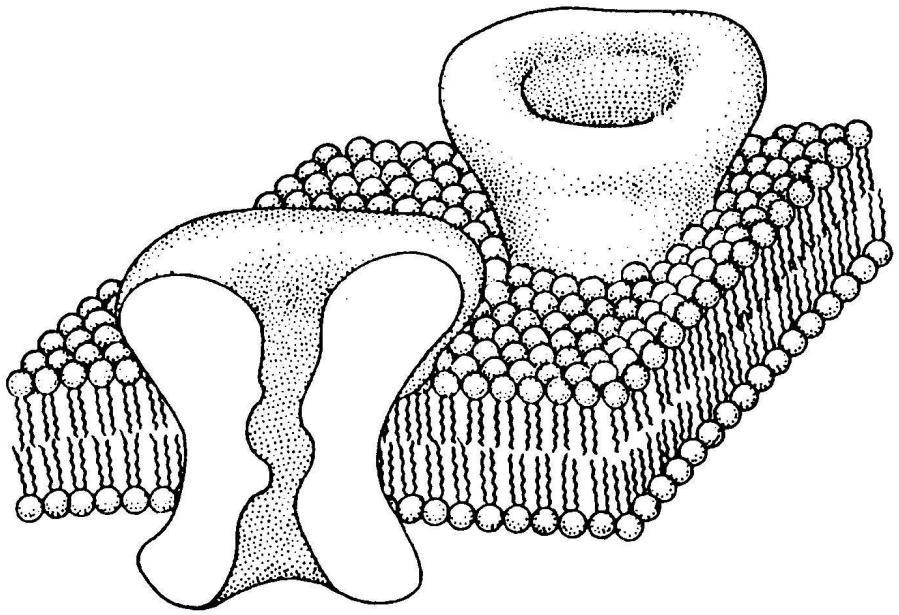

Figure 1.1: An Artist's conception of ion channels in a lipid bilayer membrane (taken from [85]).

Remarkably, the existence of ion channels was only postulated and verified quite recently. It has been known since the middle of last century that large currents flowed across biological membranes. For example, Hodgkin and Huxley [87] carried out a study of the ionic basis of nerve impulses in 1952 in which they measured the conductance of sections of nerve axon membrane. The conductances measured in such experiments were quite large, in the order of $2 \times 10^{-2}\ \Omega^{-1}\text{cm}^{-2}$, so they knew that there must be a mechanism for transporting ions across the largely impermeable membrane. Furthermore, Hodgkin and Huxley deduced that this ion permeation occurred at localised sites in the membrane. The concept of water filled pores was first postulated to explain the large currents measured moving across synthetic lipid bilayers [19, 86] and later through nicotinic acetylcholine-gated channels in biological membranes [146]. That these pores were formed by proteins was only established in the mid 1970s [85].

The development of the patch clamp technique in 1976 [146] shed further light on the situation. In this technique a tiny glass pipette is applied to the surface of a cell and clamped there by providing suction. This isolates a small patch of membrane through which currents can be measured. Indeed it was found that current did flow through small isolated sections of membrane in identifiable quanta, giving credence to the idea of pores. In fact, these experiments were measuring the current passing through single ion channels. The reality of ion channels was finally demonstrated by using electron diffraction to observe water filled protein pores, which identified the so called 'gap junction' channels in 1984 [204] and nicotinic acetylcholine gated channels in 1988 [202].

1.2 Ion channel characteristics

1.2.1 Gating

Ions are not free to move through channels at any time, but are tightly controlled such that currents arise only at particular times. This process is known as 'gating' - channels are said to 'open' and 'close' in response to various stimuli. The opening and closing of channels is clearly visible in single channel current recordings which show long periods within which no current flows when the channel is closed, interspersed with periods of quantified current when the channel is open. Different channels respond to different stimuli, but fall into 3 main categories. Channels may open or close in response to a change in the potential difference across the membrane (voltage-gated channels), to the binding of specific chemicals to the protein (ligand-gated channels) or to a mechanical pressure (mechano-sensitive channels).

The exact process of channel gating is not well known and in any case will vary between the different types of channels. Voltage gated channels contain a section of the protein known as the 'voltage sensor' which is highly charged and moves in response to potential changes opening the channel [85]. In ligand gated channels, the energy gained in binding the ligand is used to produce channel activation [94]. In at least one case (KcsA potassium channel) it is known that gating involves the widening of the pore. But, whether or not gating involves an actual opening and closing of the pore in all cases is not yet known. It is possible that conformational changes that result in moving charged residues closer to or further from the pore could also create gating without physically blocking the pore.

1.2.2 Permeation

The primary role of ion channel is to transport ions across the membrane, or in other words to conduct currents into or out of the cell. Differing concentrations of ions or different potentials on either side of the membrane act to drive ions through an open channel. These differences are created by the active processes of carrier proteins (or 'ion pumps') which use metabolic energy to transport ions across the membrane creating or maintaining ionic differences and potentials.

Typical currents of many picoamps flow through open channels. Since single channel current measurements became possible using the patch clamp technique, the currents passing through the channel have been measured in a host of different situations. The most commonly measured property is the current passing through the channel under different membrane potentials - the I-V curve. Under physiological potentials ($|V| < 100$ mV) these curves are usually linear. However, non-linearities are often found at higher potentials and can be used to study the energetics of ion permeation.

Another common study is the influence of ion concentration on channel current. Measuring the current while holding the potential fixed and varying the permeant ion concentration yields the concentration-current curve, which usually saturates at large concentrations. Similar studies using mixtures of ions, or both concentration and potential gradients, lead to more complex conductance properties.

The steps involved in ion transport through channels are not fully understood. In some channels ions move through the channel individually. In others, the channel is permanently occupied by ions and permeation takes place when another ion enters and shuffles the resident ions through the channel. The conductance experiments provide experimental benchmarks against which channel models can be tested. A good model should explain the steps involved in the dynamic process of ion permeation as well as reproducing and elucidating the origins of the current measurements.

1.2.3 Selectivity

The function of ions channels means that they have to control the permeability of the cell membrane to Na^+, K^+, Ca^{2+} and Cl^- ions separately. To do this, different ion channels discriminate between the types of ions that can pass. Some channels only allow potassium ions to pass, some sodium ions and so on. When coupled with different gating stimuli in different channels this allows for the fine control of ion flows.

The discrimination between anions and cations is presumably based on their charge. The presence of positive charges in the protein close to the pore would attract anions and repel cations, and vice versa for negative partial charges. Discrimination between like charged ions appears to be more complex, relying, for example, on the differing size of Na^+ ($r = 0.95$Å) and K^+ ($r = 1.33$Å) ions [3, 58, 174].

1.3 The role of ion channels

The importance ion channels in biological processes cannot be overstated. Indeed, the roles of channels are so varied, and essential to such a large range of processes that I can only attempt to give a broad indication of them here.

One of the most important roles of ions channels is the conduction of electrical signals in the brain and nerves. Ion pumps in the cell membranes work tirelessly to set up concentration differences on either side of the membrane. These pumps move sodium ions out of the cell at the same time as moving potassium ions in. This means that the extracellular concentration of sodium ions is very high, and the intracellular concentration is low; and vice versa for potassium. In the process of creating these concentration differences, the pumps move more ions out of the cell than in, thus creating a potential difference across the membrane, with the outside positive with respect to the inside.

A neural signal is passed from one nerve cell to another through the release of neurotransmitter chemicals. When these neurotransmitters bind to ligand-gated sodium channels in the next cell they cause the channel to open and sodium ions to rush into the cell. This causes a reduction in the potential difference across the membrane which in turn stimulates the opening of voltage-gated sodium channels. The depolarisation propagates along the cell as it continually stimulates more channels to open, and results in what is known as the 'action potential'. After a time these channels inactivate preventing further ion flow. As the sodium channels inactivate, potassium channels open, and potassium ions flow from inside the cell to outside, thus re-establishing the normal membrane potential so that another signal can pass shortly behind the first. Once the action potential reaches a synapse where the signal is to be sent to a neighbouring cell, it stimulates the release of neurotransmitters. This is done principally by opening voltage-gated calcium channels - the influx of calcium creates a chemical stimulus that opens vesicles storing the neurotransmitter chemicals. This whole process takes place in milli-seconds so that messages can be sent throughout the body without noticeable delay. All the time, the ion pumps work to reset the concentration gradients so that the process

can be continually repeated. Electrical signaling in the body is thus controlled and propagated by ion channels.

Another important role of ion channels is in sensory transduction, the process by which stimuli such as light, sound, taste, heat or pH in areas of the body are converted into signals which can be sent to the brain or that initiate unconscious responses. An interesting example is in the process of hearing. The sacculus hair cell of frogs is a cell which detects sound vibrations in the ear. When small hairs attached to the cell are moved by as little as 1 nm, they stretch the proteins that form mechano-sensitive ion channels in the cell membrane. This alteration causes the channels to open resulting in an increase of current flowing through these cation selective channels. The rise in positive charge in the cells in turn stimulates the release of neurotransmitter chemicals which open channels in neighbouring nerve axons. The electric signal caused by ion flow through these channels is then fed between nerve cells to the brain [85].

Channels are also used to translate an electrical signal into a reaction in the body. For example, when an electrical signal reaches the muscle fibres, it opens voltage gated calcium channels. The calcium ions then provide a chemical stimulus that prompts the muscle fibres to contract. Other roles of ion channels include the excitation of muscle fibres by adjacent nerve cells, the regulation of cell volumes; egg fertilisation as well as many others [45].

Apart from their biological significance, another reason that ion channels are particularly interesting is that most drugs, toxins and hormones act by altering ion channel function [85]. Discovering how these drugs alter channels at a molecular level will be important in designing targeted drugs in the future. Furthermore, since channels exist in all excitable cells and perform a host of functions, channel malfunction has been linked to a host of diseases. Mutations within genes coding ion channels can lead either to channel malfunction or an over- or under-expression of the channel proteins. Such mutations are now commonly linked to hereditary disease [16, 119]. Other diseases arise when the regulation of channel function is altered, for instance when ligands required for channel gating are not produced in the proper quantities. In some cases large non-selective channels are actually secreted into cells by organisms such as bacteria, and their presence quickly results in cell death. Understanding the detailed mechanisms of channel function will help discover how to combat these problems.

1.4 Ion channel structure

Knowledge of the 3 dimensional atomic structure of channels is important for understanding the mechanisms underlying channel function. The two most important details required are the shape and size of the water filled pore, and the location of partial charges within the protein. Knowing which atoms line the pore, and the location of charged groups is essential if one wants to make a detailed model of the interactions between the ions and the channel. Unfortunately, such information has only recently become available for only a few simple channel proteins.

For a long time, detailed physiological measurements had been made without any direct evidence of the underlying channel structure. The first step in understanding the details of channel structures came with the discovery of the amino acid sequences of the channel forming proteins. This was first done for the nicotinic acetylcholine receptor channel, and soon after for many others. Although such studies could not say anything about the 3 dimensional geometry of the channel, they demonstrated that channels fall into families, similar not only in their functional properties, but also in their protein composition. The similarities in amino acid sequences has since formed the justification for deducing the approximate structure of a large number of channels from the few which have been experimentally determined.

The conventional method for determining protein structures has been X-ray crystallography. In this, many copies of the channel are crystalised in a lattice, and studied by shining X-rays from various angles at the specimen and analysing the diffraction patterns. Unfortunately, membrane proteins, and channels in particular, have been difficult to crystalise as they are only stable in their native conformation when surrounded by the lipid membrane.

For this reason, the first direct pictures of the 3 dimensional structure of ion channels came from the electron microscope. In these studies, channels were quick frozen in their lipid bilayer surroundings and electron micrographs made at different angles and focal planes. The first low resolution pictures were obtained of gap junction channels [204] and the acetylcholine receptor channel from the torpedo electric ray [202]. These indicated that the acetylcholine receptor channel consists of two 20 - 25 Å wide openings, one of which extends for about 60 Å from the bilayer membrane, whilst the other extends for about 20 Å. These entrances are joined by a thin segment that spans across the membrane. This is only about 30 Å long and less than 10 Å wide. Higher resolution pictures have been obtained more recently, but although such pictures give valuable information about the channel geometry the resolution is not sufficient to give evidence about the location of particular amino acid residues with this.

As structures of biological channels were so difficult to obtain, many theoretical efforts turned to a simpler case: the gramicidin A (GA) channel. GA is an antibiotic that forms channels in lipid membranes. Its simplicity lies in the fact that it is comprised of only about 500 atoms, unlike biological channels that often consist of tens of thousands. High resolution structural data was obtained for the GA channel using nuclear-magnetic-resonance (NMR) spectroscopy in the early 1980s [15]. Since then GA became a focus for ion channel theorists as details of the locations of all the atoms within the channel protein were at least approximately known. The gramicidin channel itself is a long narrow cylindrical pore, about 25 Å in length and only 2Å in radius, which turns out to be quite different from biological channels.

The breakthrough in determining biological ion channel structure was made in 1998 when first the KcsA potassium channel from *Streptomyces lividans* [58] and then the *Myobacterium tuberculosis* MscL mechanosensitive channel [32] structures were obtained using X-ray crystallography. Determining the KcsA structure was particularly important, because similar potassium channels carry out important functions in nearly all biological organisms. Although it is significantly simpler than most potassium channels in human cells, the KcsA channel has a very similar physiology and is thought to contain an essentially similar pore forming structural core. Furthermore, sodium and calcium channels are believed to have evolved from potassium channels and to share many characteristics in the pore forming region [128]. This channel was found to be around 45 Å in length. The inner end of the pore appears to be an 18 Å long tunnel only around 6 Å in diameter. The center of the channel widens to contain a 10 Å diameter cavity. The outer end of the pore narrows again to only around 3 Å in diameter, and is believed to be responsible for the channels ability to select which cations pass through it. Both ends of the pore contain negatively charged regions which prevent anions from entering the channel. Furthermore, the locations of potassium ions in the channel can also be seen, indicating possible binding sites.

One difficulty in the KcsA structure is that it appears to be in a closed conformation. The intracellular end narrows to a size through which potassium ions could not pass. Determining what structural changes take place in moving to the open state has been an interesting puzzle in the field.

Very recently, crystal structures have been obtained for a CLC chloride channel (in a closed state) [59] and for a calcium gated MthK potassium channel (in an open state) [97]. The advances in crystallography mean that more channel structures can be expected in the near future.

Already there are common features emerging within the known channel struc-

tures. Ion channels have to be able to rapidly transport ions, which is most easily achieved by a wide pore. But channels also have to be able to select between ions, which is most easily achieved in a narrow pore. It seems that in general a compromise is reached between these cases by channels having a short narrow section responsible for discriminating between ions (known as the 'selectivity filter') while the rest of the pore is much wider. Also, within the narrow section of the channel there are usually some highly charged amino acid residues which act to both attract ions into the channel and help discriminate between them.

1.5 Why models are needed

Physiological experiments and the determination of channel structures have given us an important insight into the operation of ion channels. But such experiments provide only the first step in determining how channels actually work. There are many aspects of ion channel function that cannot be investigated directly through such experimental procedures, and theoretical modelling can provide an understanding not otherwise available.

The dynamics of ions can only be inferred from experiments, whereas they can be observed and quantified in models. Hopefully this means that the physical causes of various physiological properties can be determined. For example, when measuring currents in a channel, it is impossible to determine exactly what ions are doing within it. One can count the number of ions crossing the channel, but this cannot be used to determine exactly how the ions are interacting with the protein or with other ions in the channel. Knowing the structure of a channel assists in determining which residues line the pore and so might provide an important interaction with passing ions. Experiments replacing particular residues can also assist in determining the importance of various amino acids to the channel function. But, in models it is possible to determine the various forces that influence an ion's motion, quantities that cannot be determined experimentally. In this way, for example, the contributions of particular charged residues can be quantified and compared with other forces that act on a permeating ion. In a simulation it is possible to visualise an ion moving through the channel, to see where it dwells, or whether other ions also enter to assist the movement of the first.

The sudden rush of structural information from experiments has ushered in a new era of ion channel research. Models of ion channels can now include this new level of detail, and knowledge of molecular details allows the specific interactions between the ions and the channel to be described in detail. The structural information can

be used in models to determine how a permeating ion interacts with the protein wall and the charges contained within. The role of individual amino acid residues, or more generally how the physical components of the channel can influence its function, can be elucidated. The new structural information makes it feasible to use models to relate the permeation, selectivity and gating of the channel to specific physical processes.

Obviously, a model must always be compared with experimental evidence so that its validity can be tested. A successful model should accurately reproduce available data. But a good model should do more than just this, it should also concisely summarise and explain this data. Furthermore, a model should be useful for making new testable predictions. Ultimately good models should provide a guide to experiment, highlighting, for example, important residues that can be examined with mutagenesis, or suggesting novel experiments.

Chapter 2

Models of Channel Conductance

2.1 Introduction

Since the main role of ion channels is the conduction of ionic currents, people have naturally tried to find ways to theoretically predict the magnitude of the current that will pass through a particular channel so as to understand the mechanisms by which channels select and transport ions. Initially these models of ion conductance aimed to give some insight to the mechanisms involved in ion permeation, without focusing on too many physical details. But recently, since the crystal structure of some biological channels has become known, the effort has been to directly relate these structures to the channel's function.

Although the primary goal of this thesis is to examine the dynamic process of ion permeation, much insight can be gained from static or equilibrium models. Determining factors such as the forces acting on ions, or the energy landscape encountered by them can be just as illuminating as a direct modeling of ion dynamics. Indeed, Poisson's equation is used frequently throughout the thesis to determine these quantities and to quantify the factors influencing permeation. In this chapter I will start by discussing electrostatic calculations before focusing on models that can be used with the aim of modeling and predicting channel currents moving from simpler to more detailed models. Reaction rate theory is a simple model that describes the permeation of an ion as kinetic hopping between states. The theories of electrolytes have been used to study ion channels, in simple forms such as Ohms and Fick's law as well as in some more complex techniques such as Poisson-Nernst-Planck theory. The next level of complexity is to start treating the atoms in the system individually in simulations. In some such techniques only some atoms are described individually such as in Brownian dynamics in which the ions are treated individually whilst the protein and water is not. In others, in particular molecular dynamics, all the atoms are included.

Although much can be gained from the simpler models, they may often overlook or incorrectly describe some of the mechanisms involved in ion permeation. For this reason people often seek to make more realistic models which necessarily contain a greater level of detail. But, it is not always the case that the greater the level of detail in the model the better. At times simplifications provide a way of determining the important physical processes without getting lost in details. At a more practical level simplicity is also a blessing as the computations required in some models provide great limitations on their use. For example, the number of calculations required to carry out quantum mechanical molecular dynamics simulations are such that it is only feasible to simulate dozen or so atoms for one or two pico seconds. This makes it impossible to simulate ion conduction through a protein molecule containing thousands of atoms which takes in the order of a micro second. Modeling ion conduction is therefore a delicate balance between gaining the level of detail necessary to examine the mechanisms of interest without being swamped by calculations and numbers that make it impossible to reach your goal.

2.2 Electrostatic calculations

The dynamic behaviour of ions in and around ion channels is ultimately determined by the forces acting on them. Thus when studying ion permeation it is of interest to examine these forces and the energy landscape encountered by ions in the channel to help elucidate the permeation mechanisms. These forces are also required in dynamic permeation models such as Brownian dynamics simulations. Calculating these forces microscopically is very difficult due to the number of atoms in a typical system. In this thesis such microscopic calculations are not attempted, and continuum electrostatics is used as a practical alternative. The use of continuum electrostatics allows for forces to be calculated at a rate that can be used in Brownian dynamics simulations or other permeation models used to calculate ion currents.

In continuum electrostatics, atoms are not treated in a discrete manner, but rather are represented as a continuous media described by a dielectric constant. An important feature of dielectric materials is that when placed in an electric field a polarisation is induced. This means that dipoles are formed which orient with the electric field. These dipoles may be permanent molecular dipoles (such as those between the hydrogen and oxygen atoms in water) or due to electronic polarisation in the atom itself. The strength of the dipoles and their ability to orient with an external field is characterised by the *dielectric constant*. If no dipoles are induced,

as in the case of a vacuum, then the material is said to have a dielectric constant of one. The higher the dielectric constant above this, the stronger the dipoles that are induced. The net charges of atoms and molecular dipoles can still be included as point charges in the model. For ion channels, the dielectric constant is typically assumed to be uniform throughout the lipid bilayer and protein (usually with a value of $\epsilon_{protein} = 2 - 5$), with another uniform value for the bulk water (typically $\epsilon_{water} = 80$), with possibly an intermediate value inside the pore. The accuracy of these electrostatic calculations in ion channels will be discussed in more detail in chapter 9. A diagram indicating how a protein pore is represented using dielectric regions is given in Fig. 2.1.

Once the dielectric regions have been determined, fixed charges can be assigned to atoms in the protein or at any other location with charge density $\rho(\mathbf{r})$, and the potential in the system found by solving Poisson's equation:

$$\epsilon_0 \nabla \cdot [\epsilon(\mathbf{r}) \nabla \phi(\mathbf{r})] = -\rho(\mathbf{r}) \tag{2.1}$$

with the boundary conditions

$$\phi_1 = \phi_2, \qquad \epsilon_1 \nabla \phi_1 \cdot \hat{\mathbf{n}} = \epsilon_2 \nabla \phi_2 \cdot \hat{\mathbf{n}} \tag{2.2}$$

where $\hat{\mathbf{n}}$ is the unit vector normal to the dielectric boundary, and the subscripts refer to the values on the two sides of the boundary.

Poisson's equation can be used to find the energy landscape encountered by ions in the channel. To do this, an ion is placed at a number of positions and the potential energy found by solving Poisson's equation at each position. By moving the ion along the permeation pathway the energy profile experienced by a conducting ion can be found. Energy wells can be related to binding sites and the crossing of energy barriers would represent the rate limiting steps in conduction. Multi ion channels can also be investigated by placing additional ions in the channel when calculating the energy of the first. Techniques for gaining solutions of Poisson's equation are described in chapter 3. The applicability of Poisson-Boltzmann theory, an extension of Poisson's equation including a continuous equilibrium description of the electrolyte, to ion channels is assessed in chapter 5.

Induced surface charges

An important consequence of the use of the dielectric representation is that an ion near the protein induces surface charges of the same polarity on the protein-water interface. When a cation in an electrolyte solution is placed near a slab of protein, water molecules near the ion align themselves such that the oxygen atoms,

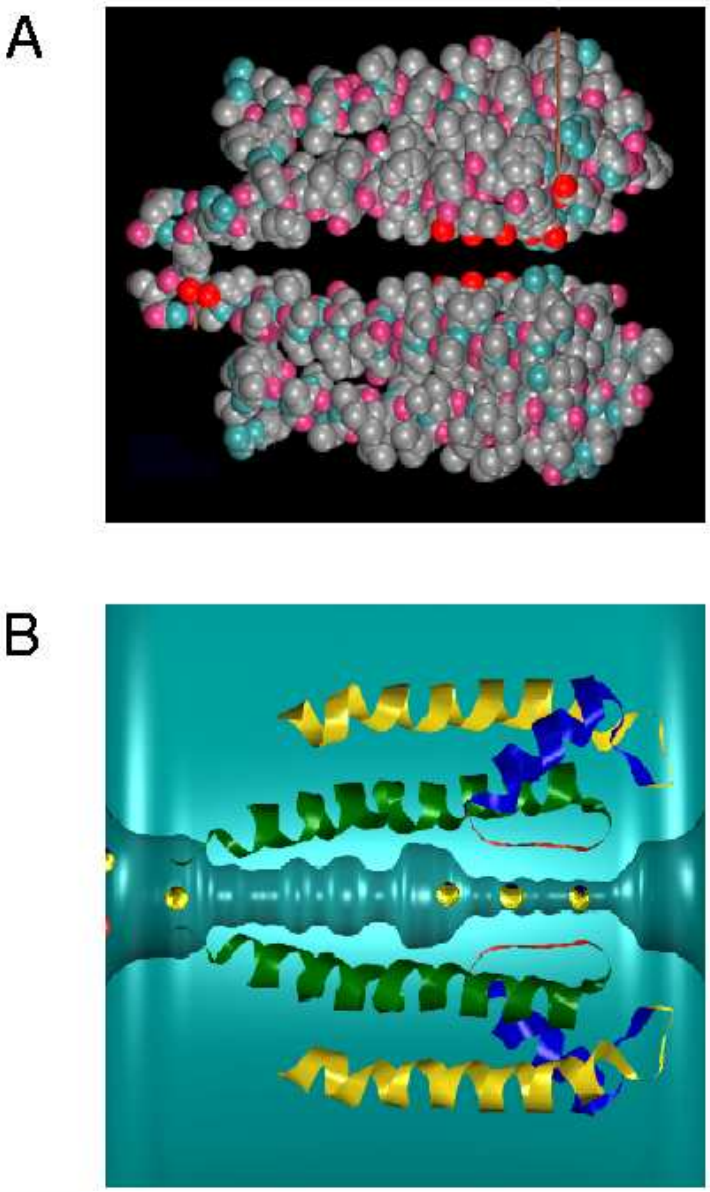

Figure 2.1: Diagram of how a protein pore is represented as a dielectric medium. (A) An atomic space filling diagram of the atoms from two of the four subunits that form the KcsA potassium channel [58]. The missing subunits are identical to the two shown and lie into and out of the page, and they have been removed so that the pore can be seen lying horizontally between the subunits. (B) A rigid dielectric picture of the KcsA pore. The pore boundary is formed by tracing around the born radii of the pore lining atoms. The protein and membrane are then represented as a rigid dielectric medium indicated in blue. The pore itself, and the regions on either end of the pore are assigned dielectric constants $\epsilon_{channel}$ and ϵ_{bulk} respectively. The atomic detail of the protein in (A) is represented as a ribbon diagram for reference. The partial charges of the protein atoms can be included as charges inside the dielectric region representing the protein.

with their partial negative charges, are positioned nearest to the ion. Because polar or carbonyl groups on the protein wall cannot rotate as freely as the water molecules, there will be excesses of hydrogen atoms at the water-protein interface. Viewed from the ion, these excess hydrogen atoms at the boundary appear as surface charges, exerting a repulsive force on it as depicted in Fig. 2.2. In general, if an ion is in a region of dielectric constant ϵ, then it will induce a surface charge of the same sign on the boundary with a region with lower dielectric constant and of opposite sign with a region of higher dielectric constant.

Macroscopically, we say that a charge q located at a distance d from a protein surface induces surface charges on the dielectric boundary. For an idealized infinite plane, the magnitude of the repulsive force this ion experiences is the same as when we place another charge q', on the other side, at a distance d from the surface, and remove the boundary. The magnitude of this image charge q' is related to the relative permittivities of the protein ($\epsilon_p = 2$) and water ($\epsilon_w = 80$), given by

$$q' = \frac{\epsilon_w - \epsilon_p}{\epsilon_w + \epsilon_p} \frac{q}{\epsilon_w}. \tag{2.3}$$

As the ion comes nearer to the boundary, the repulsive image force it experiences grows as $1/d^2$. We can also consider the potential energy of an ion approaching a dielectric interface. The potential energy created by the interaction of its own charge with the dielectric interface (or 'self energy') can be expressed as [114]:

$$U_s = \frac{1}{4\pi\epsilon_0\epsilon_w} \frac{\epsilon_w - \epsilon_p}{\epsilon_w + \epsilon_p} \frac{q^2}{4d} \tag{2.4}$$

A similar self energy and repulsive force acts on an ion that is about to enter an ion channel. However, in this case the force can be more than an order of magnitude larger due to the dielectric boundary being wrapped around the ion, enhancing the effect. The size of the self energy can be evaluated in an infinite cylinder, and if $\epsilon_w >> \epsilon_p$ is given by

$$U_s \backsimeq \frac{1}{4\pi\epsilon_0\epsilon_w} \frac{\epsilon_w - \epsilon_p}{\epsilon_p} \frac{q^2}{5.8d} \tag{2.5}$$

For comparison, if we consider a monovalent ion 4 Å from the boundary then we find $U_s(plane) = 0.4$ kT whilst $U_s(cyl.) = 12$ kT. In a realistic ion channel the self energy may be less than in an infinite cylinder as the channel is finite with wide entrances. However, an ion entering a pore formed by membrane proteins encounters a significant energy barrier due to the induced surface charges, the height of which increases rapidly as the radius of the pore decreases. This energy barrier plays an important role in determining permeation properties of ions across a narrow pore as will become evident in chapters 5, 6 and 7, and any description of ion movement near a dielectric interface must take account of the effects of induced surface charge.

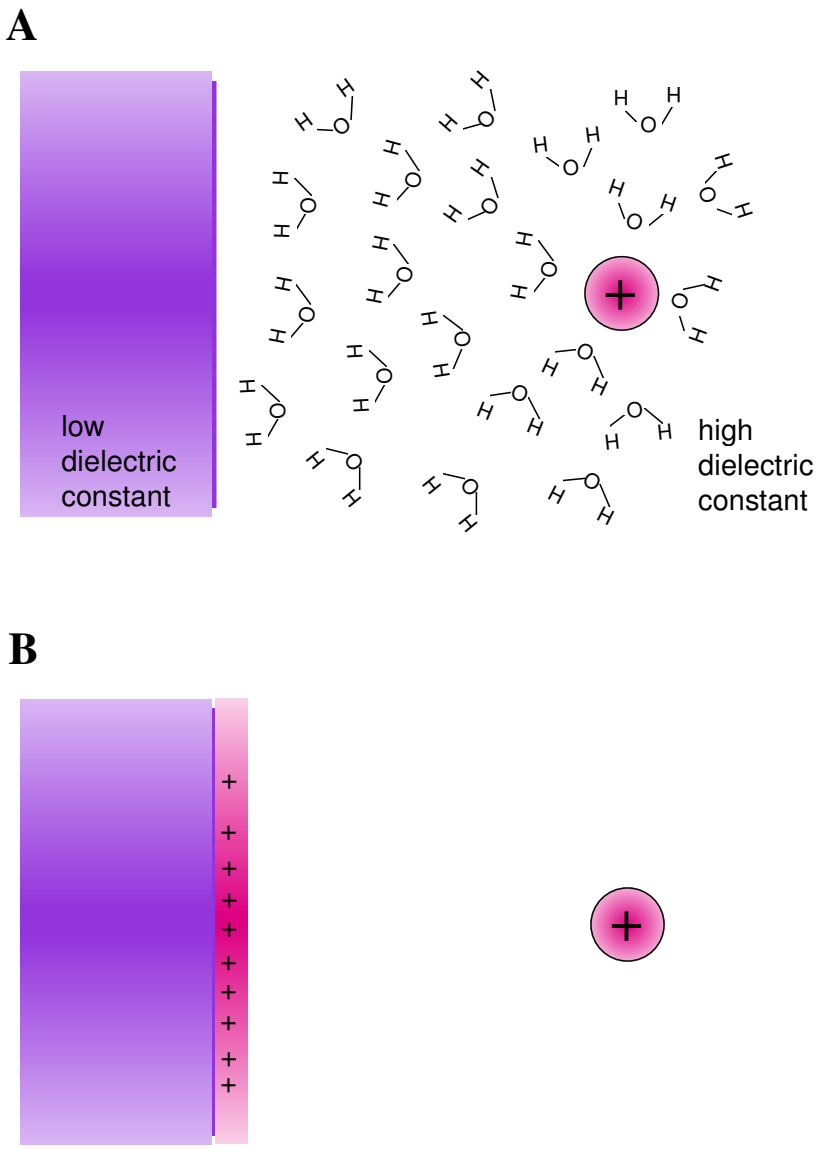

Figure 2.2: An example of the induced surface charge at the boundary of regions of differing dielectric properties due to the presence of a nearby ion. An ion in aqueous solution aligns the dipoles of the water molecules surrounding it as in **A**. As these dipole charges along the dielectric boundary at the channel wall are not cancelled out by the weak dipoles induced in the protein, the net effect is of a line of charge forming just inside the channel wall as shown in **B**.

2.3 Reaction rate theory

Reaction rate theory provides a simple way to predict currents in an ion channel. In this theory the channel is represented very simply as a series of energy wells and barriers. The process of ion conduction is then described as the hopping of an ion between wells, or between states of the system. The different states of the system represent the different distribution of ions between energy wells.

For example, a simple ion channel might be represented by two energy wells shallow enough to hold only one ion each. The system then has four possible states: both wells empty, both wells full or an ion in only one of the two wells. The allowed transitions can be mapped out and their probabilities represented by rate constants. In this example one transition would be forbidden, as an ion could only move from one well to another if the second well is empty. The current passing through the channel can then be represented by an equation involving the transition probabilities, or 'reaction rates', between the relevant states in the conduction process.

Reaction rate theory was originally developed to describe the rate of chemical reactions [66], before being applied to diffusive processes [65] and then generalised to any rate process. Its early application to chemical reactions used statistical mechanics to use information about the proportions of reactants and products to estimate the transition rates. Provided the system was near equilibrium, this allowed reaction rates to be determined theoretically. However, in many applications of the theory, the reaction rates cannot be determined independently from the measurements they are trying to predict. This means the theory becomes a pedagogical tool rather than a predictive theory.

Reaction rate theory has been useful in chemistry and biochemistry, particularly in explaining the action of enzymes, which act to reduce the energy barriers in particular reactions. The theory has also had extensive use in ion channels where it has been used to model conduction in single and multi-ion channels. Sophisticated models have also been developed, for example to allow for fluctuations in the barrier heights that may be caused by conformational changes in the protein. A good review of these applications is given by Cooper et. al. [45].

The application of the theory to diffusive processes, however, is more dubious than its chemical counterpart. Reaction rate theories necessarily discretise space into specific locations corresponding to the energy wells. Describing the random motion of a particle by sequential hopping between a finite number of states is a bad model if the energy varies only slowly across the region. Reaction rate hopping models are much more appropriate if there are sharp changes in energy [100]. This

poses a problem in applying reaction rate theory to ion channels in which diffusion is believed to be the main mechanism of transport. To model channels accurately in this way would involve modeling the channel by many close shallow energy wells. Unfortunately, all existing studies of channels only include a few energy minima.

Reaction rate theories are very simple, particularly when contrasted to simulations. They have been surprisingly successful in elucidating the permeation mechanism as some channels do involve a process akin to ions hopping in and out of binding sites. But, the main problem with such theories, particularly as far as the aim of this project is concerned, is that there is very little relation between the model and the channel structure. These barrier models involve a highly simplified representation of the channel and although the energy wells are meant to represent binding sites in the channel, no direct connection is made with the physical structure of the channel [125, 150]. These models do not tell what creates the energy wells or barriers. Indeed, it is not even possible to relate the rate constant in the model to the actual height of the energy barrier that the ion is crossing [11]. Rate-theory models do not provide a way to predict currents from a given channel structure, nor the inverse, predicting a channel structure from its conductance properties.

2.4 Continuum theories

Continuum theories provide a way to model the diffusive aspect of ion permeation using the mean field theories developed for bulk electrolytes and are able to relate this directly to the channel structure. They were introduced as an alternative to rate models of ion channels in the 1980's and have flourished since then.

2.4.1 Ohm, Fick and the Nernst-Planck equation

Ions in electrolytes (and channels) diffuse due to potential or concentration gradients. The relationship between the current density and the potential gradient (or the electric field) is expressed by Ohm's law

$$\mathbf{J} = -g\nabla\varphi = g\mathbf{E}, \tag{2.6}$$

where g is the conductivity of the electrolyte solution whose values are determined from experiments under various conditions. An estimate of the current passing through a channel can be made for any given geometry using the more familiar form of Ohm's law $I = VG$, where I is the channel current, V is the membrane potential, and G is the channel conductance. For example, in a simple cylindrical channel of radius r and length L, the channel conductance is given by

$$G = \pi r^2 g/L. \tag{2.7}$$

The physical basis of Ohm's law can be easily understood in terms of the microscopic motion of ions in water. Ions in an electrolyte solution incessantly collide with the surrounding water molecules and as a result execute a random Brownian motion with an average collision time τ. When an electric field $\mathbf{E}$ is applied, an ion with mass m and carrying a unit charge e accelerates, on average, for time τ, gaining a drift velocity, $\mathbf{v}_\mathrm{d} = (e\mathbf{E}/m)\tau$ before the next collision. Substituting this drift velocity into the definition of current density gives Ohm's law.

Ohm's law, simple as it may be, can provide us with useful insights about the permeation mechanisms across a transmembrane pore. As an example, we consider the GA channel, a cylindrical pore whose radius r and length L are approximately 2 Å and 25 Å, respectively. The experimentally determined conductivity of 150 mM K^+ ions is $g = 8.4 \times 10^{-3}$ S/cm. Substituting these values in Eq. 2.7, we obtain $G = 42$ pS. For an applied potential of 200 mV, the current across the pore is then expected to be 8.4 pA. This is about 3 times larger than the current measured experimentally in gramicidin A [9]. This example illustrates that ion permeation across channels is not just a passive process as envisioned in Ohm's law—ions moving from one side of the membrane to the other under a uniform driving field, confined by the channel walls but not interacting with them. In fact, ions do interact with the fixed and induced surface charges on the channel walls, which creates energy wells and barriers along the permeation path, the net effect of which is to reduce the current from that of a purely passive pore. Thus a correct calculation of the ion-channel interactions is of utmost importance in order to obtain reliable results from a permeation model.

The relationship between the current of ions and the concentration gradient across a channel is given by Fick's Law:

$$\mathbf{J} = -ezD\nabla n, \tag{2.8}$$

where D is the diffusion coefficient of ions and n is the ion number density. As shown by Einstein in 1905, the underlying physics is the same as in Ohm's law, namely, the Brownian motion of ions. In the case of ion channels, when one side of the membrane has a higher concentration than the other ($n_1 > n_2$), ions will flow to the other side with a flux, $J = ezD(n_1 - n_2)/L$.

In general, there could be both a potential and a concentration gradient driving the ions across an ion channel. This situation is described by the Nernst-Planck

equation that combines Ohm's and Fick's laws

$$\mathbf{J}_\nu = -ez_\nu D_\nu \nabla n_\nu - g_\nu \nabla\varphi = -ez_\nu D_\nu \left(\nabla n_\nu + \frac{z_\nu e n_\nu}{kT}\nabla\phi\right), \tag{2.9}$$

in which the Einstein relation, $g = nz^2e^2D/kT$, is used to rewrite the expression and the subscript, ν refers to the ion species. Because the potential in an ion channel depends on the ion concentrations there, use of the Nernst-Planck equation with a predetermined or assumed potential is problematic. To avoid the question of self-consistency, one has to include contribution of the ions to the potential, which we discuss below. While the Nernst-Planck equation is primarily used to describe current flow, in the special case of a vanishing current, it makes an important statement about the electrochemical equilibrium in cells. Using $\mathbf{J} = 0$ in Eq. 2.9 and integrating once, we obtain the celebrated Nernst equation

$$\varphi_1 - \varphi_2 = -\frac{kT}{e}\ln(n_1 - n_2) = -59\log\frac{c_1}{c_2}\ (\text{mV}), \tag{2.10}$$

that gives the potential difference required to maintain the equilibrium when the concentrations are different on the two faces of the membrane. The numerical factor in Eq. 2.10 is obtained using $T = 298$ K. In practice, the Nernst equation is often used to estimate the membrane potential generated by asymmetric solutions in cells.

2.4.2 Poisson-Nernst-Planck theory

The Nernst-Planck equation describes how potential and concentration gradients lead to currents. However, they do not include information about how the potential is created, nor the effect that the concentrations of ions itself has on the potential. Combining all these features within one framework leads to the so called Poisson-Nernst-Planck (PNP) theory. In this theory, the potential in equation 2.9 is determined by solving Poisson's equation (Eq. 2.1). The two equations are solved simultaneously to yield consistent solutions for the potential, concentration and flux of ions moving through the channel.

Analytic solutions of the PNP equations are very difficult except in some special cases [195, 196], but the equations can be tackled numerically. When applying PNP theory to calculate currents through ion channels the shape of the channel, the partial charges of the protein atoms, an applied field and the concentrations of ions either side of the channel can all be included. This means that PNP is probably the simplest non-equilibrium theory that can relate the current passing through a channel to its structure. For this reason it provides a very promising start to modeling the structure function relationship inside ion channels.

During the last decades continuum theories of electrolytes have found a new niche in the description of physical processes in the salty waters of cells [64, 213]. Continuum theories were originally developed for bulk electrolytes early in the century, and their validity has been firmly established since then [23]. The more recent applications in biology usually involve mesoscopic systems, and it is not clear from the outset that the assumptions made for bulk solutions are justified for solutions confined to small volumes. Of these, the mean field approximation which assumes that the potential can be determined from a continuous distribution of the mobile charges in an electrolyte is most suspect. The basic question is whether the predicted concentrations in continuum theories, which represent the space average of ion densities, are in accordance with the average motions of individual ions, and whether the potentials found using an average ion distribution reflect those experienced by discrete ions. In this respect, the Debye length provides a useful guide. If the system size is much larger than the Debye length, as in the case of large proteins and membrane surfaces, the mean field approximation inherent in the continuum theories should be relatively safe. On the other hand, membrane pores that transport ions across a cell usually have radii smaller than the Debye length [85], and the use of continuum theories in such systems is questionable. Applications of continuum theories to membrane channels have nevertheless flourished in recent years (for reviews see, for example, [45, 61, 62, 122]).

In chapter 6 I discuss PNP theory in more detail. Unfortunately I also demonstrate that it is not appropriate to use in narrow ion channels due to problems with the mean field treatment of ions. Treating the ions via their average concentrations, as is done in PNP theory, is not valid in narrow ion channels where only one or two ions enter at a time. The forces felt by individual ions cannot be accurately represented using time averaged concentrations. In particular, the surface charges induced by ions become important, but cannot be treated accurately in this mean field approach.

2.5 Brownian dynamics simulation

Brownian dynamics (BD) simulation is a technique in which the motions of individual ions are followed for some short period of time. Thus BD simulations differ from the continuum models in that charge is localised rather than being dispersed in a continuous manner and time is reintroduced. The ions, however, are assumed to be moving in a continuous solution as in PNP, rather than in the presence of discrete water molecules. The effects of this water is taken into account

by including frictional and random forces on the ion caused by their interactions with water molecules thus leading to random Brownian motion of the ions. BD is the primary conduction model used in this study. I will introduce it briefly here, but a full description of the method is given in chapter 3.

Brownian motion has been well described and quantified as a stochastic process but has only recently been used to model ion channels. The first applications were carried out in one-dimension [38], and the technique has only been extended to three dimensions very recently - firstly by our research group to study ion movement in model acetylcholine receptor channels and the KcsA potassium channel [42, 127] and more recently by others to study Porin channels [93, 157, 185].

To carry out a BD simulation of an ion channel, a model channel shape and dielectric structure must first be devised. Ions are then assigned an initial position and thermal velocity. Then, the forces on each ion are calculated and related to the position and velocity of the ions using the Langevin equation (Eq. 3.1). In the Langevin equation the forces acting on an ion are broken into 3 components: random, frictional and systematic forces. The random force represents the incessant collisions of the ion with its surrounding water molecules, and rapidly fluctuates about a zero mean. The frictional force, on the other hand, is the drag created by passing through the water molecules. The systematic force is all the remaining forces, not created by the surrounding water. This includes the electrostatic force created by other ions, fixed charges in the protein, the applied potential, and from induced surface charges at the dielectric (water/protein) boundary. The system is evolved forward for a short time step, each ion being moved to a new position calculated from the Langevin equation. This process is repeated for many time steps to model the movement of ions over a short time.

The advantage of BD compared to other simulation techniques is that the simplifications involved make it feasible to simulate long time periods. This means that currents passing through the channel can be directly computed, unlike in molecular dynamics (discussed below). This means that current-voltage and current-concentration relationships can be calculated and compared directly with experimental results. Simulations can also be carried out with mixtures of ions to determine the selectivity ratios of the channel. Unfortunately, however, ions of the same valence are treated in a similar manner in these simulations (apart from their different radii) which makes it difficult to determine the selectivity between different ions of the same valence. In this case the selection of ions is most likely related to more subtle properties such as the strength of binding to the neighbouring water molecules which can only be dealt with in a more detailed theory such as molecular

dynamics.

BD simulations can also be used to study permeation kinetics. Ion trajectories can be analysed to determine the average concentrations throughout the channel. This is useful in finding binding sites and determining the average number of ions involved in conduction. Also, the important rate limiting steps in conduction can be determined from the ion trajectories. The trajectories themselves can be animated to view the motions of ions through the channel which can be an invaluable tool in understanding the mechanisms of conduction.

BD is a phenomenological theory with a number of simplifications and parameters that need to be validated or derived from a more fundamental theory. For example, although the ions are treated as discrete particles, the water molecules are still modeled as a continuum, greatly reducing the number of computations required to carry out the simulation. Far from any boundary, where the water molecules are free to move and align as they wish, this is a reasonable assumption. However, in small confined regions, such as inside a very small radius channel, when the size of the region is of the same order of size as the size of the ions and water molecules this assumption may break down. The water molecules will be constrained and so no longer be able to align as they wish, and the hydration shells of the ions will be forced to interact with the channel walls. Also the protein is taken to be a rigid structure which does not move as ions pass through the channel. This seems to be a reasonable approximation for the narrow gramicidin A channel as recent NMR experiments have shown that any conformational changes in the channel protein are very small [199, 200]. The amount of flexibility in other protein channels is yet to be determined.

In BD simulations the systematic (electrostatic) forces are typically found by solving Poisson's equation. This means that the protein and water are treated as uniform dielectric environments. Determining what value of the dielectric constant to use is important, but probably even more important is whether or not the dielectric continuum description is valid at all. I examine the possibility that this description breaks down in chapter 9. BD itself, however, only deals with the dynamic behaviour of ions and does not specify how the forces are determined. If the continuum electrostatics is shown to be invalid in particular cases, then BD may still be useful if the forces can be determined in another way. The other parameter required in BD simulations is the diffusion coefficient of ions. These can be determined from MD simulations.

BD simulations provide a good compromise between detailed all atom simulations and the continuum theories. They can be used to calculate experimentally

measurable properties of channels (namely the currents passing through them) and relate this to the channel structure. But, unlike in continuum theories, the ions are treated as discrete entities rather than through their average concentrations. This avoids many potential problems that can arise in the continuum models which are highlighted in chapters 5 and 6. These simulations also escape many of the difficulties encountered in more complex simulations, however ultimately the assumptions used in BD must be validated from a more fundamental theory.

2.6 Molecular dynamics simulation

Molecular dynamics (MD) is a simulation technique in which *all* the atoms in the system are treated explicitly. For ion channels, this involves simulating the motion of all the protein and lipid atoms, the water molecules and ions. In a similar manner to BD, the simulation is broken into small timesteps. The forces acting on all the atoms are calculated at a given time, before the atoms are moved a short distance corresponding to their motion in one timestep. During a simulation the computer keeps track of the positions of all the atoms, but making sense of this vast amount of data can be challenging. Also, the number of calculations required during the simulation is enormous due to the huge number of atoms being simulated. The computational power required places severe limits the types of problems that can be tackled with MD. But, despite the complexity, the availability of several user-friendly MD packages such as AMBER [212], CHARMM [25] and GROMOS [81] have made the MD method accessible to any researcher with a modest workstation. As computer power increases, hopes have been raised that biological processes will soon be able to be studied at a microscopic level. MD, however, has to be used with some caution, as its accuracy is yet to be demonstrated in many biological situations [207]. Below I will present the basics formalism of MD and discuss some of the complexities, before examining its application to ion channels

2.6.1 Basic formalism

In MD simulations, one follows the trajectories of N particles interacting via a many-body potential $U(\mathbf{r}_1, \mathbf{r}_2, \ldots, \mathbf{r}_N)$ using Newton's equation of motion:

$$m_i \frac{d^2\mathbf{r}_i}{dt^2} = \mathbf{F}_i, \tag{2.11}$$

where m_i and $\mathbf{r}_i$ denote the mass and position of the i'th particle, and the force on it ($\mathbf{F}$) is given by the gradient of the potential U. Because all the atoms in the

system (including water molecules) are represented explicitly in MD, there are no frictional or random forces to deal with as in BD. This makes the integration of Eq. 2.11 rather trivial. Most commonly, if the positions are known at a time t and a short time before this $t - \Delta t$, they are calculated at a later time using the Verlet algorithm:

$$\mathbf{r}_i(t + \Delta t) = 2\mathbf{r}_i(t) - \mathbf{r}_i(t - \Delta t) + \frac{\mathbf{F}_i(t)}{m_i}\Delta t^2. \tag{2.12}$$

At every time step, the potential function is recalculated using the new positions of the particles before moving them again. This process is iterated for a number steps until a statistically satisfactory data set is generated. The trajectory data thus generated is stored at certain intervals, which are analyzed later to determine the structural and dynamical properties of a system. Quantities such as free energy, mean square displacement, radial distribution and other correlation functions are calculated from an ensemble average of several simulations.

Despite being conceptually simple, MD is in practice very complex. Determining the forces, finding suitable boundary conditions and analysing and interpreting the results can all be quite difficult. A full discussion of these issues can be found in one of the many textbooks on the subject [2, 67, 165].

2.6.2 Force fields

Since the force fields (or potential functions) are the crucial inputs in MD simulations it is essential that they are chosen correctly when simulating a biomolecular system (see [210] for a recent review).

The forces acting on atoms are typically broken into two components: 'bonded' interactions representing covalent bonds existing between atoms, and all the remaining 'non-bonded' interactions. In classical MD the non-bonded interactions are determined by empirically fitting parameters to make the simulations reproduce experimentally measured properties (usually things such as radial distribution functions in bulk electrolyte solutions). In *ab-initio* MD these forces are determined at each timestep from electronic structure calculations.

Bonded interactions

The atoms in proteins and lipids are not free but bonded to their nearest neighbors by covalent interactions. In MD these bonds are represented by three types of bond interactions: stretching of a bond length between two atoms, bending of a bond angle formed by three atoms and torsion of a dihedral angle between the

planes of four atoms. The first two are normally represented by harmonic potentials, whilst the torsion potential is written in terms of periodic functions. The bond interactions allow a certain degree of flexibility to the protein atoms forming an ion channel, which may change their configuration in response to a permeating ion. Unfortunately, with the currently available run times it is difficult to quantify the amount of flexibility in ion channel proteins using MD. It remains an open question whether protein flexibility plays an important role in ion permeation.

Non-bonded interactions

If the atoms in a system could be represented as charged balls, they would simply interact via the Coulomb potential. Unfortunately the electrons around atoms are not inert but move according to quantum mechanical laws, which modify this simple classical picture in subtle ways. Incorporation of the effects of electrons in classical MD simulations has been an ongoing concern since the inception of the method in the 1960s. Electronic contributions to the intermolecular interaction can be divided into three groups: polarization, attractive (or van der Waals) dispersion and short-range repulsion.

Polarisation refers to the shift in the position of the electron cloud with respect to the nucleus when an atom is placed in an electric field. An exact description of polarization requires the solution of the Schrödinger equation. In classical MD, however, the polarisation is usually ignored or approximated using a simple classical picture where electrons move in a harmonic potential. This induced dipole, in turn, creates an electric field of its own which further polarizes the surrounding atoms. Thus polarization is a many-body effect that needs to be taken into account self-consistently via iteration of the polarization and dipole field equations. Because this procedure is quite costly computationally, in most force field parameterizations polarization effects are incorporated implicitly by invoking a mean field approximation. That is, an average induced dipole term is added on top of the monomer value so as to reproduce the bulk properties of a system.

The dispersion forces arise from quantum fluctuations that leads to correlations between the electrons of two atoms. Virtual excitations of electrons in one atom generate a spontaneous dipole moment that polarizes the neighboring atoms yielding an induced dipole-induced dipole interaction. Unlike polarization, the dispersion force is a purely quantum phenomenon with no classical analogue. Although there are no polarization forces between neutral atoms, they are still attracted by the dispersion forces.

The repulsion term has its origins in the Pauli exclusion principle that forbids two

electrons occupying the same quantum state. When two atoms come into contact, the orbitals of electrons starts overlapping, which leads to a sharply rising repulsive potential. The dispersion and repulsive potentials are often combined in a so-called Lennard-Jones (LJ) 12–6 interaction that has become almost an industry standard in MD force fields. Compared to the Coulomb and polarization interactions, the LJ potential is weaker and has a much shorter range.

In most MD force fields the polarization interaction is neglected, and the parameters in the Coulomb (partial charges on atom centers) and the LJ interactions are determined from fits to the bulk properties (e.g., enthalpy of vaporization and density for water). The pair potentials determined in this way incorporate many other effects in their parameterizations, and therefore do not have much in common with the actual dimer interaction in vacuum. The justification for such a simplified phenomenological approach is ultimately its success in reproducing experimental observations. In this regard, more fundamental approaches based on accurate many-body interactions have been much less successful [209].

Ab-initio calculations provide a way to avoid approximate parameterizations of the atom interactions. The inter-atomic forces can be found by solving the Schrödinger equation using either Hartree-Fock theory [159] or density functional theory (DFT) [108]. Both of these techniques can only be used to study small systems, especially the former in which the basis set expansion of the electron wave function limits its applicability. Car and Parrinello [30] made a breakthrough when they developed an algorithm for combining DFT with MD. The motions of atoms are still simulated by classical mechanics but the forces between them are calculated quantum mechanically. The main difficulty with these techniques is the number of calculations required is much greater than in classical MD. This means a huge amount of computer time is required, and so presents limits to the system sizes that can be studied. Such ab-inito methods have been applied to crystals [26] and an ion in bulk water [135]. A first application of DFT to ion channels has also been recently reported [73] although it could only conclude that polarization is likely to be important in ion permeation. The application of *ab-initio* techniques to ion channels promises to be exciting new frontier.

2.6.3 Boundaries

A major problem in MD simulations is how to achieve a bulk-like environment when using a relatively small system. Indeed in a simulation of 1000 atoms in a box, about half of the atoms are in direct contact with the surfaces. The traditional way to avoid the surface effects is to impose periodic boundary conditions. That

is, the simulation system is replicated in all directions, filling all space. Such a boundary condition seems to be a reasonable choice for bulk solutions, but for a grossly inhomogeneous system such as an ion channel, periodicity introduces its own artifacts. These artifacts can be monitored by checking the dependence of results on the system size, though such precautions are rarely exercised in practice because of the time required. It is expected that the errors introduced by periodicity are much less severe than those that would result from the use of vacuum as a boundary. As a result, the periodic boundary conditions are adapted almost universally in current MD simulations of biomolecules. A better justification of its use in simulations of ion channels is needed to substantiate accuracy of the current MD results.

Using periodic boundary conditions raises the question of how to handle the long-range Coulomb forces in the resulting infinite system. In early simulation work, cutoffs were often employed to truncate the Coulomb forces. Now, more elaborate techniques such as Ewald summation in which the Coulomb interaction is split into a long and a short-range part to reduce the computational costs are most commonly used.

2.6.4 Application to ion channels

The application of MD to ion channels is severely hampered by the computational cost involved. The MD algorithm assumes that the forces acting on atoms are constant over a timestep. Thus, very short timesteps are required to keep this assumption at least approximately correct. The rotational motion of water, in particular, is very fast, and so time steps of at most 2 fs have to be used. An ion takes more than 10 ns to pass through an ion channel under physiological conditions, and to gain statistically reliable measurements of current would require simulations of the order of 1 μs. Even for a very small ion channel system, about 1,000,000 calculations are required per timestep, and gaining an estimate of current would take close to a year of CPU time on a modern supercomputer (and this would only yield one data point on an I-V or current-concentration plot!). This is obviously more than most researchers can afford. In a recent 100 ns MD simulation, Crozier et al. [50] calculated the conductance of a simplified artificial channel in somewhat extreme conditions (1 M solution with a 1.1 V applied potential). This gives hope that it may be possible to determine conductance of biological channels from MD studies under physiological conditions in not too distant future. But, given that I-V curves are generally non-linear at large potential and the simplicity of the artificial channel, it is not clear what this result has to say about biological channels in physiological conditions. Typical MD simulations of biological channels can be run

for about 10 ns, which is too short to estimate the channel conductance, or even to explore the dynamics of a single conduction event. Currently, MD cannot be used to determine biological channel currents.

This does not mean that MD has no use in studying ion channels. There is important information that can be gained from simulations other than currents. Perhaps most useful is the potential of mean force (PMF) of an ion moving along the permeation path. This can be calculated from the average force acting on or the average distribution function of an ion at a given position. The PMF represents the energy landscape experienced by the ion, and describes the work required to push an ion through the channel. This energy profile can tell one much about the permeation process. Wells in the profile would represent binding sites where ions are delayed, and the number and size of the energy barriers would imply information about the rate limiting steps in conduction, and could be used to gain an indication of the transit rate. Furthermore, the PMF can be fed into a coarser grained model, such as BD, to model currents and remove some of the uncertainties in the forces acting on ions. PMFs have recently been calculated for permeating ions in the GA channel [102, 176, 215].

The calculation of the PMF in the GA channel has, however, highlighted some potential problems in the use of MD in ion channels. Although the profiles obtained predict energy wells at appropriate positions, they also predict huge energy barriers ($\sim$ 15 - 40 kT) that would prevent ion permeation. These results are in obvious contradiction with experiments in which ions pass readily through the GA channel. Most likely, the problem arises from using invalid force fields, particularly from the neglect of polarization.

MD simulations can also be used to gain an indication of channel selectivity by using free-energy perturbation calculations. In this technique, an ion at a position in the channel is slowly transformed into an ion of another type and the energy difference between the two end states calculated [141]. The ion species with the lower free energy is more likely to enter the channel and the selectivity ratio can be estimated from the free energy difference via a Boltzmann factor. This technique has been used to determine the correct selectivity sequence in the GA channel [172, 179] as well as predicting the selectivity of the KcsA channel for potassium over sodium [3]. Because these calculations involve the energy difference for the transformation of an ion of one type into another at the same location, inaccuracies in force fields are likely to cancel out, making such predictions more robust compared to the PMF of an ion along the permeation path. Moreover, ions with the same valence cannot readily be distinguished in BD; hence, MD offers the only method for understanding

their selectivity sequences.

Macroscopic parameters such as diffusion coefficients of ions and the dielectric constant of water in the channel are two other local properties that can be estimated from MD. These quantities are required as input parameters in BD simulations that would otherwise have to be determined from fits to experimental data. Studies have suggested that both the dielectric constant [183, 217] and diffusion coefficients of ions [5–7, 131, 175, 190, 191] will be substantially lower inside a narrow pore than in bulk solution.

Considering the simplicity of the force fields in current use, MD techniques have been remarkably successful in studies of lipid-protein systems. The average treatment of polarization appears to work well as long as one retains the bulk-like environment for the molecules in question [201, 209]. In applications of MD to ion channels, however, there is likely to be problems in this regard because ions move from bulk water into a narrow pore formed by protein molecules with very different polarization characteristics. This problem is probably responsible for the overly large energy barriers predicted in the GA channel. Thus the force fields currently employed in most MD programs appear not to be sufficiently accurate for the purpose of PMF calculations in channels, and the construction of new, polarizable force fields is desirable. A longer term goal is to use *ab-initio* MD methods to derive the force field parameters directly from the electronic structure calculations rather than determining them empirically from fits to data [114].

As MD simulations involve the interactions of all the atoms in the channel protein, it is only reliable if the relative positions of all the atoms, that is the molecular structure, is known. For this reason most early MD studies were made on the GA channel, which for a long time was the only channel with a known atomic structure. Since the crystal structure of the KcsA channel was determined in 1998, it has become the main target of simulations [3, 6, 13, 21, 74, 75, 130, 174, 188]. These studies have provided valuable information on the selectivity mechanism and the energetics of ion permeation in the channel, but do not make predictions about the conductance.

Although MD cannot be used to determine currents in biological channels at the current time, it can play a complementary role to BD in many respects. By making estimates of diffusion coefficients, dielectric constants, and possibly the PMF and using these in BD, one can reduce the arbitrariness in the choice of free parameters that so often plagues the application of phenomenological models to realistic systems.

2.7 Conclusions

In this chapter I have introduced many theories used to model permeation through biological ion channels. I discussed the dielectric representation involved in continuum electrostatics and how Poisson's equation can be applied to the channel. Solutions to Poisson's will be an important focus of this project and I will return to these in the following chapter. Reaction rate theories have been used to explain the basic steps involved in conduction, but unfortunately the parameters in these models cannot be related to the physical structure of the channel. The simplest way to examine the structure function relationships is to use a continuum theory such as PNP. Continuum theories provided a major advance over rate models, but as I will discuss in chapter 6 they cannot be used to accurately model the processes involved in ion permeation. Simulation techniques provide a further step forward in accurately modeling channels. Molecular dynamics simulations in which all the atoms in the system are modeled will provide the most accurate descriptions of permeation in the future. But currently they are too slow to be used to describe permeation, and the accuracy of the approximations currently used in the classical MD force fields is not clear. Brownian dynamics, in which only the ions are treated discretely, provides a more practical approach. It is both fast enough to model currents, avoids many of the problems of the continuum theories, and has potential to explain much, but not all, the mechanics of channels. BD will be the principal tool used in this study as it is currently the only model that can relate ionic currents to channel structure in a realistic way.

Chapter 3

Brownian Dynamics Simulations

The most important methodology used in this study is Brownian dynamics (BD) simulations. Such simulations are used in all the following studies, and so it is worthwhile to explain the technique and the practical issues involved in its implementation carefully before proceeding.

3.1 Basic formalism

In BD, the channel walls are taken to be rigid and the protein and membrane atoms are assumed to form a continuous medium as with the electrostatic calculations described in chapter 2. The water molecules in the electrolyte are described as a continuous dielectric medium. The motion of individual ions, however, are simulated explicitly using the Langevin equation:

$$m_i \frac{d\mathbf{v}_i}{dt} = -m_i \gamma_i \mathbf{v}_i + \mathbf{F}_R(t) + q_i \mathbf{E_i} + \mathbf{F_S}, \tag{3.1}$$

where m_i, q_i and $\mathbf{v}_i$ are the mass, charge and velocity of the ith ion. In Eq. 3.1, the effect of the surrounding water molecules is represented by an average frictional force with a friction coefficient $m_i\gamma_i$, and a stochastic force $\mathbf{F}_R$ arising from random collisions. The frictional and random forces are related through the fluctuation–dissipation theorem [218]:

$$m_i \gamma_i = \frac{1}{2kT} \int_{-\infty}^{\infty} \langle F_R(0) F_R(t) \rangle dt, \tag{3.2}$$

in which the angled bracket notation denotes ensemble averages.

The third term on the RHS of Eq. 3.1 is the total electric force (where $\mathbf{E}$ is the electric field) acting on the ion due to other ions, fixed and induced surface charges at the channel boundary, and the applied membrane potential. The last term, $\mathbf{F_s}$ represents additional short range forces used to more accurately mimic the ion–ion and ion-protein interactions at short distances as described below.

The Langevin equation can be solved to relate the position and velocities of ions at one time to that a short time later in a process described by van Gunsteren and Berendsen [206]. The Langevin equation is integrated from an initial time t to a later time t_n to give

$$\dot{x}(t)\exp(\gamma t) - \dot{x}(t_n)\exp(\gamma t_n) = \frac{1}{m}\int_{t_n}^{t}[F_R(t') + F(t')]\exp(\gamma t')dt', \tag{3.3}$$

in which F is the total systematic force acting on the ion (the sum of the electrical and short range components) and the ion subscripts i have been dropped for simplicity. If this systematic force is expanded to third order as $F(t) = F(t_n)+\dot{F}(t_n)(t-t_n)$ then equation 3.3 can be partly integrated giving

$$\begin{aligned}\dot{x}(t) = \dot{x}(t_n)\exp(-\gamma(t-t_n)) &+ \frac{F(t_n)}{m\gamma}(1-\exp(-\gamma(t-t_n))) \\ &+\frac{\dot{F}(t_n)}{m\gamma^2}(\gamma(t-t_n) - 1 + \exp(-\gamma(t-t_n))) \\ &+\frac{\exp(-\gamma t)}{m}\int_{t_n}^{t}F_R(t')\exp(\gamma t')dt'.\end{aligned} \tag{3.4}$$

The position of the particle after a short time Δt can be found by integrating equation 3.4 from t_n to $t_n + \Delta t$. The last term is integrated by parts and the result defined as a new variable, X related to the random force:

$$X_n(\Delta t) = (m\gamma)^{-1}\int_{t_n}^{t_n+\Delta t}[1-\exp[-\gamma(t_n+\Delta t-t)]]F_R(t)dt. \tag{3.5}$$

The final result of the integration is then:

$$\begin{aligned}x(t_n+\Delta t) &= x(t_n) + \frac{\dot{x}(t_n)}{\gamma}(1-\exp(-\gamma\Delta t)) \\ &+\frac{F(t_n)}{m\gamma^2}(\gamma\Delta t - 1 + \exp(-\gamma\Delta t)) \\ &+\frac{\dot{F}(t_n)}{m\gamma^3}(1-\gamma\Delta t + (1-\gamma\Delta t)^2/2 - 1 - \exp(-\gamma\Delta t)) \\ &+X_n(\Delta t).\end{aligned} \tag{3.6}$$

The velocities can then be eliminated from equation 3.6 by adding $\exp(-\gamma\,\Delta t)x(t_n+\Delta t)$ [206] to give the final expression:

$$x(t_n+\Delta t) = x(t_n)[1+\exp(-\gamma\Delta t)] - x(t_n-\Delta t)\exp(-\gamma\Delta t)$$

$$
\begin{aligned}
&+m^{-1}F(t_n)(\Delta t)^2(\gamma\Delta t)^{-1}[1-\exp(-\gamma\Delta t)] \\
&+m^{-1}\dot{F}(t_n)(\Delta t)^3(\gamma\Delta t)^{-2}[\frac{1}{2}\gamma\Delta t[1+\exp(-\gamma\Delta t)] \\
&-[1-\exp(-\gamma\Delta t)]] + X_n(\Delta t) + \exp(-\gamma\Delta t)X_n(-\Delta t),
\end{aligned}
\tag{3.7}
$$

where

$$X_n(-\Delta t) = X_{n-1}(\Delta t)G(\gamma\Delta t)/C(\gamma\Delta t) + Y, \tag{3.8}$$

in which Y are sampled from a Gaussian with zero mean and

$$G(\gamma\Delta t) = \exp(\gamma\Delta t) - 2\gamma\Delta t - \exp(-\gamma\Delta t) \tag{3.9}$$

$$C(\gamma\Delta t) = 2\gamma\Delta t - 3 + 4\exp(-\gamma\Delta t) - \exp(-2\gamma\Delta t), \tag{3.10}$$

The computational steps in implementing this algorithm are then as follows:

1. Assume that the locations, and forces acting on each ion in the previous time steps, $x(t_n)$,$x(t_{n-1})$, $X_{n-1}(\Delta t)$ and $F(t_{n-1})$ are known
2. Evaluate the total systematic forces $F(t_n)$.
3. Compute the derivative of the systematic force

$$\dot{F}(t_n) = [F(t_n) - F(t_{n-1})]/\Delta t \tag{3.11}$$

4. Calculate the random terms $X_n(\Delta t)$ and $X_n(-\Delta t)$
5. Calculate the new ion positions from equation 3.7.

In practice, ions are randomly assigned an initial position and thermal velocity from the Boltzmann distribution. The forces on the ions are then calculated before the system is evolved forward for a short time step, using the above procedure. The forces on the ions are then recalculated at their new locations and the system evolved forward once more. This process is repeated to simulate the motion of the ions over the desired time interval.

Figure 3.1 shows a typical BD system. The shape of the channel boundary is first traced out as desired and inserted into a protein / membrane region represented in brown. This protein region is typically assigned a dielectric constant $\epsilon_{protein} = 2$. The inside of the pore and the regions at either end are given higher values, $\epsilon_{channel}$ and ϵ_{bulk}. Ions are then placed in reservoirs at each end of the pore. These ions are contained by reservoir boundaries which form a hard barrier to the ions (but do not represent dielectric boundaries). The motions of the ions in the system are

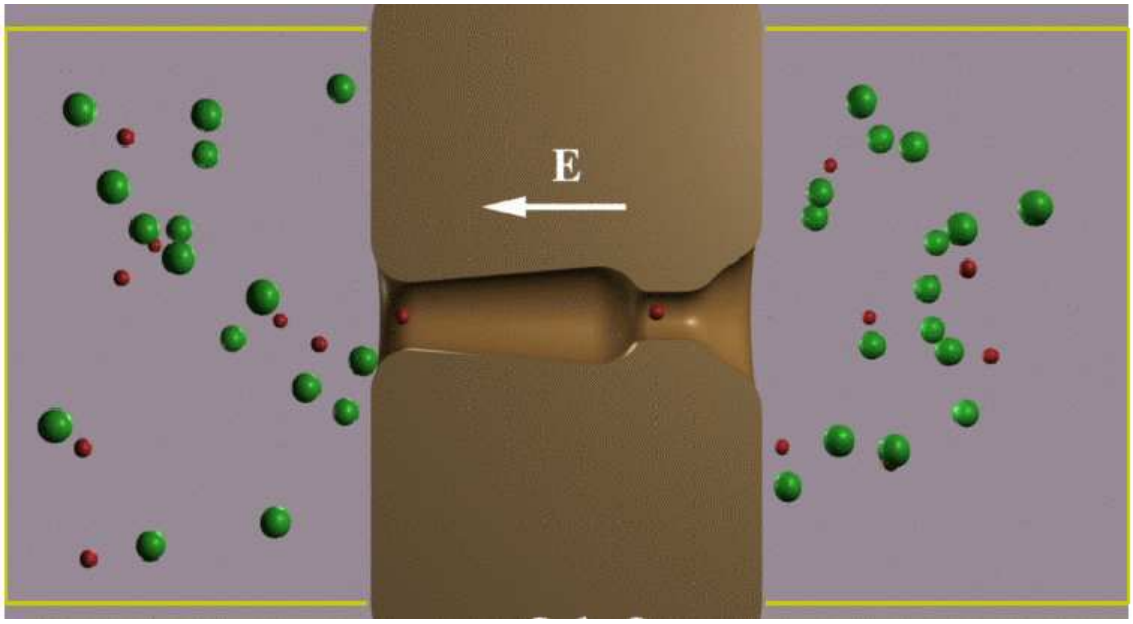

Figure 3.1: Diagram of the BD system used to study the calcium channel in chapter 8. Calcium (red) and chloride (green) ions are placed in the water solution (purple) in reservoirs on either side of the protein (brown). The intracellular space is on the lefthand side of the channel, and the extracellular space on the right. The reservoir walls which are used to contain the ions are indicated by the yellow lines. The calcium channel pore passes through the center of the protein. In this case a membrane field is applied to drive ions through the channel and the motions of the ions are simulated using the Langevin equation.

then followed as described above. The situation in this figure actually represents a model of the L-type calcium channel discussed in chapter 8. The baths contain calcium (red) and chloride ions (green).

Note that the friction coefficient, γ, is related to the diffusion coefficient via the Einstein relation $D = kT/m\gamma$. The friction coefficient is also related to the 'relaxation time constant', γ^{-1}, which corresponds to the time required for a particle that is suddenly displaced to relax back to its equilibrium position. Unlike earlier BD algorithms, this one is not limited by the condition $\Delta t << 1/\gamma$, which would require $\Delta t << 10$ fs for typical ions and make the simulation of conductance computationally expensive.

The two remaining requirements that limit the size of the time steps are that the average distances traveled by ions in each time step must be much smaller than the dimensions of the system, and that the time derivative of the electric forces must also be small compared to the magnitude of the force. In previous simulations using this algorithm, the time step was systematically increased to see its affect on ion trajectories [91, 127]. It was found that when the time step was greater than 100 fs the trajectory of the test particle deviated from that found with shorter time steps. Thus in these studies a maximum time step of 100 fs is employed. To simulate the short range forces more accurately we use a multiple time step algorithm in the simulations described in chapters 8 and 9. In these cases, a shorter time step of 2 fs is used across the channel where short range ion-ion and ion-protein forces have the most impact on ion trajectories. Elsewhere a longer time step of 100 fs is used. If an ion is inside the short timestep region at the beginning of a 100 fs period then that ion is simulated by 50 short steps while the other ions in the long-time regions are frozen to maintain synchronicity.

Results are obtained by running numerous simulations, each typically simulating $0.1\mu s$ of real time. For successive simulations, the final positions and velocities of the ions in the previous simulation are used as initial positions and velocities in the next trial. The current passing through the channel is calculated by counting the number of ions that cross the channel, and averaging the values obtained in repeated simulations. Concentration distributions can also be constructed by averaging the number of ions in a given region of the channel during a simulation.

To maintain the specified concentrations in the reservoirs, a stochastic boundary is applied: when an ion crosses the channel, say from left to right, an ion of the same species is transplanted from the right reservoir to the left. For this purpose, the ion on the furthermost right-hand side is chosen, and it is placed far left-hand side of the left reservoir, making sure that it does not overlap with another ion.

The stochastic boundary trigger points, located at either pore entrance, are checked at each time step of the simulation. The membrane potential is created by adding a constant electric field throughout the system. (Note that this does not result in a linear potential drop across the system due to the presence of the dielectric boundaries). These boundary conditions are described in more detail and tested in chapter 4

The BD program is written in FORTRAN, vectorized and executed on a supercomputer (Fujitsu VPP-300 or Compaq SC). The basic BD program was written by Toby Allen, Matthew Hoyles, and Siu Cheun Li at the Protein Dynamics Unit at the ANU. I have contributed to the development of the program and have made significant improvements and modifications. These have included improving the short range forces, implementing the geometries discussed later and allowing for non-symmetric boundaries, implementing the Grand Canonical Monte Carlo boundaries, allowing the use of finite difference solutions to Poisson's equation, adding numerous data analysis modules for calculating conductances and concentrations and much more.

3.2 Calculation of forces

3.2.1 Electric forces

In most cases the electric forces acting on the ions are found by solving Poisson's equation for the given channel boundary and ion locations using one of the numerical techniques described below. Rather than solving Poisson's equation at each time step, which would be computationally prohibitive, a system of lookup tables is used [91]. The electric field and potential due to one- and two-ion configurations are pre-calculated at a number of grid points and stored in a set of tables. During simulations, the potential and field at desired points are reconstructed by interpolating between the table entries and using the superposition principle. For this purpose, the total electric potential ϕ_i experienced by an ion i is broken into four components

$$\phi_i = \phi_{\mathrm{X},i} + \phi_{\mathrm{S},i} + \sum_{j \neq i} (\phi_{\mathrm{I},ij} + \phi_{\mathrm{C},ij}), \tag{3.12}$$

where the sum over j runs over all the other ions in the system. In Eq. 3.12, $\phi_{\mathrm{X},i}$ is the external potential due to the applied field, fixed charges in the protein wall, and charges induced by these; $\phi_{\mathrm{S},i}$ is the self potential due to the surface charges induced by the ion i on the channel boundary; $\phi_{\mathrm{I},ij}$ is the image potential due to the charges induced by the ion j; and $\phi_{\mathrm{C},ij}$ is the Coulomb potential due to the ion j. All the

channel models described in this thesis are symmetric about the channel axis. This means that the first 3 potential terms in Eq. 3.12 can be stored in, respectively, 3, 2 and 5 dimensional tables (dimension is reduced by one in the latter two cases by exploiting the azimuthal symmetry of the system's geometry). Similar tables are constructed for each component of the electric field which are calculated from the gradient of the potential at the grid points. The electric forces required in the simulations are then obtained at each time step by interpolating between values in the lookup tables. The accuracy in interpolating potential values from precalculated tables depends on the number and distribution of storage points in the tables. Values are stored using a set of generalised coordinates which allow for variations of grid spacing, and the forces on ions can be very accurately determined [91].

3.2.2 Short range forces

The Coulomb interaction between two ions is modified by the addition of a repulsive $1/r^9$ potential, which arises from the overlap of their electron clouds [156]. The hydration forces between two ions add further structure to the ion pair potential in the form of damped oscillations [71, 72]. Together these effects can be approximately represented by

$$U_{\rm sr}(r) = U_0 \left\{ (R_{\rm c}/r)^9 - \exp[(R-r)/a_{\rm e}] \cos[2\pi(R-r)/a_{\rm w}] \right\} . \qquad (3.13)$$

Here the oscillation length $a_{\rm w} = 2.76$ Å is given by the water diameter and the other parameters are determined by fitting Eq. 3.13 to the potentials of mean force obtained from MD given by Guàrdia et al. [71, 72]. For anion-cation pairs, $R_{\rm c} = r_1 + r_2$ but for like ions the contact distance is pushed further to $R_{\rm c} = r_1 + r_2 + 1.6$ Å. The origin of the hydration force R is slightly shifted from $R_{\rm c}$; by $+0.2$ Å for like ions and by -0.2 Å otherwise. The exponential drop parameter is determined as $a_{\rm e} = 1$ Å for all ion pairs. A full list of parameters used for the various ion types considered is given in table 3.1.

Fig. 3.2 A shows a plot of this short range potential for the NaCl solution used in our Brownian dynamics simulations. This potential agrees well with the potential of mean force derived by Guàrdia et al. ([71, 72]). The short range force in Eq. 3.1 is determined from the derivatives of the potential in Eqs. 3.13.

BD simulations using this combination of Coulomb and short range forces accurately mimic the results of molecular dynamics simulations. In Fig. 3.2 B, we show the radial distribution functions for Na-Na, Na-Cl and Cl-Cl pairs obtained from 2.5 ns BD simulation of a 1.79 M NaCl solution (22 Na^+ and 22 Cl^- ions) confined in a large cylinder with a diameter and height of 30 Å. To avoid the edge effects, ions

Table 3.1: Parameters used for short range ion–ion forces.

Ions	U_0 (kT)	R_c (Å)	R (Å)
Na–Na	2.5	3.50	3.70
K–K	2.5	4.26	4.46
Ca–Ca	0.8	3.58	3.78
Na–Cl	8.5	2.76	2.56
K–Cl	5.2	3.14	2.94
Ca–Cl	16.8	2.80	2.60
Cl–Cl	1.4	5.22	5.42

within 8 Å of the boundary at any timestep are excluded from the sampling. As expected, the resulting peaks in the distribution function are located at the minima of the potential of mean force and also match closely those locations found in the radial distribution functions from molecular dynamics simulations [132] (indicated by the arrows). We have found that simpler ion-ion interactions that ignore hydration effects employed previously in BD studies of other channels (*e.g.*, [40, 42]) are not suitable in many cases. In the calcium channel, for example, the simpler interactions allow cations to pass each other in the selectivity filter, unlike when the realistic interaction described above is used.

The short range forces are also used to keep the ions in the system and to mimic other interactions between ions and the protein. In order to prevent ions from leaving the system, a hard-wall potential is activated when the ions are within one ionic radius of the reservoir boundaries, which elastically scatters them. For the ion-protein interaction U_{IW}, we use the usual $1/r^9$ repulsive potential

$$U_{\mathrm{IW}}(r) = \frac{F_0}{9} \frac{(R_i + R_w)^{10}}{(R_c(z) + R_w - a)^9}, \tag{3.14}$$

where R_i is the ion radius, R_w is the radius of the atoms making up the channel wall, $R_c(z)$ is the channels radius as a function of the z coordinate, and a is the ion's distance from the z axis. We use $R_w = 1.4$ Å and $F_0 = 2 \times 10^{-10}$ N in Eq. 3.14, which is estimated from the ST2 water model used in molecular dynamics [192].

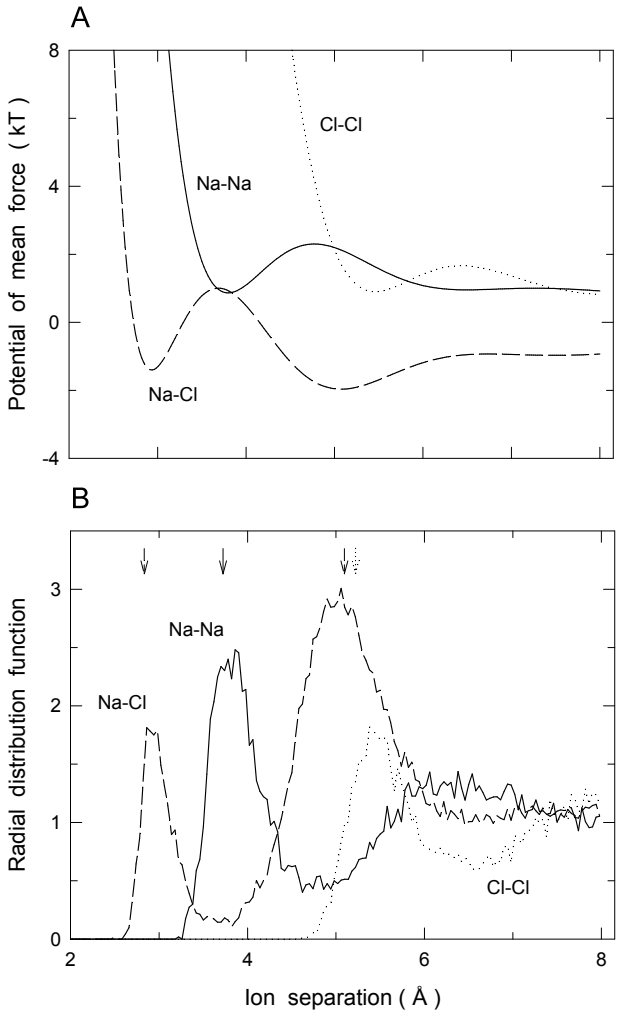

Figure 3.2: Ion-ion forces used in BD simulations. (A) The inter ion potentials for Na^+ - Na^+ (solid line), Na^+ - Cl^- (dashed line) and Cl^- - Cl^- (dotted line) ion pairs are plotted against the ion separation as given by Eq. 3.13. (B) The radial distribution functions for 1.79 M NaCl solution derived from BD simulations (the same line styles as in A are used). The locations of the maxima found in the molecular dynamics simulations of Lyubartsev and Laaksonen [132] are indicated by the arrows at the top of the graph.

3.2.3 Other force calculations

It is worth noting that the BD algorithm only describes the dynamic behaviour of ions in terms of the forces acting on it and does not specify what those forces are. The forces acting on the ions in BD can be calculated in any way, and need not rely on the solutions of Poisson's equation. Indeed, in chapter 9 I discuss the possibility that the continuum picture used in Poisson's equation fails in the narrow GA channel due to problems with assigning a uniform dielectric constant. In this case we employ an 'inverse method' in which we guess the potential energy profile in the channel and thus the forces acting on an ion in the channel. This potential profile replaces the electric forces in the Langevin equation 3.1. Although we calculate the electric forces using Poisson's equation in all cases other than those mentioned in chapter 9, this need not be so. A different method for calculating the forces such as using a PMF derived from MD or an 'inverse method' can easily be used within the BD formalism.

3.3 Solutions of Poisson's equation

As mentioned above, the electric forces in the BD simulations are usually found by solving Poisson's equation. These solutions are also informative in their own right, as they can be used to find the energy landscape encountered by ions in the channel. Analytic solutions to Poisson's equation exist for some special shapes of the dielectric boundary, however, none of these, with the exception of a toroidal boundary, resemble the shape of biological ion channels [115]. Thus one generally has to resort to numerical solutions. The two methods of numerical solution used in this study are described briefly below.

3.3.1 Boundary element method

In the boundary element method, introduced by Levitt [120] the dielectric boundary is represented by small segments of area s_i. The change in the electric field across the boundary is represented by a polarisation charge density, σ_i induced in each segment. By placing an infinitesimal Gaussian pillbox about the segments, the induced charge density can be related to the electric field:

$$(\mathbf{E}_1 - \mathbf{E}_2) \cdot \hat{\mathbf{n}} = \frac{\sigma}{\epsilon_0}. \tag{3.15}$$

The induced charge density can thus be calculated to be

$$\sigma = 2\epsilon_0 \frac{\epsilon_2 - \epsilon_1}{\epsilon_2 + \epsilon_1} \mathbf{E}_{ex} \cdot \hat{\mathbf{n}}, \tag{3.16}$$

where $\mathbf{E}_{ex}$ is the field created by all sources other than the charge on the segment of interest. This external field is calculated from the normal derivative of the external potential at $\mathbf{r}_i$ due to polarisation charges on other segments and other charges q_k:

$$\phi_{ex}(\mathbf{r}_i) = \frac{1}{4\pi\epsilon_0} \Big[\sum_{j \neq i} \frac{\sigma_j s_j}{\mid \mathbf{r}_i - \mathbf{r}_j \mid} + \sum_k \frac{q_k}{\epsilon_k \mid \mathbf{r}_i - \mathbf{r}_k \mid} \Big], \tag{3.17}$$

in which j is summed over all the segments and k over all the charges.

The solution to Poisson's equation can be found by starting with an initial polarisation charge density $\sigma = 0$ and iterating equations 3.16 and 3.17 until the results converge. As Poisson's equation has a unique solution inside a closed boundary, the converged potential must be the solution we are after.

This method has been further improved to account for the curvature of the segments by including a self interaction which arises from other points within the segment and is dependent on the geometry of the segment [92]. This procedure provides fast accurate solutions provided enough boundary sectors are employed. In this thesis I use a program developed by Matthew Hoyles for solving Poisson's equation using the boundary element approach. The main downsides to using this package is that it has been developed assuming cylindrical symmetry in the system which reduces the problem to 2 dimensions but limits its applicability to axially symmetric channel shapes. Also, the potential energy and forces acting on an ion approach infinity as it is brought close to a dielectric boundary. This makes it difficult to assign different dielectric constants inside the channel to the bulk water, which creates a dielectric interface through which ions will pass.

3.3.2 Finite difference method

An alternative way to find numerical solutions to Poisson's equation is to use a finite difference approach. In this technique a grid is placed over the system, and the continuous variables, ϕ and ϵ are approximated by discrete values at the grid points in the case of the potential, and at the mid point between grid points in the case of the dielectric constant.

Poisson's equation can then be discretised using a similar method to that used to commonly discretise the Poisson-Boltzmann equation [106]. (A description of the discretisation of the Poisson-Boltzmann equation can be found in chapter 5.)

Poisson's equation is integrated over the volume of a grid element v, of side lengths h_x, h_y, and h_z centered on a grid point giving:

$$\int_V \nabla \cdot [\epsilon(\mathbf{r}) \nabla \phi(\mathbf{r})]\, dV = -\int_V (\rho_{\rm ex}/\epsilon_0) dV. \tag{3.18}$$

Using Gauss' theorem, the left hand side of Eq. 3.18 is converted to a surface integral, and then the derivatives of ϕ are written as finite differences

$$\int_V \nabla \cdot [\epsilon(\mathbf{r}) \nabla \phi(\mathbf{r})]\, dV = \int_S \epsilon(\mathbf{r}) \nabla \phi(\mathbf{r}) \cdot d\mathbf{S} = \sum_{j=1}^{6} \epsilon_j \, \frac{\phi(\mathbf{r}_i + h_j \hat{\mathbf{j}}) - \phi(\mathbf{r}_i)}{h_j} \, \frac{V}{h_j} \,. \tag{3.19}$$

Here the sum is over the six surfaces of the rectangular box with $h_1 = h_4 = h_x$, $h_2 = h_5 = h_y$, $h_3 = h_6 = h_z$, and $\hat{\mathbf{j}} = \hat{\mathbf{x}}$, $\hat{\mathbf{y}}$, $\hat{\mathbf{z}}$ for $j = 1, 2, 3$, and $-\hat{\mathbf{x}}$, $-\hat{\mathbf{y}}$, $-\hat{\mathbf{z}}$ for $j = 4, 5, 6$. The term on the right hand side of Eq. 3.18 is evaluated similarly by replacing the integrands with their average values at the grid point

$$\int_V (\rho_{\rm ex}/\epsilon_0) dV = V \rho_{\rm ex}(\mathbf{r}_i)/\epsilon_0 = q(\mathbf{r}_i)/\epsilon_0. \tag{3.20}$$

Substituting Eqs. 3.19 and 3.20 back into Eq. 3.18, we obtain an expression for the potential at the i'th grid point in terms of the values of the potential, charge and dielectric constant at this grid point and its immediate neighbours

$$\phi_i = \frac{\sum_j \epsilon_j \phi_j / h_j^2 + q_i/(\epsilon_0 V)}{\sum_j \epsilon_j / h_j^2}. \tag{3.21}$$

Equation 3.21 is solved using an iterative relaxation scheme. The potential values at the edge of the grid are set using appropriate boundary conditions. Both Jacobian and Gauss-Seidal relaxation techniques are considered [160]. In Jacobian relaxation, an initial guess is made for the potential at all grid points, which are then used in Eq. 3.21 to recalculate the potential at each grid point. This process is iterated until the potential values at all grid points converge to a stable solution. In Gauss-Seidal relaxation, when available, updated values of the potential in neighbouring points are used in evaluating Eq. 3.21. This speeds up the convergence, hence it is the preferred method in scalar machines. In Jacobian relaxation, the number of iterations required for convergence is larger. However, because the program can be vectorized readily with this method, it may be more suitable for use in a vector machine.

For faster convergence, we also employ an over- or under-relaxation method [160]. After each iteration, the value of the potential at a grid point is updated according to $\phi = (1 - \omega)\phi_{\rm old} + \omega \phi_{\rm new}$, where ω is the relaxation parameter that varies in the range $[0, 2]$. The case of $\omega = 1$ obviously corresponds to no relaxation, $\omega < 1$ is called under-relaxation and $\omega > 1$ over-relaxation. Under-relaxation is useful in

situations where the potential diverges or oscillates around the actual value after each iteration. Barring these occurrences, over-relaxation is preferred as it leads to a faster convergence.

I devised and wrote a program in FORTRAN90 for finding these finite difference solutions. A simple extension of the program also allows it to solve the Poisson-Boltzmann equation as discussed in chapter 5 as the Poisson-Boltzmann equation reduces to Poisson's equation when the electrolyte concentration is set to zero.

We have subjected this finite difference code to several tests to check its convergence properties and accuracy. Here I describe one test of the program in the GA channel presented in chapter 9. In these tests the dielectric constant in the channel, $\varepsilon_c = 80$ is employed for ease of comparison with the boundary element method. Figure. 3.3 A shows the grid size dependence of the potential energy profile of a monovalent cation as it is moved along the central axis. As the grid size in the finite difference method is reduced from 0.8 Å to 0.4 Å, the results are seen to converge rapidly. In Fig. 3.3 B, we compare the potential energy profile obtained from the finite difference solutions (dashed line) with that obtained from the boundary element method (solid line). A general agreement is obtained between the two methods (differences are much smaller compared to the thermal energy of an ion), which establishes the validity of the finite difference solutions.

Further tests of this program and the accuracy of its solutions are discussed in section 5.4.1.

3.4 Parameters used in simulations

A list of parameters required for the BD simulations is given in table 3.2. A temperature of 298 K is used throughout.

Table 3.2: Parameters used for BD simulations.

	Ca	Na	K	Cl
Mass ($\times 10^{-26}$ kg)	6.6	3.8	6.5	5.9
Diffusion coefficient ($\times 10^{-9} m^2 s^{-1}$)	0.79	1.33	1.96	2.03
Ionic radii (Å)	0.99	0.95	1.33	1.81

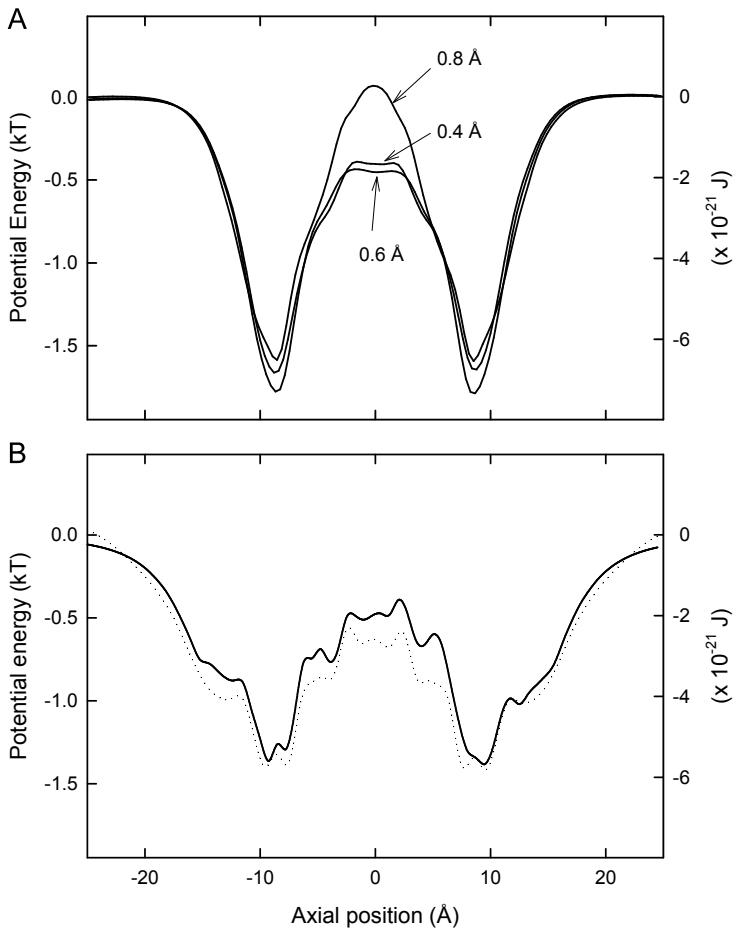

Figure 3.3: (A) Convergence of the potential energy profile with the grid size used in the finite difference solution of Poisson's equation. (B) Comparison of the energy profile obtained from the finite difference solution (dashed line) with that obtained from the boundary element method (solid line) for the axially symmetric boundary. $\epsilon_c = 80$, and $\epsilon_p = 2$ are used in both cases.

3.5 Testing the dynamic behaviour of ions

It is important to check that the dynamic behaviour of ions in the BD simulations faithfully reproduce what should be expected in reality. Such tests were carried out on this BD program by Siu Cheung Li and his colleagues [127]. They checked that the mean-square displacement, velocity distribution and the velocity autocorrelation function found from simulations were in accord with theoretical expectation, in simulations carried out without any dielectric boundaries.

An expression for the mean square displacement of ions can be obtained by integrating the Langevin equation 3.1 twice when there are no electric or short range forces to give:

$$\langle x^2 \rangle = \frac{2kT}{m\gamma} \left[t - \gamma^{-1}(1 - \exp(-\gamma t) \right] . \tag{3.22}$$

in which γ^{-1} is the relaxation time constant, which corresponds to the time required for a particle that is suddenly displaced to relax back to the original equilibrium position. For K^+ and Cl^-, γ^{-1} is about 30 fs. At times much greater than this relaxation time, the mean-square displacement should obey the relation

$$\langle x^2 \rangle = \frac{2kT}{m_i \gamma_i} t, \qquad for \qquad t >> \gamma_i^{-1}. \tag{3.23}$$

The velocity distribution should be Maxwellian with the form [166]

$$F(v)dv = 4\pi n [\frac{m_i}{2\pi kT}]^{1/2} \exp(-m_i v^2/2kT) v^2 dv \tag{3.24}$$

In which $F(v)dv$ is the mean number of ions per unit volume with a velocity between v and $v + dv$, and n is the number density of ions.

The velocity autocorrelation function is of the form [166]

$$\langle v(0)v(s) \rangle = \frac{kT}{m_i} \exp(-\gamma_i |s|), \tag{3.25}$$

showing that regardless of the initial velocity the following velocities of the particle will be correlated over a time interval of order $1/\gamma_i$, the relaxation time constant of the system.

In all cases the results of the BD simulations agreed very closely with these theoretical measures [127], yielding confidence that the simulations accurately characterise the motion of particles undergoing Brownian motion in a fluid.

3.6 Conclusions

In this chapter I have presented the details of the BD technique that is used to study ion permeation in biological channels in the remainder of this thesis. BD simulations are introduced as a means to examine the dynamic behaviour of ions, and efficient algorithms for carrying out such simulations have been presented and tested. These simulations provide a practical method for the calculation of ion channel conductance from a given structure. The solutions of Poisson's equation are used to calculate electrostatic forces acting on ions in the BD simulations and are also useful for determining the energy landscape encountered by an ion in the channel. Two methods for solving Poisson's equation in arbitrary geometries were presented: the boundary element technique and the finite difference technique.

Chapter 4

Boundary Conditions in Brownian Dynamics Simulations

4.1 Abstract

The boundary conditions used in our BD simulations are checked for validity. The simple stochastic boundary that we have been employing to maintain ion concentrations in our BD simulations is compared with the recently proposed grand canonical Monte Carlo method. Different methods of creating transmembrane potentials are also compared. The results confirm that the treatment of the reservoir boundaries is mostly irrelevant to the conductance properties of an ion channel as long as the reservoirs are large enough.

4.2 Introduction

In our BD simulations, we have concentrated on representing the forces acting on ions accurately because ultimately they are responsible for driving the ions across the channel. The calculated conductance values could be very sensitive to errors in electric fields and potentials. For example, conductance has an exponential dependence on the size of energy barriers in channels. In contrast we regard the reservoir boundaries conditions, required to maintain ion concentrations and create driving potentials, as a secondary issue. However, recently questions have arisen about the methods of implementing the boundaries in BD simulations of ion channels. The purpose of the reservoirs is to move the necessarily unphysical system boundaries away from the critical part of the simulation - the channel. Provided the reservoirs are large enough, a simple implementation of the boundaries should then suffice. We implement the boundaries by applying a uniform electric field across the channel and keeping a fixed number of ions in the reservoirs. In our simulations the

chosen concentration values in the reservoirs are maintained by recycling ions from one side to the other whenever there is an imbalance due to a conduction event. This process mimics the current flow through a closed circuit. There has, however, been a great deal of debate in the field about the appropriateness of such a simple stochastic boundary. Most recently, Im et al. [93] have proposed a more elaborate treatment of boundaries using a grand canonical Monte Carlo (GCMC) method. In this paper, they also question the validity of the simple method, but unfortunately do not support this criticism with any hard evidence, such as a comparison of the two methods.

The source of this preoccupation with boundaries in BD appears to arise from the association with MD simulations where the correct treatment is known to be crucial [180]. However, the nature of the electrostatic forces in BD is very different from those in MD – firstly an ion's electric field (or potential) in water is reduced by a factor of 80 due to the dielectric shielding, and secondly, shielding due to the counter ions completely annuls the remaining field strength beyond 4 Debye lengths. For physiological concentrations (150 mM) this length scale is about 30 Å. With this provision on the reservoir dimensions, we believe that a simple boundary method should be adequate for the purpose of calculating the conductance of a channel from BD.

In view of the debate outlined above, however, it seems prudent to perform additional tests on the validity of our simple stochastic boundaries. The work of Im et al. [93] provides us with an opportunity to do so. We have modified our computer programs to deal with the more sophisticated boundaries, and have carried out BD simulations of model channels using the two different methods. We have also experimented with different methods of representing the transmembrane potential. The purpose of these tests is to determine whether or not the alternative ways of maintaining ion concentrations or applying a membrane potential make any difference to the conductance of the model channel, or to the concentrations of ions near the mouths of the channel. If not, we feel safe in concluding that the reservoirs are adequately insulating the channel from the boundary conditions, and that our simulations accurately reflect the physical processes taking place in ion channels.

4.3 Ion concentrations

We apply stochastic boundaries to maintain the specified concentrations in the reservoirs. Here, we compare the use of a simple boundary that maintains a fixed number of ions in the system with a more sophisticated GCMC boundary that allows fluctuations in the number of ions.

4.3.1 Simple stochastic boundary

The simple stochastic boundary is designed to maintain the desired ion concentrations in the reservoirs by keeping the number of each ion species in the system fixed. When an ion crosses the channel, say from left to right, an ion of the same species is transplanted from the right reservoir to the left. For this purpose, the furthermost ion on the right-hand side is chosen, and it is placed at the far left-hand side of the left reservoir, making sure that it does not overlap with another ion. The stochastic boundary trigger points, located at either pore entrance, are checked at each time step of the simulation. In this way the total number of each type of ion in each reservoir remains constant throughout the simulation. We emphasize that the exact placement of the trigger points is not crucial as the change in potential inside the channel due to moving an ion from one reservoir to another is only a few mV (as found by explicitly measuring the potential in the channel just before and just after the ion is moved). This is much smaller than the potentials from most other sources e.g., other ions, induced charges on the boundary, applied potential and fixed charges. The current is identical (within statistical errors) wherever the trigger point is placed in the channel.

4.3.2 Grand Canonical Monte Carlo

In an electrolyte solution, the total number of ions within a given region varies with time as ions wander in and out. To allow such fluctuations in the number of ions in the reservoirs, we implement as an alternative a grand canonical Monte Carlo (GCMC) stochastic boundary as developed by Im et al. [93]. We use essentially the same procedure but include a brief description of the method for completeness.

Fluctuations in the number of particles in an open system are described using the grand canonical ensemble with the grand partition function

$$\mathcal{Z} = \prod_{\alpha} \sum_{n_\alpha \geq 0} \frac{\bar{n}_\alpha^{n_\alpha}}{n_\alpha!} \exp[n_\alpha \bar{\mu}_\alpha / kT] \int dV \exp[-W(\{n_\alpha\})/kT], \tag{4.1}$$

where $\bar{n}_\alpha$ and $\bar{\mu}_\alpha$ refer to the expected number and chemical potential of ions of species α, $W(\{n_\alpha\})$ is the free energy of the configuration $\{n_\alpha\}$, and the volume integral is carried over all the ion coordinates in the system. The probability for a particular configuration $\mathcal{P}(\{n_\alpha\})$ can be read off from Eq. 4.1 by removing the sum and integral, and dividing by $\mathcal{Z}$. To achieve a variable number of ions in a finite BD simulation, ions must be created or destroyed from within the reservoirs. Using the principle of detailed balance and $\mathcal{P}(\{n_\alpha\})$, one can derive the following expressions for the transition probabilities corresponding to the creation and destruction of ions of species α [93]

$$\mathcal{P}_{\rm cre}(n_\alpha \to n_\alpha + 1) = \frac{(\bar{n}_\alpha/n_\alpha + 1)\exp[-(\Delta W - \bar{\mu}_\alpha)/kT]}{1 + (\bar{n}_\alpha/n_\alpha + 1)\exp[-(\Delta W - \bar{\mu}_\alpha)/kT]}, \tag{4.2}$$

$$\mathcal{P}_{\rm des}(n_\alpha \to n_\alpha - 1) = \frac{1}{1 + (\bar{n}_\alpha/n_\alpha)\exp[(\Delta W + \bar{\mu}_\alpha)/kT]}. \tag{4.3}$$

Here ΔW is the free energy difference between the final and initial configurations.

The probabilities in Eqs. 4.2–4.3 are employed in Monte Carlo steps to create or destroy ions in the reservoirs as follows. First a random number between 0 and 1 is picked and a creation is attempted if it is less than 0.5 and a destruction if it is greater (equal probability is required to preserve microscopic reversibility). In case of creation, an ion of species α is introduced in a random location and the probability in Eq. 4.2 is calculated. If it is greater than a newly picked random number, the creation is accepted, otherwise the ion is removed. Similarly in the case of destruction, one of the ions of species α is randomly chosen and the probability of its removal from the system is calculated using Eq. 4.3. If a random number is below this value then the ion is removed from the system, otherwise it remains.

Such particle creation and destruction is unphysical and is meant to represent the movement of ions into and out of the reservoirs. So, we must make sure that this does not affect the dynamics of ions near the ion channel by limiting such events to 'buffer regions', sufficiently distant from the channel. Fig. 4.1 depicts the BD system used with the GCMC boundary conditions. An ion channel (cylindrical in this case, but any shape is possible) is connected to reservoirs at each end. Cylindrical reservoirs are used here to be consistent with our previous BD simulations, although again any geometry is possible. Ions move throughout this channel - reservoir system according to the BD algorithm described previously. The outside edge of the reservoirs form the buffer zones in which the GCMC creation/destruction routine takes place. In our studies we used a buffer thickness of 10 Å.

The chemical potential is calculated from the excess solvation energy, $\Delta\mu_\alpha$, of each ion type for the specified average concentration in the relevant buffer. In a

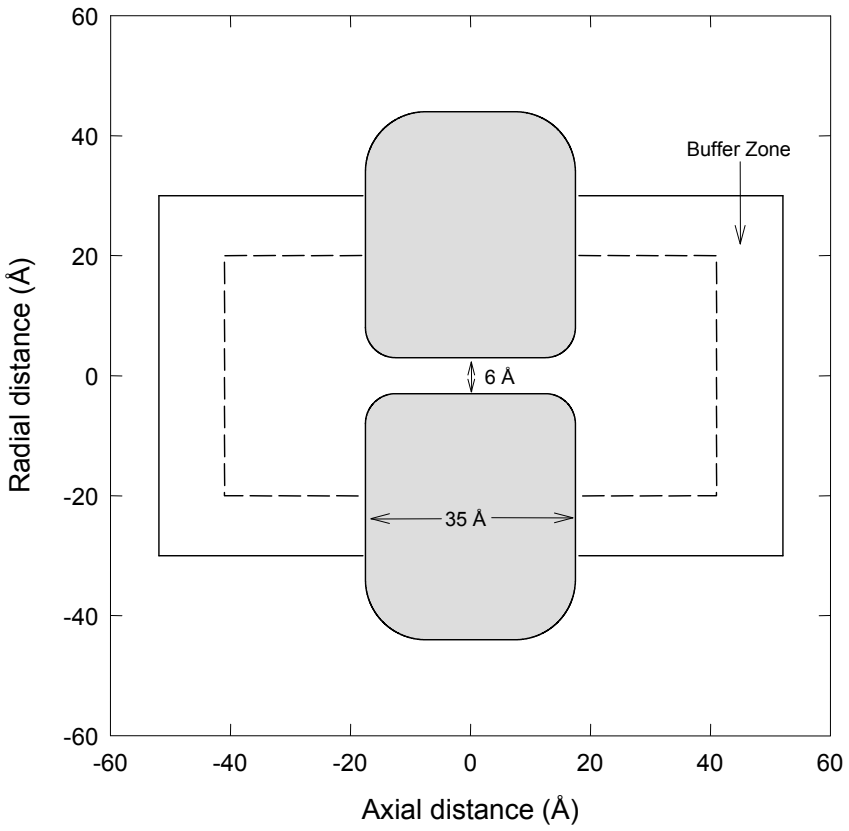

Figure 4.1: Diagram of the channel and reservoir system used in BD/GCMC simulations. The protein and membrane (shaded region) forms a 3 dimensional channel when rotated about the central axis by 180 degrees. In this case the channel is cylindrical although it may have any shape. Attached to each end of the channel are cylindrical reservoirs. During BD simulations, ions move within this channel and reservoir system. When the GCMC procedure is used to maintain ion concentrations in the reservoirs, ions are created and destroyed in the buffer zones around the outside edge of the reservoir indicated by the dashed lines. The dimensions shown are those for the cylindrical channel discussed in the text.

similar fashion to Im et al., we employ the hypernetted chain (HNC) approximation [78]. The method used follows closely that of Rossky and Friedman [170] and incorporates the short-range and hydration interactions described in chapter 3, instead of the Lennard-Jones potential used by Im et al. that ignores the contributions of solvent molecules. (Note that the solvation energies could be calculated in other potentially more accurate ways, such as direct Grand Canonical simulation.) Once the excess solvation energies are determined, they are adjusted to account for any driving potentials in the system as follows:

$$\bar{\mu}_{\alpha\beta} = \Delta\mu_\alpha + q_\alpha V_\beta, \tag{4.4}$$

where q_α is the charge on ion type α and V_β is the potential in buffer β.

To allow the GCMC boundary procedure to accurately enforce the boundary conditions, many GCMC steps (a creation or destruction of each type of ion in each reservoir) should be performed for every BD timestep. In this study, 10 GCMC steps are performed for every BD step. The concentration in the reservoirs varies during a GCMC-BD simulation as ions are created and destroyed. The average concentration, though, is found to be always slightly lower than the specified input value.

4.3.3 Comparing the techniques

Below we describe a number of tests carried out to compare the simple and GCMC stochastic boundaries.

Equilibrium ion distribution

We first demonstrate that the BD simulations with either the simple or GCMC procedure maintains the desired equilibrium conditions by examining the relative distribution of ions in bulk solution. For this purpose, we set all dielectric constants in the system equal to 80 so that there are no dielectric boundaries in the system, and ignore ions that are within 8 Å of the reservoir boundaries to avoid edge effects in sampling. In Fig. 4.2, we show the radial distribution functions for K–Cl (A) and K–K (B) ion pairs, obtained from BD simulations of a 500 mM KCl solution for 10^6 timesteps (0.1 μs), in one case with the GCMC routine in place (triangles) and in another without (filled circles). When testing the GCMC procedure, the buffer regions are enlarged to occupy the entire reservoirs (so that ions can be created or destroyed anywhere) as the test is for a bulk solution. The curves agree closely and depict the peaks due to the contact and solvent separated minima in the potential

of mean force. They also closely follow the results obtained from the HNC equations indicated by the solid line. This agreement indicates that the equilibrium structure of the electrolyte is accurately reproduced in BD simulations with or without the GCMC routine.

Cylindrical channels

As we are interested in comparing different treatments of the boundary in BD simulations, it matters little which channel model we use. Thus, for simplicity, we first make our comparisons in a simple cylindrical channel, before demonstrating the robustness of these results in a more complex potassium channel model.

The cylindrical channel model is formed by rotating the curve shown in Fig. 4.1 about the central axis. The channel radius is set to 3 Å and its entire length to 35 Å. Firstly we set the dielectric constant of the protein to 80, equal to that of the electrolyte in the channel and reservoirs. In this case, as there is no dielectric boundary, no reaction field can be induced. Although not realistic, this provides the simplest case in which to test the stochastic boundary methods, and it also helps in showing the importance of the reaction field when these results are compared to those with a realistic choice of dielectric constant. The overall concentration in the simple boundary simulations is set to be the same as the average concentration during the GCMC simulations. For compatibility with later simulations, all studies in the cylindrical channels are carried out using NaCl solution.

Ion distributions and fluctuations

Im et al. [93] show that when the GCMC method is used, the number of ions in the reservoirs fluctuates considerably during a BD simulation, and therefore, they claim "BD with a fixed number ions cannot describe the permeation process in a satisfactory manner". Such a connection between channel current and variations in the ion numbers is far from being obvious. For one thing, fluctuations in concentration in any volume in the vicinity of the channel occur at a much faster rate than conduction of ions, and hence a direct correlation between the two quantities is unlikely. Secondly, even if such fluctuations did have an effect on channel current, these will be at the level of noise in the stochastic BD simulations, and will be lost when the average current is determined (which should depend only on the average concentration). Finally, fixing the total number of ions in the reservoirs does not mean that the number of ions near the channel mouth does not fluctuate where such effects, if important, should be modeled correctly.

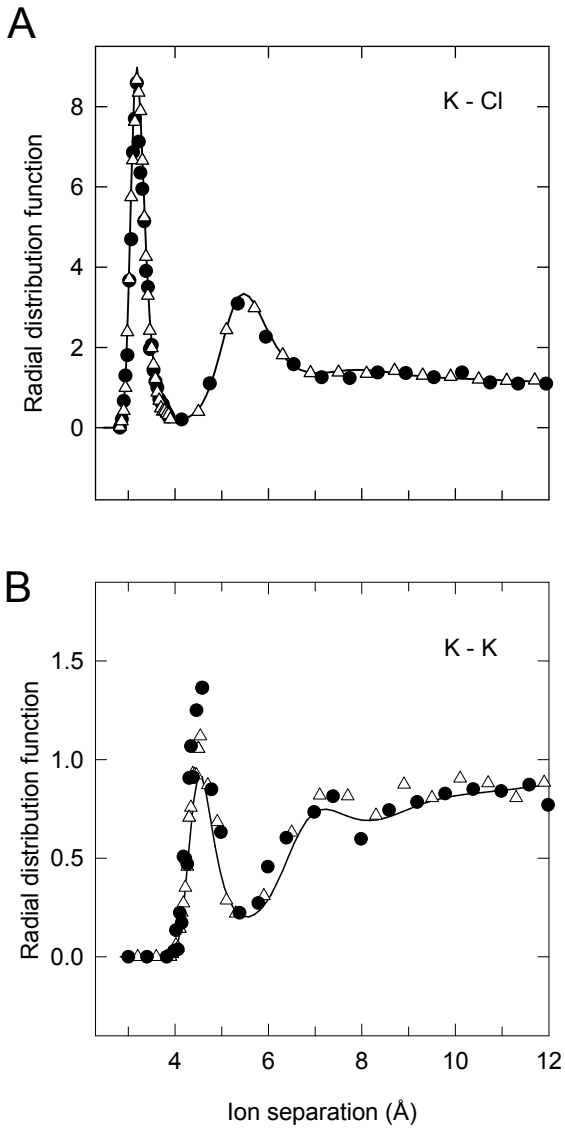

Figure 4.2: Radial distribution function for (A) $K^+ - Cl^-$ and (B) $K^+ - K^+$ ion pairs moving in the reservoirs as found from BD with the GCMC routine in place throughout the reservoirs (triangles), BD simulations without the GCMC routine (filled circles), and the HNC equations (solid line). The BD plots were calculated by sampling from simulations using a cylindrical channel with no dielectric boundaries and ignoring ions within 8 Å of the reservoir boundaries.

In Figs. 4.3 and 4.4, we demonstrate this third point by comparing the predictions of the simple boundary (A) with the GCMC method (B) for the distribution of ions near the channel. In each figure, the probability of finding a given number of ions in a fraction of the reservoir volume around the channel mouth (denoted by x) is plotted. In Fig. 4.3, $x = 0.5$ corresponding to all the volume outside the buffer zone in the GCMC method as indicated by the dashed line in Fig. 4.1. In Fig. 4.4, $x = 0.25$, that is, half of the volume used in Fig. 4.3 (around the mouth of the channel). Given N particles in a box, the probability of finding n of them occupying fraction x of the volume is given by the binomial distribution

$$\mathcal{P}(n, x) = \frac{N!}{n!(N-n)!} x^n (1-x)^{N-n}, \tag{4.5}$$

which is indicated by the dashed line in Figs. 4.3 and 4.4. As expected, the probability distributions when using the simple boundary method show that the number of ions in these regions varies significantly during a simulation, the distributions closely following the binomial one in both Figs. 4.3 A and 4.4 A. Even though the total number of ions in the reservoir is constant during the simulation, the number of ions near the channel is not fixed. The GCMC distribution is slightly more spread out in Fig. 4.3 B, where the effect of the number fluctuations in the buffer zone is maximal. But, as shown in Fig. 4.4 B, as soon as one moves away from the buffer boundary, the GCMC distribution also reverts to the binomial distribution. Thus, away from the boundary regions, ion numbers fluctuate according to the binomial distribution regardless of whether one fixes the total number of ions in the system or allows it to fluctuate according the GCMC method.

We emphasize that the boundary conditions imposed in either method contains unphysical elements and one has to make sure that these regions are well separated from the channel. The rule of thumb is to put the boundaries at about 4 Debye lengths away from the channel mouths to allow for near complete ionic screening. Once the boundaries are at such distances, their effects are totally washed out in the vicinity of the channel so that all methods should lead to similar fluctuations in ion numbers there.

Channel currents

Since the distribution of ions and the fluctuations in ion numbers are very similar near the channel mouth with both the simple and GCMC methods, they should also lead to similar conductance properties. To demonstrate that the choice of stochastic boundary makes no difference on the channel conductance, we next compare the

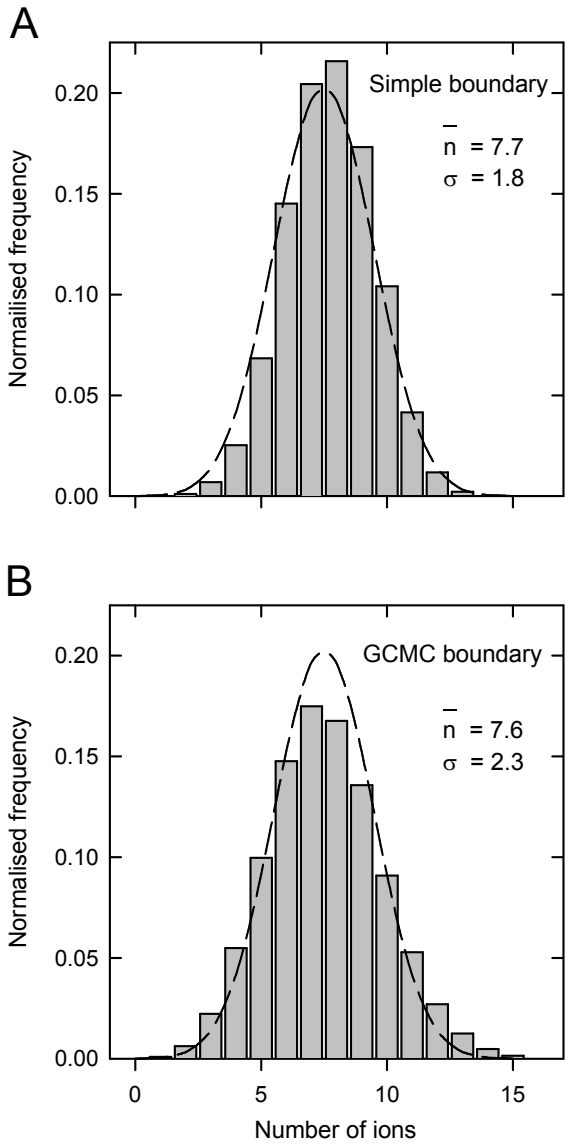

Figure 4.3: Fluctuations in cation numbers in a region around the channel mouth comprising 50% of the volume of one reservoir when (A) the simple stochastic boundary is used and (B) when the GCMC procedure is used. A dielectric constant of 80 is used everywhere. The number of ions in the region is sampled every 100 BD steps and the relative frequency is calculated during a 0.2 μs simulation period. The average concentration in the simulation is $\approx$ 280 mM corresponding to 15 ions of each type in each reservoir. The average number of ions in the region and the standard deviations are indicated by $\bar{n}$ and σ respectively. The dashed line shows the corresponding binomial distribution from Eq. 4.5 with $N = 15$ and $x = 0.5$.

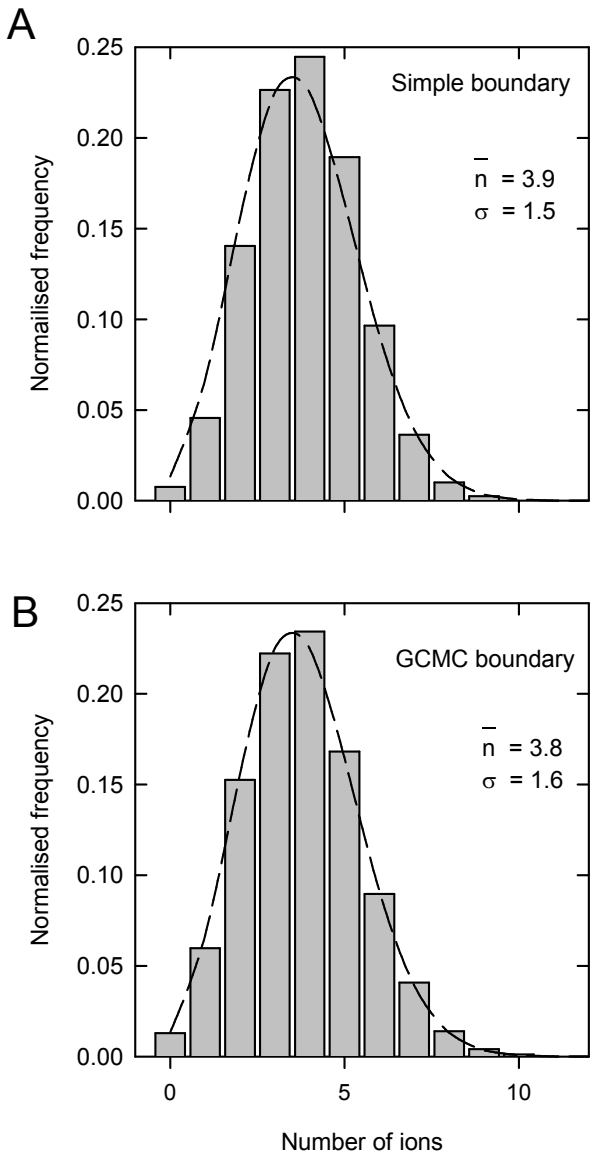

Figure 4.4: Fluctuations in cation numbers as in Fig. 3 except in a smaller region near the channel mouth containing 25% of the entire reservoir volume using (A) the simple boundary and (B) the GCMC boundary.

current passing through the cylindrical channel during BD simulations with the simple and GCMC boundaries.

In Fig. 4.5 we plot the current-voltage curve in a 3 Å radius cylindrical channel found from BD simulations employing either the simple stochastic boundary (filled circles) or the GCMC boundary (triangles). For this plot $\varepsilon = 80$ is used everywhere so that there are no dielectric boundaries and thus no ion self energies or image charges. This situation is the same as that used in the control study of chapter 6 and is similar to the simulations of Im et al. [93], in which reaction fields are ignored. As there are no fixed charges or other sources which can bias the potential, both cations and anions pass through the channel in opposite directions. The current carried by the cations and anions are plotted separately in the figure, and there is a greater anion current due to chloride having a larger diffusion coefficient than sodium. Rather than being Ohmic, the current-voltage relationship is notably non-linear. This is most likely a consequence of the fact that at larger voltages the ion transit time through the channel is shorter. As the channel is too narrow for ions to pass each other, yet cations and anions are trying to permeate through the channel in opposite directions, the shorter transit time would aid conduction by clearing the channel ahead of the next conduction event. It is clear from this plot that the currents calculated using either the simple or the GCMC boundaries are essentially the same, the two agree to within the statistical uncertainty of the data. Thus, the channel current does not depend on which boundary technique is used.

If we change the dielectric constant of the protein to the realistic value of 2, then a dielectric boundary is formed and reaction field effects come into play. When an ion approaches a protein boundary with a lower dielectric constant it induces surface charges which repel the ion away from this interface. Indeed as discussed in chapter 5 and 6, these reaction fields can be the dominant electrostatic effect in ion channels and should not be ignored. In this case, the repulsive forces prevent ions from entering the channel, and so the current is reduced to zero. Not surprisingly, the choice of stochastic reservoir boundary has no effect – no ions cross the channel with either technique. The most important physical effects for simulating the channel are those between the ion and the channel itself, not those due to the reservoir boundaries or ions far from the channel.

Next we create a conducting cylindrical channel with dielectric boundaries by including fixed charges in the channel walls. A ring of 8 monopoles are placed at each end of the channel (at $z = \pm 12.5$ Å), each carrying a charge of $-0.09e$. These charges help cations overcome the image forces and enter the channel, while preventing anions from entering, creating a cation selective channel. The cation

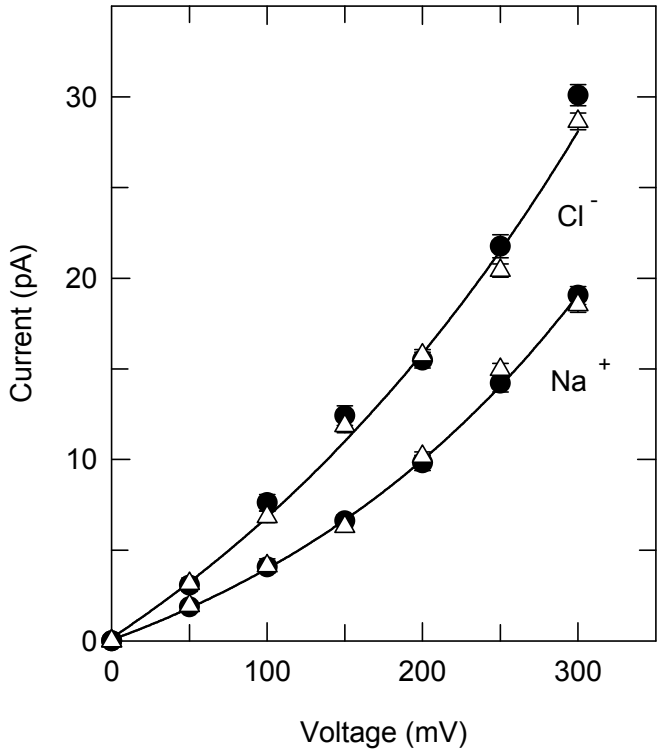

Figure 4.5: Comparison of the current-voltage curves in a cylindrical channel using the simple stochastic boundary (filled circles) or the GCMC boundary (triangles). A 3 Å radius channel is used with $\varepsilon = 80$ everywhere and 265 mM NaCl solution. Ions are driven across the channel by an electric field of 2×10^7 V/m corresponding to a potential drop of approximately 200 mV across the system. Sodium and chloride currents are plotted separately and each set of results is fitted by the solid line.

current passing through the channel is plotted against the driving potential using both the simple and GCMC boundaries in Fig. 4.6. As in the case of Fig. 4.5, the currents found from simulations employing the GCMC boundary are almost identical to those found using the simple boundary. Note that the non-linearity in this case results from the residual barriers in the potential energy profile.

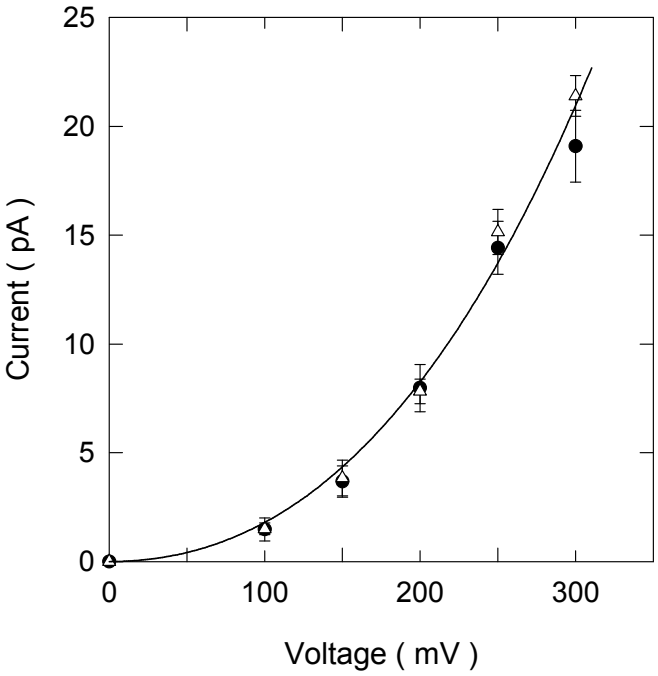

Figure 4.6: Comparison of the current-voltage curves in a cylindrical channel with fixed charges using the simple stochastic boundary (filled circles) or the GCMC boundary (triangles). A 3 Å radius channel is used with 8 monopoles placed at each end as described in the text. A dielectric constant of 2 is assigned to the protein and 80 everywhere else.

More complex channels

We have seen that the choice of stochastic boundary used to maintain concentrations in the simulation reservoirs has no effect on the currents flowing through simplified cylindrical channels. As a final test, we check to make sure that this conclusion is valid in a more complex and realistic multi-ion channel that we have modeled previously, as well as checking it at a range of concentrations. To do this we

use the KcsA potassium channel model that has been described in an earlier paper [4]. An open state KcsA channel shape has been constructed using MD from the known closed state crystal structure [3]. A dielectric interface is then constructed by tracing out a boundary using a water molecule and assigning the dielectric constant a value of 2 in the protein and 60 in the channel. The final shape, and the pore forming peptide helices are shown at the top of Fig. 4.7. Charges are assigned at positions corresponding to the protein atoms using the extended CHARMM-19 parameter set. More details can be found in the above references.

In Fig. 4.7 we plot the current-concentration curve in the KcsA potassium channel surrounded by KCl solution under a driving potential of 200 mV. The results of our simulations show a saturation of channel current with increasing conductance, and are fitted by a Michaelis – Menton curve to indicate this. The data from simulations carried out using the simple stochastic boundary, indicated by the filled circles, are those published elsewhere [4]. When the GCMC boundary is employed, the new data shown by the triangles reproduces this curve well at all concentrations studied. Thus, once again the choice of stochastic boundary has little effect on channel currents, even over a large range of concentrations.

4.4 Potentials

A second issue to do with reservoir boundaries is how to apply a potential difference that drives ions through the channel. There are at least three possibilities that have been considered in the past, and there has been debate as to which is most appropriate.

4.4.1 Techniques for applying a membrane potential

In all our recent BD simulations and those in the remainder of this thesis, we create a transmembrane potential by simply applying a uniform electric field through the system. This applied field is included in the solution of Poisson's equation with the dielectric boundaries so that it induces surface charges of its own. The resulting potential is far from being linear across the system – it drops much more rapidly through the channel than in the reservoirs.

Another approach is to fix the potential at the desired values along the far ends of the reservoirs. This creates an equipotential surface at each end, which can be set independently to create a potential drop across the channel. This is similar to placing electrodes at the far end of each reservoir, though in an actual experiment, the electrodes would be much farther from the channel than in a typical simulation.

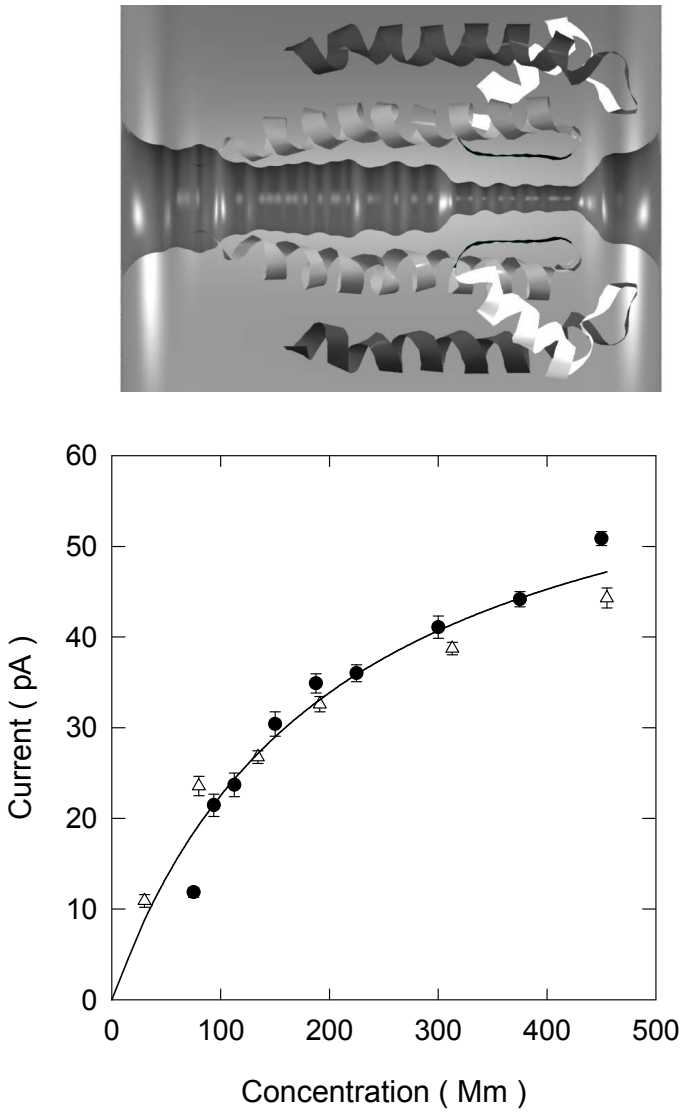

Figure 4.7: Conductance concentration curve in a model KcsA potassium channel found from BD simulations employing the simple stochastic boundary (filled circles) and GCMC boundary (triangles). An electric field of 2×10^7 V/m is used to drive the ions across the channel. The results represent the averages of a 1.5–2.0 μs simulations. The inset shows the shape of the channel and indicates the major peptide helices.

To use such a scheme, we solve Poisson's equation with the specified boundary potentials using the finite difference method. The results due to the transmembrane potential, fixed charges in the protein wall, and charges induced by these are stored in the three dimensional lookup table.

A final method, which has been introduced by Im et al. [93], is to make the fixed potential more realistic by moving the fixed potential surfaces far away from the simulation system. The electrolyte solution in between the reservoir and the fixed potential surface is treated as a continuum by solving the PB equation in this region. The potential in the system is thus calculated using a modified Poisson-Boltzmann equation, which reduces to Poisson's equation in the BD simulation system where ions are treated explicitly. We implement this procedure by using the finite difference method to solve the modified Poisson-Boltzmann equation when constructing the three dimensional lookup table.

4.4.2 Comparing the techniques

The membrane potential which drives ions through an ion channel arises from ion clouds on each side of the membrane or a distant electrode. Thus setting the potential at the back edges of the reservoirs in our simulations is not entirely realistic as it fails to allow for variations at these positions caused by the movement of mobile ions. The use of the modified Poisson-Boltzmann equation avoids some of these difficulties by taking into account the effects of mobile ions when determining the potentials at each end of the BD simulation. The uniform field approach does not include the cause of the transmembrane potential, rather just takes it as given, a bias which could be created by ionic clouds or polarisation external to the BD system.

But, rather than entering a debate as to which is the most realistic way to create the transmembrane potential, we simply demonstrate here that it again makes no difference which method is used, by directly comparing the three. In Fig. 4.8 we plot the average potential along the central axis of the channel during a BD simulation using the constant field, fixed potential, and modified-PB approaches. In all cases, the majority of the potential drop occurs in the channel with the potential remaining relatively flat in the reservoirs. When the fixed potential or modified PB methods are used, a slightly greater charge separation occurs in the reservoirs due to ions being attracted to the potential generating electrodes. This is especially true near the outside edge of the reservoir, and leads to the drop in the magnitude of the potential there. The boundary effects created in these techniques are, however, quickly screened out by the mobile ions in the system. It is worth noting that in the

modified PB method we solve the modified PB equation only once before doing the BD simulation. Thus, the electrolyte outside of the reservoirs does not react to the presence of the explicit ions in the BD simulation. If the modified PB equation was solved at each BD timestep, it is possible that the electrolyte would act on average to cancel some of the charge separation seen in the BD simulation. This, of course, would only act to bring the potential closer to the constant field case, and would not alter our conclusion. Inside the channel, the potentials are almost identical in all cases, and good agreement is maintained until around 20 Å from the channel mouth. Thus, no matter which technique is used to create the transmembrane potential, the average potential seen by ions in or near the channel is the same. As it is the potentials in and around the channel which drive ions through it, the choice of technique for creating a transmembrane potential is, therefore, irrelevant when it comes to calculating the current passing through the channel in a BD simulation.

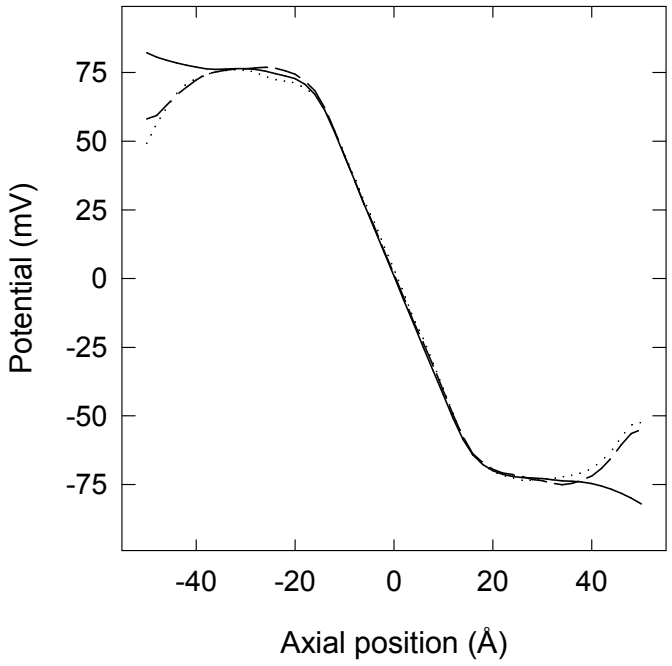

Figure 4.8: Average potential profiles along the channel axis during a BD simulation when the transmembrane potential is set via the uniform field (solid line), fixed potential (dashed line) and modified PB (dotted line) methods. The cylindrical channel model is used, with a dielectric boundary but no fixed charges. The potential is plotted between the two ends of the reservoirs. In all cases the potential at each point is averaged over a 0.1 μs BD simulation.

4.5 Conclusions

We have presented a number of results which demonstrate that it does not matter whether the simple stochastic or the GCMC stochastic boundary is used to maintain ion concentrations in the reservoirs during BD simulations. In both cases, the edge of the reservoirs or the GCMC buffer zones must be at a reasonable distance from the channel, ideally 3–4 Debye lengths, such that any unphysical edge effects or particle creation/destruction are screened from the channel. When these precautions are followed, the number of ions near the channel fluctuates according to the binomial distribution and the current passing through the channel is the same with either method. Similarly it does not matter how the transmembrane potential is set. Provided the reservoirs are large enough, mobile ions redistribute themselves, causing the potential drop across the channel to be the same in all cases.

The simple boundary method is conceptually simpler, involves less calculations, and is considerably faster. For a typical simulation presented here with a 300 mM solution, a 1 μs simulation takes around 45 hours of CPU time to complete using the simple boundary and 115 hours with the GCMC boundary method. The greater time is due to the potential energy of the system having to be recalculated for each GCMC creation or destruction step. The simple boundary also allows one to specify beforehand the exact concentration that will be used in a given simulation. Thus for BD simulations of solutions at the usual physiological concentrations, the added complexity of the GCMC method provides no perceptible advantages compared to the simple boundary method.

One situation where the GCMC boundary does have an advantage over the simple boundary method is the simulation of solutions at very low concentrations. For example, to simulate an ion species in the μM range using the simple boundaries would require reservoirs thousands of times larger than those described here in order to contain at least one ion of this type. This is not only cumbersome, but also makes including a second ion species at a higher concentration (say in the mM range) problematic – the reservoir would have to contain thousands of ions of the second type, making it too slow to simulate. The GCMC boundary can reach such low concentrations using a small reservoir as there need not always be an ion of each type in the simulation – the low concentration species is simply created in the buffer regions at a proportionally lower rate. Of course, the simulation may still take a long time if one waits for the low concentration ion to enter the channel. Also, the GCMC method may be useful if the channel protein carries a net charge. The GCMC technique allows for the electrolyte to be in equilibrium without having the same number of cations and anions in the system.

Of course, it is possible to treat the boundaries in other ways not discussed here. For example, a periodic boundary could be used to maintain ion concentrations and potentials, such as that typically used in Non Equilibrium Molecular Dynamics simulations [50, 198]. These techniques have their own advantages, such as avoiding any explicit potential boundary, and disadvantages such as only being able to model symmetric solutions at each end of the channel. But, from what we have seen here, it should be apparent that the choice of boundary does not matter, provided some common sense precautions are observed.

Although the GCMC boundary opens up some new avenues for simulation at low concentrations, it is no more accurate method than the simple stochastic boundary that we have been employing in our BD simulations. The results presented here support the expectation that as long as the reservoirs are large enough so that the edge effects are completely screened out near the channel, one need not worry about the exact implementation of the system boundaries. Instead, it is more important to describe the ion dynamics in and near the the channel accurately, including the effects of image forces.

Chapter 5

Testing Poisson - Boltzmann Theory

5.1 Abstract

We test the validity of the mean field approximation in Poisson-Boltzmann theory by comparing its predictions with those of Brownian dynamics simulations. For this purpose we use spherical and cylindrical boundaries as well as a catenary shape similar to that of the acetylcholine receptor channel. The interior region filled with electrolyte is assumed to have a high dielectric constant and the exterior region representing protein a low one. Comparisons of the force on a test ion obtained with the two methods show that the shielding effect due to counter ions is overestimated in Poisson-Boltzmann theory when the ion is within a Debye length of the boundary. As the ion gets closer to the boundary, the discrepancy in force grows rapidly. The implication for membrane channels, whose radii are typically smaller than the Debye length, is that Poisson-Boltzmann theory cannot be used to obtain reliable estimates of the electrostatic potential energy and force on an ion in the channel environment.

5.2 Introduction

The use of continuum theories of electrolytes to model biological processes has flourished in recent years. But, as noted in section 2.4.2, the use of continuum theories inside the confined regions of ion channels is questionable. One reason for the popularity of the continuum theories that deal with concentrations of ions rather than individual ions, used to be that the alternative methods were computationally intractable. As noted earlier, this is still true for molecular dynamics simulations. To study ion permeation across a membrane channel using molecular

dynamics, one needs supercomputers that are several orders of magnitude faster than currently available. In comparison, the situation with Brownian dynamics, where only the motion of ions are traced, is much better. As stressed in a recent series of commentaries on ion permeation [125, 137, 143, 150], the time is ripe for a realistic assessment of continuum theories as models of ion channels, and if they fail the tests, to move on to more accurate theories.

In this and the following chapter, I aim to provide such a test for two prominent continuum theories; Poisson-Boltzmann (PB) in the present chapter and the Poisson-Nernst-Planck in the next one. PB theory has become an important tool in studies of proteins and membranes, leading to many insights on the key role played by electrostatic interactions [90]. The availability of efficient computer programs for solving the PB equation [52, 187] has increased its use tremendously during the last decade. In ion channels, the PB equation was initially used to include the effects of ionic atmosphere on the potential energy profile of an ion in schematic channel models [29, 101, 121]. More recently, the PB calculation of potential energy profiles has been extended to realistic channel structures in numerous articles [1, 37, 54, 163, 171, 181, 182, 189, 211]. In PB calculations, ionic shielding greatly reduces the potential energy of an ion in a channel compared to that of a single ion calculated from Poisson's equation. The PB equation is a mean field theory. That is, it assumes that the properties of the system can be accurately described by time averaged rather than time dependent quantities. To assess the reliability of the PB calculations, it is important to check that this shielding effect is not an artifact of the mean field assumption.

The total electrostatic force acting on an ion inside and near the vicinity of a channel determines its dynamic behaviour. Therefore, it is the most important quantity to check in judging the accuracy of the PB theory. Here we test the validity of the mean field approximation in the PB theory by comparing its predictions for the force on a test ion as well as potential energy and concentration profiles with those obtained from BD simulations. BD is eminently suitable for this task because the motion of all the ions in the system are traced individually according to the Langevin equation. As both the BD and PB approaches treat the protein as and water as rigid dielectric environments, differences between their results can be isolated to the treatment of the electrolyte. Furthermore, the long-time average of physical quantities in BD should reflect the actual physical behaviour of the system more accurately than the continuum methods. The main point of this article is demonstrated using a spherical geometry which serves as a generic example of an electrolyte confined in a small volume. Cylindrical channels with varying radius

provide testing grounds for schematic channel models, while a catenary shape similar to that of the acetylcholine receptor channel is used for tests in a more realistic geometry.

5.3 Poisson-Boltzmann theory

Poisson-Boltzmann theory provides a classical electrostatic description of a system in which fixed external charges, represented by a density ρ_{ex}, are surrounded by mobile ions in a dielectric medium. The main assumption of the theory is that at equilibrium, the distribution of mobile ions in the system can be approximated by a continuous charge density, ρ_{el}, given by the Boltzmann factor

$$\rho_{\text{el}}(\mathbf{r}) = \sum_{\nu} z_\nu e n_{0\nu} \exp\left[-z_\nu e\phi(\mathbf{r})/kT\right], \tag{5.1}$$

where $n_{0\nu}$ is the bulk (or reference) number density of ions of species ν and $z_\nu e$ is their charge. Here n_0 (in SI units) is related to concentration c_0 (in moles/liter) by $n_0 = 1000 N_A c_0$ where N_A is Avogadro's number. The average electric potential $\phi(\mathbf{r})$ in Eq. 5.1 is obtained from the solution of Poisson's equation where the charge density is broken into components from fixed charges, ρ_{ex} and from the electrolyte, ρ_{el}.

$$\epsilon_0 \nabla \cdot [\epsilon(\mathbf{r})\nabla\phi(\mathbf{r})] = -\rho_{\text{el}} - \rho_{\text{ex}}. \tag{5.2}$$

Combining Eqs. 5.1 and 5.2 for a 1:1 electrolyte, which is our main interest here, we obtain the following PB equation

$$\epsilon_0 \nabla \cdot [\epsilon(\mathbf{r})\nabla\phi(\mathbf{r})] = 2en_0 \sinh\left[e\phi(\mathbf{r})/kT\right] - \rho_{\text{ex}}. \tag{5.3}$$

Apart from a few special cases this equation cannot be solved analytically. Therefore, a linearized form proposed by Debye and Hückel [53] has been commonly used in practical applications. Expanding the sinh term in Eq. 5.3 and keeping only the leading term in ϕ yields the linear PB equation for a bulk electrolyte with no fixed charges ($\rho_{\text{ex}} = 0$)

$$\nabla^2\phi = \kappa^2\phi, \tag{5.4}$$

where $1/\kappa$ is the Debye screening length given by

$$\frac{1}{\kappa} = \sqrt{\frac{\epsilon_0 \epsilon kT}{2e^2 n_0}}. \tag{5.5}$$

At room temperature ($T = 298$ K) in water ($\epsilon = 80$), the Debye length is related to concentration as $\kappa^{-1} = 3.07/\sqrt{c_0}$ Å. While the approximation in Eq. 5.4 is no

longer necessary with the availability of high-speed computers, the intuitive picture of shielding provided by the Debye-Hückel theory still plays a useful role. Here we use it to indicate where and why the PB theory may break down. The solution of Eq. 5.4 in bulk is well known (e.g., [140]), and yields the following screened Coulomb potential around a central ion of radius $a/2$

$$\phi = \frac{e \exp[-\kappa(r-a)]}{4\pi\epsilon_0\epsilon(1+\kappa a)r}. \tag{5.6}$$

The radial density of the screening charge $p(r)$ is proportional to this potential

$$p(r) = 4\pi r^2 \rho_{\rm el} = -4\pi r^2 \epsilon_0 \epsilon \kappa^2 \phi = \frac{-e\kappa^2}{1+\kappa a} r \exp[-\kappa(r-a)], \tag{5.7}$$

which is seen to peak at $r = 1/\kappa$ and then decay exponentially. The volume integral of this shielding charge is of interest, and for a sphere of radius r, it is given by

$$q(r) = -e\left[1 - \frac{1+\kappa r}{1+\kappa a} \exp[-\kappa(r-a)]\right], \tag{5.8}$$

Equation 5.8 shows that $-q(r)/e$ increases monotonically with r, leading to a 25% screening of the central charge at about $r = 1/\kappa$, rising to 80% at $r = 3/\kappa$. Thus for a $c_0 = 150$ mM electrolyte under bulk conditions, length scales of around 25–30 Å are required for near complete screening of an ionic charge. When a boundary is imposed at a smaller distance, the system tries to maintain equilibrium by increasing the counter-ion concentration in the volume between the ion and the boundary. However, because of the physical size of ions and electrostatic repulsion effects, there is a limit to this increase, and one anticipates that as the ion gets closer to the boundary, the counter ion density will eventually become much smaller, producing less shielding than expected from bulk PB theory. This prediction can be tested directly by comparing the PB results with those obtained from BD simulations where all ions are treated on an equal footing as particles with a finite size and charge, rather than as a continuous charge density.

For this purpose, we have solved the PB equation (5.3) numerically using a finite difference algorithm for various boundaries as described below. From the numerical solution of the PB equation, one obtains the potential at discrete grid points. These potential values are then fed into the Boltzmann factor (Eq. 5.1) to determine the concentration of ions. The components of the force on a test ion at a particular grid point is calculated by numerical differentiation, from the difference of the potential at two opposing neighbouring points in the x, y and z directions.

5.4 Numerical solutions

We employ a finite difference method to solve the PB equation similar to that discussed for solving Poisson's equation in section 3.3.2. The problem is discretized by placing a rectangular grid of points with cell dimensions $h_x \times h_y \times h_z$ over the region of interest. The value of the potential at each grid point represents the average value of ϕ in the rectangular box centered at the grid point. Each surface element between neighbouring grid points is assigned a dielectric constant according to the position of the mid-point, that is, $\epsilon = 80$ if it is in the electrolyte and $\epsilon = 2$ if it is outside. Similarly, a value of $\rho_0 = 2en_0/\epsilon_0$ (see Eq. 5.3) is assigned to grid points that are in the electrolyte, and $\rho_0 = 0$ to points that are outside. To correspond with the BD simulations, ions around the test ion are excluded from a spherical zone with radius $r_t + r_i$, where r_t is the radius of the test ion and r_i is that of the anions or cations. Thus, unlike the primitive model, a different exclusion zone can be employed for anion and cation concentrations if they have different radii.

To obtain the finite difference form of the PB equation, we integrate Eq. 5.3 over a rectangular box of volume $V = h_x h_y h_z$ around each grid point i at position $\mathbf{r}_i$ [106]

$$\int_V \nabla \cdot [\epsilon(\mathbf{r}) \nabla \phi(\mathbf{r})]\, dV = \int_V \rho_0(\mathbf{r}) \sinh\left[e\phi(\mathbf{r})/kT\right] dV - \int_V (\rho_{\rm ex}/\epsilon_0) dV. \tag{5.9}$$

Using Gauss' theorem, the left hand side of Eq. 5.9 is converted to a surface integral as described in section 3.3.2.The terms on the right hand side of Eq. 5.9 are evaluated similarly by replacing the integrands with their average values at the grid point

$$\begin{aligned} \int_V \rho_0(\mathbf{r}) \sinh\left[e\phi(\mathbf{r})/kT\right] dV &= V \rho_0(\mathbf{r}_i) \sinh\left[e\phi(\mathbf{r}_i)/kT\right], \\ \int_V (\rho_{\rm ex}/\epsilon_0) dV &= V \rho_{\rm ex}(\mathbf{r}_i)/\epsilon_0 = q(\mathbf{r}_i)/\epsilon_0. \end{aligned} \tag{5.10}$$

Substituting Eqs. 3.19 and 5.10 back into Eq. 5.9, we obtain an expression for the potential at the i'th grid point in terms of the values of the potential, charge and dielectric constant at this grid point and its immediate neighbours

$$\phi_i = \frac{\sum_j \epsilon_j \phi_j / h_j^2 + q_i/(\epsilon_0 V)}{\sum_j \epsilon_j / h_j^2 + \rho_{0i} \sinh(e\phi_i/kT)/\phi_i}, \tag{5.11}$$

where the subscripts i and j on ϕ, q, and ρ_0 refer to the grid positions $\mathbf{r}_i$ and $\mathbf{r}_i + h_j \hat{\mathbf{j}}$, respectively. Note that a similar expression for the linear PB equation can be obtained from Eq. 5.11 by substituting $\sinh(e\phi_i/kT)/\phi_i \to e/kT$ leading to

$$\phi_i = \frac{\sum_j \epsilon_j \phi_j / h_j^2 + q_i/(\epsilon_0 V)}{\sum_j \epsilon_j / h_j^2 + \rho_{0i} e/kT}. \tag{5.12}$$

Equation 5.11 is solved using an iterative relaxation scheme as for Poisson's equation in section 3.3.2. In the present PB calculations, Gauss-Seidal relaxation has been employed throughout.

It is well known that the algorithm for the linear PB equation (5.12) converges to a stable solution [148]. In the non-linear case, this algorithm was shown to converge in most cases if under-relaxation is employed [96]. In practice, we have found that the algorithm converges to stable solutions for all the situations we consider with both over-relaxation (typically, $\omega = 1.6$) and under-relaxation ($\omega = 0.6$). The convergence criteria used is that the maximum change in potential between successive iterations at any grid point is smaller than the tolerance value, which is typically set to 10^{-6} V.

The PB program is executed on an alpha cluster, where a typical run with 1 Å grid size takes 5-20 minutes, depending on the boundary conditions employed.

5.4.1 Tests of accuracy

In all the situations considered, convergence to a stable solution is achieved using a tolerance of 10^{-6} V, which is sufficiently accurate for our purposes. The input parameter that influences the accuracy of results most is the grid size used in discretizing the system. Errors decrease with the grid size while computation time increases with it. Therefore a compromise has to be made for efficient running of the program with an acceptable range of errors. Since the force on an ion is the most sensitive quantity to the grid size, it is used in choosing the optimal size. A range of grid sizes are considered for the various geometries and configurations investigated. In the absence of fixed charges in a cylindrical channel, a uniform grid spacing of 1 Å is found to be adequate. Larger grid sizes lead to unacceptably large errors in force (e.g., for 2 Å, the relative error could be as high as 100%), while not much is gained by using a smaller grid (going to 0.5 Å reduces the error by a few percent). Since fixed charges in the channel lead to a more rapid variation in the potential, a smaller grid size (≈ 0.5 Å) needs to be employed in such cases to obtain a similar level of accuracy. With decreasing grid size, the force gets smaller, i.e., it converges to its actual value from above. Therefore, as a consequence of these optimal choices, we anticipate that the presented PB results for forces and potentials are slightly larger than their actual values.

We have performed a number of tests to ascertain the validity and accuracy of the numerical solutions of the PB equation. The simplest test cases are those involving a single ion (zero concentration) where the PB results can be compared with those obtained from the solution of Poisson's equation found either analyti-

cally or using complimentary numerical methods (e.g., boundary element method, see 3.3.1). While these do not provide a complete test for the PB solutions, they nevertheless serve to check the Poisson part of the program, an important consideration especially in cases with dielectric boundaries. For an ion in a uniform dielectric medium, the numerical solution is found to converge to the analytic result, $\phi = e/4\pi\epsilon_0\epsilon r$, within a few percent when a 1 Å grid is used. The accuracy improves when the grid size is made smaller as noted above. Other tests are carried out for a single ion in spherical and cylindrical boundaries, which are employed in the rest of the article. Numerical solutions of the PB equation in these cases are compared to the solutions of Poisson's equation obtained with the boundary element method. In all cases, the potential obtained from solution of the PB algorithm is found to agree with the alternative solution to within a few percent. A similar agreement is found for the force on a test ion.

Tests of the PB solutions in the case of an ion in electrolyte are not easy to perform as there are no suitable analytical solutions. We use instead the linear PB equation for this purpose, for which the solution for a test ion in bulk is quoted in Eq. 5.6. In the PB algorithm, linearizing involves simply switching from Eq. 5.11 to 5.12 in the calculation of the potential, hence such a test should be sufficient in checking the overall integrity of the program. Both the potential and concentration obtained from the numerical solution of the PB equation agree with the analytic results to within a few percent. An analytic solution can also be obtained for a fixed ion located at the centre of a sphere filled with electrolyte. A similar level of agreement is also found in this case.

5.5 Brownian dynamics

In most cases in this chapter, forces are calculated on a fixed ion during BD simulations. In these cases the ions are initially assigned random positions in the reservoirs, except for the test ion which is held in a fixed position. This ion is held in place for a period of 20,000 time steps, while the system reaches equilibrium. After this, the system is allowed to evolve for a further 200,000 or 1,000,000 time steps. At each time step, the force acting on the fixed ion (and other ions) is calculated, and from the time average of these a value for the force is computed for the entire simulation. Each simulation is repeated from between 5 to 16 times to obtain a value for the average force on an ion at each position along the central axis of the system. The duration of simulations are varied from 150 to 300 ns according to the statistical accuracy of the results. The potential profile of an ion is constructed by

integrating the force curve along a given path.

5.6 Results

Comparisons of the PB theory with BD simulations are carried out for three different geometries: a sphere, cylindrical channels of varying radius and a catenary shaped channel. The cylindrical channels are used in the majority of comparisons since they provide a prototype channel model that has been employed in numerous applications of the continuum theories to ion channels. The sphere is included for control studies and pedagogical reasons, and the catenary channel to show the robustness of the results for a more realistic channel shape. Each case is discussed in a separate subsection in the following. We note for future reference that the Debye lengths for 150, 300, and 500 mM solutions are, respectively, 7.9, 5.6, and 4.3 Å.

5.6.1 Electrolyte in a sphere

While our main concern is cylindrical pores, the spherical geometry is useful for purposes of control studies in a bulk-like environment, as well as in illustrating the effect of a confining dielectric boundary on the shielding of ions in a simple situation. In the following comparisons, a sphere of radius 20 Å containing an electrolyte of concentration $c_0 = 500$ mM is employed. In BD simulations, this concentration is represented by 10 anions and 10 cations, including the test ion. (The systems used here and in the following channel models are always chosen to be electroneutral.) The above choice for concentration is dictated by the BD considerations of having a sufficient number of ions in the system to obtain good statistics but not too many so as to encumber the simulations. Since the main variable is the distance of the test ion from the boundary, the choice of radius does not have much influence on the results. In order to compare the results with the analytic solutions of the linear PB equation (Eq. 5.4), both the cation and anion radii are taken as 1 Å in the sphere studies. A dielectric constant of $\epsilon = 80$ is used everywhere in bulk simulations. When emulating a protein boundary, $\epsilon = 2$ is used outside the sphere.

In solving the PB equation, we use a sharp spherical boundary around the test ion, which emulates a hard wall potential that prevents its overlap with other ions. Such an infinite potential is not practical to implement in BD simulations. Therefore a $1/r^9$ potential is used instead, which is both easier to handle and more physical. As seen in Fig. 5.1 A, the two potentials differ near the contact region and overlap once the ions are slightly separated. As a result of the softer potential used in BD, the ions (especially counter ions) are expected to be more broadly distributed near

the contact region with the test ion. This is exemplified in Fig. 5.1 B where we compare the radial distribution functions $g(r)$ in PB and BD for a bulk electrolyte. Here the PB results are obtained by fixing a test cation at the origin and those of BD by averaging over the ion-ion distributions. To avoid the finite size effects in the BD simulations, ion pairs are included in the average only when at least one of them is inside an imaginary $r = 10$ Å sphere. The linear PB results (not shown) for anion-cation distribution is somewhat higher than the non-linear one at the maximum but this appears to be mostly due to the finite mesh size used in numerical solutions of the PB equation. Otherwise, there is little difference between the linear and nonlinear PB results, especially at larger radii. The broadening of the sharp peak at contact in BD simulations is expected to influence the results at distances less than 3 Å. The shifting of counter charge density to smaller radii means that the BD simulations should provide a better shielding at short distances compared to the PB theory. At larger distances, the radial distribution functions overlap, and as far as the force on the test ion is concerned, one should obtain similar results within the two approaches. We note that using a hard-wall potential in BD would have led to larger forces on the test ion at short distances due to less shielding. However, as will be seen in the comparisons below, this issue is mostly irrelevant because the force results in BD follow closely that of a single ion. That is, there is little shielding due to counter ions, and therefore details of their interaction with the test ion at short range cannot have much influence on the results.

The shortcomings of the continuum theories of electrolytes in confined volumes are most succinctly illustrated in a spherical geometry because it involves a single parameter – the distance of a test ion from the boundary. In Fig. 5.2 A, the force on a test cation held fixed at a given position is plotted as a function of the radial distance. A single ion (no electrolyte) experiences a repulsive force due to induced surface charges at the sphere boundary. This force is shown by the dashed line for reference purposes. As the ion moves from the center of the sphere towards the dielectric wall, the repulsive force acting on it is seen to increase steeply. The PB calculations (solid line) exhibit the expected results from ionic shielding: the force on the test ion due to the boundary charges is significantly reduced compared to that of a single ion. In contrast, little shielding is observed in BD calculations of the force (filled circles with error bars), which follows quite closely the dashed line for the force on a single ion. The discrepancy between the PB and BD results become appreciable at 8 Å from the boundary, which corresponds to about 2 Debye lengths. As the ion gets closer to the boundary, this discrepancy grows, and at the closest BD simulation point (4 Å), it becomes a factor of 3. We note that even

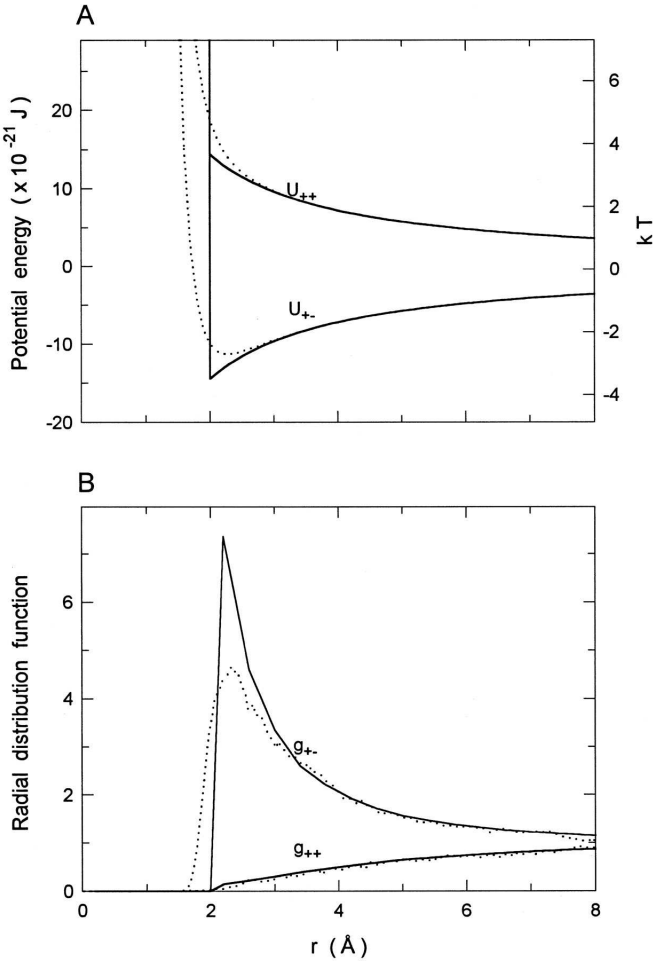

Figure 5.1: (A) Comparison of the hard-wall (solid line) and $1/r^9$ (dotted line) ion-ion potentials for a positive (U_{++}) and negative (U_{+-}) test ion around a fixed positive ion in a 500 mM bulk electrolyte, (B) the resulting radial distribution functions in PB (solid lines) and BD (dotted lines) for anions (g_{+-}) and cations (g_{++}) around the fixed ion.

when $\epsilon = 80$ is used outside the sphere, there is a net force on the ion because the presence of a boundary results in an asymmetric distribution of counter ions in the radial direction. In both PB and BD, this force is much smaller than the $\epsilon = 2$ case. For example, the force acting on an ion located at 4 Å from the boundary when $\epsilon = 2$ is determined to be 2.5 pN from the PB calculations and 6.8 pN from the BD calculations. The corresponding values when $\epsilon = 80$ are 0.5 and 1.6 pN. Thus the force on the ion is mostly due to the reaction field from the dielectric boundary.

The source of the discrepancy is to be sought in the inability of the counter ions in the BD simulations to provide the level of shielding observed in the PB theory. To see this more clearly, we compare in Fig. 5.2 B the anion and cation concentrations in the two theories. The average concentrations in the region between the fixed ion and the boundary are plotted against the radial position of the ion. This region is defined by the conical section between the ion and the boundary with the ion radius as its central axis and subtends a constant solid angle of 30°. Thus as the ion gets closer to the boundary, this volume gets smaller. Concentrations in PB are obtained from the space average of charges in the defined region, whereas in BD they are obtained from the time average of ions in the region. The PB results are shown with the solid lines, and the BD results are indicated by the open (anions) and filled circles (cations) that are fitted with the dotted lines. As the test ion approaches the boundary, the PB theory predicts a rapid rise in the anion concentration, which is necessitated by the decreasing available volume between the ion and the boundary. The opposite behaviour is observed in the BD simulations, that is, the anion concentration actually decreases as the ion gets closer to the boundary. The discrepancy between the predictions of the two theories again becomes appreciable when the ion is about 2 Debye lengths from the boundary. Thus this example explicitly demonstrates when the concentrations in the PB theory starts to disagree with the average ion densities obtained from the BD simulations, signalling the break down of the mean field approximation.

The above results give a clear indication of the operating range of PB theory for an electrolyte confined within a dielectric boundary. While the Boltzmann factor (Eq. 5.1) puts a limit to the increase in anion concentration (otherwise there would be a perfect shielding with very large concentrations to provide it), it clearly does not capture the whole physical picture. Reflecting on these results, it is clear that the continuum description which distributes the ionic charges over the whole volume is ultimately responsible for the failure of the PB theory. When the integrity of the ionic charges are kept as in the BD simulations, there is an enormous repulsive force on a counter ion (due to induced surface charges) as it attempts to enter the

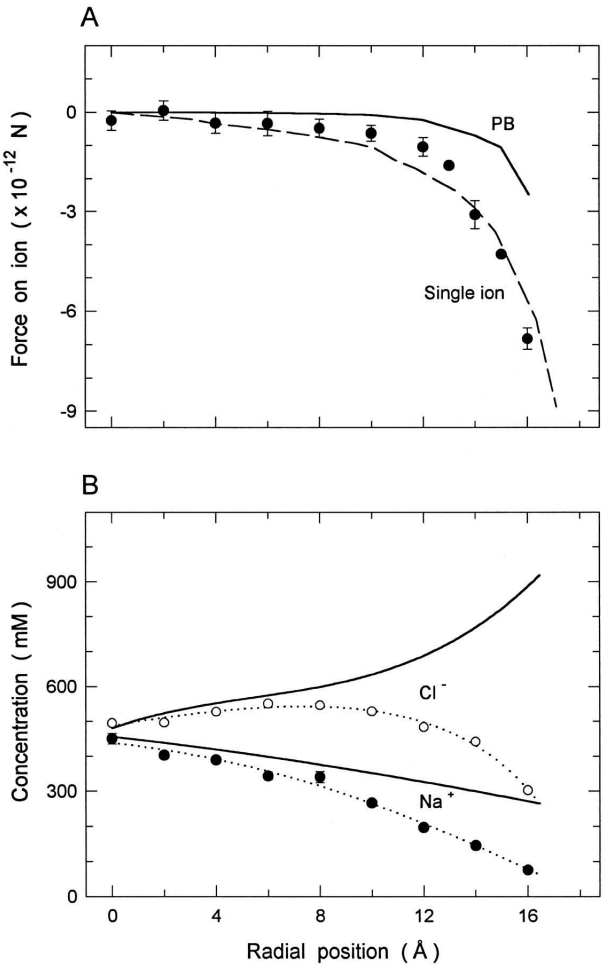

Figure 5.2: Test of the PB theory for a 500 mM electrolyte in a sphere of radius 20 Å. (A) Force acting on a fixed cation is plotted against its radial position. The solid curve shows the force obtained from the PB theory and filled circles with error bars show the BD simulation results. The dashed line indicates the force in the case of a single ion ($c_0 = 0$). The error bar on BD data points is one standard error of means and is not shown when it is smaller than the size of the data point. (B) Concentration of mobile ions in a region of constant solid angle (30°) between a fixed cation and the spherical boundary. The average concentration obtained from the PB theory (solid lines) and the BD simulations [open (Cl) and filled (Na) circles fitted with the dotted lines] are plotted against the radial position of the fixed cation.

narrow region between the test ion and the boundary. This force largely prevents the anions from entering the narrow region, and is responsible for the drop in anion concentration in BD. In PB calculations at 500 mM, an average cell with a grid size of 1 Å contains 1/3000 of a unit charge. Distribution of charge into such small units cuts down the effectiveness of the repulsive force, and hence allows relatively large anion concentrations to occur in the narrow region. While the total negative charge in this region is only about 30% of a unit charge, the PB results indicate that even this small amount could still provide a very effective shielding. This happens because the surface charges induced on the boundary are proportional to $1/r^2$, and therefore, those charge elements nearer the boundary can induce proportionately more negative charges on the surface which cancel the positive charges induced by the test ion more efficiently.

Figure 5.3 illustrates the origins of the discrepancy between the PB and BD results. In the PB theory, the electrolyte is distributed in a continuous manner, allowing negative charge to build up around the test ion, even if the ion is close to the dielectric boundary of the sphere. This counter charge can reduce, or shield the induced charges on the boundary. If the ions are treated as discrete entities as in BD, there will only be an average negative charge near the test ion if ions actually move through this region during the simulation. However, if the counter charge itself comes close to the boundary it is repelled away by the surface charges it induces. This makes it unlikely for ions to spend time in this region, and so there is little shielding of the reaction field experienced by the test ion.

5.6.2 Cylindrical model

We next consider cylindrical channels with rounded corners. The rounding is necessitated by the fact that sharp corners cause difficulties in the numerical solutions of Poisson's equation, and, in any case seems to be a more realistic depiction of real ion channels. The dimensions of the channel are outlined in Fig. 5.4, with the channel obtained by rotating the curve shown in the figure around the axis of symmetry. The radius of the channel is varied from 3 Å to 13 Å in the comparisons. The height h of the reservoir is adjusted to keep the volume fixed when the radius is varied. For $r = 3$ Å, a height of $h = 25$ Å is used. The dielectric constants are 2 for protein and 80 for water unless otherwise specified. An average concentration of 300 mM is used in all the PB calculations, which is determined from the total cation (or anion) charge in the system as in the case of the sphere. The BD simulations are carried out with a total of 24 Na^+ and 24 Cl^- ions, corresponding to an average concentration of 300 mM. The reason for using this higher value instead of the more

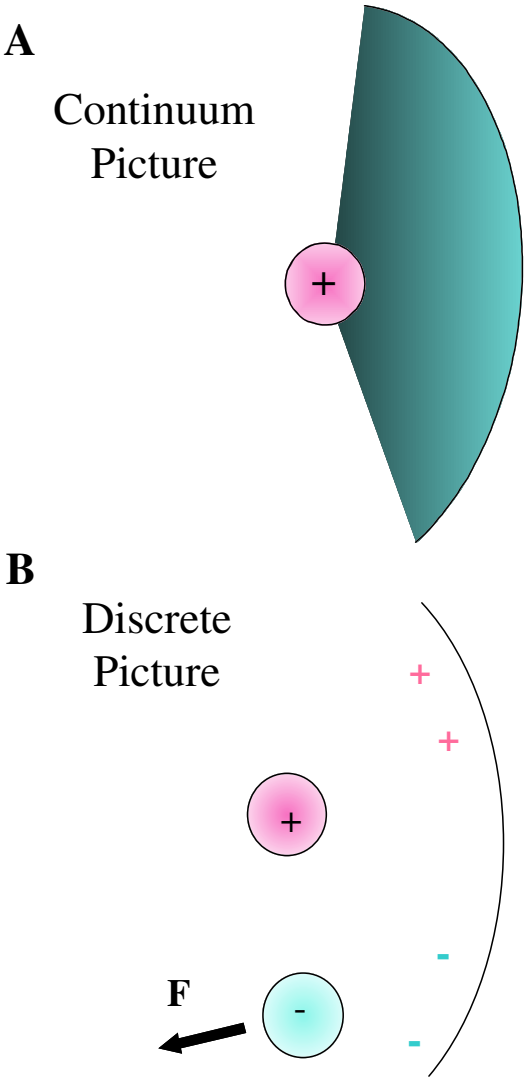

Figure 5.3: Schematic picture of the distribution of negative charge between a fixed cation and the nearby boundary of a dielectric sphere in (A) the continuum and (B) the discrete picture of the electrolyte.

physiological 150 mM is entirely statistical; twice as many ions leads to better accuracy in the BD simulations. The results are hardly sensitive to concentration in BD, and exhibit only a logarithmic dependence in PB calculations. Thus essentially similar results would be obtained using a concentration of 150 mM.

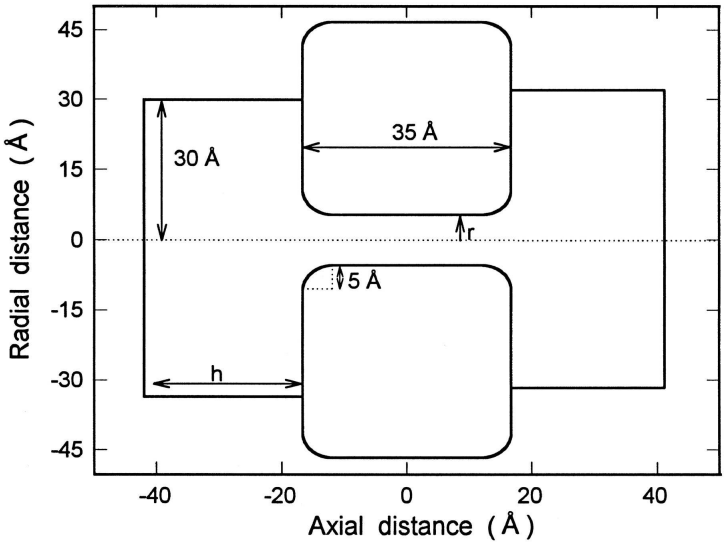

Figure 5.4: Cylindrical channel models used in comparisons of PB theory with BD simulations. A three dimensional channel model is generated by rotating the cross section about the central axis by 180°. The cylindrical section is 25 Å in length, and the rounded corners have a radius of 5 Å. The radius of the cylinder r is varied from 3–11 Å. The reservoir height h is adjusted so as to keep the total (reservoir and channel) volume constant when the radius is changed.

From the view of the dynamics of an ion in a channel environment, the quantity that is of most interest is the force acting on it at various positions in the channel. In Fig. 5.5, we compare the PB and BD calculations of the z-component of the force on a test ion as it is moved along the channel axis (only the positive side is shown since the curves are symmetric around $z = 0$). In BD, a test ion is held at a fixed position on the channel axis, and the z-component of the force acting on it is tabulated at every 10 time steps, and averaged at the end of the simulation. The ion is then moved to another position along the channel axis, and the measurement is repeated. The shielding effect in PB is seen to lead to a drastic reduction in force compared to the BD result in the $r = 3$ Å channel (Fig. 5.5 A). As the channel size is increased, the discrepancy decreases but it remains several-fold (Figs. 5.5 B-C).

Finally in the $r = 11$ Å channel, when the force itself becomes quite small, the complete shielding observed in PB theory is reproduced in BD (not shown).

Another issue that needs to be addressed in these comparisons is the effect of the ion-wall potential (or finite ion size), which is implemented in BD simulations but ignored in PB calculations. This issue of consistency between the two theories and its influence on the results presented can be addressed in two ways. One method is to implement the finite size of ions in PB equation by multiplying the right hand side of Eq. 3 by a space dependent function that will exclude the ions from the volume within 1 Å of the boundary [173]. The second method is to do the opposite, that is, shrink the activation distance of the hard-wall potential in BD from 1 Å to zero, thus allowing ion centers to come near the boundary. Because in almost all applications of the PB theory to ion channels such finite size effects are not considered and our main purpose is to provide tests for these applications, we prefer to use the second method here. In Fig. 5.6, we plot the BD results for the force on a cation in a $r = 3$ Å channel as in Fig. 5.5 A, but with the activation distance of the hard-wall potential reduced from 1 Å (circles) to 0.5 Å (squares) and 0.1 Å (triangles). It is seen that there are no discernible differences among the various results, with all falling on the force curve obtained from the solution of Poisson's equation for a single ion (dashed line). Thus even if we ignore the finite size of ions and allow them to access the whole channel volume as in PB theory, they decline to take advantage of the extra space offered. Obviously, the steep increase in image forces as an ion approaches the dielectric boundary makes these regions rather inhospitable places, a fact that is missed by the PB theory because smearing of charges dilutes the effects of the boundary forces. Since the range parameter of the hard-wall potential does not have any influence on the results, we will keep using the more realistic 1 Å range in the rest of the comparisons.

A quantity that can be more directly related to ion permeation is the potential energy profile of an ion which is obtained by integrating the force curves in Fig. 5.5. We compare the PB and BD profiles in Fig. 5.7 for $r = 3$, 4, and 7 Å channels. In the PB case, shielding reduces the energy barrier seen by a single ion by roughly an order of magnitude, virtually obliterating it. No shielding effects are seen in the BD potential energy profiles in the narrow channels ($r = 3$-4 Å). In the $r = 7$ Å channel, shielding is seen to reduce the barrier of a single ion by more than half. Nevertheless, the barrier in BD remains larger than the PB result, pointing to a sizable discrepancy despite the reduction in the potential energy values.

Compared to the sphere results, the discrepancy between the two theories is more accentuated in the cylindrical channels because the access of counter ions to

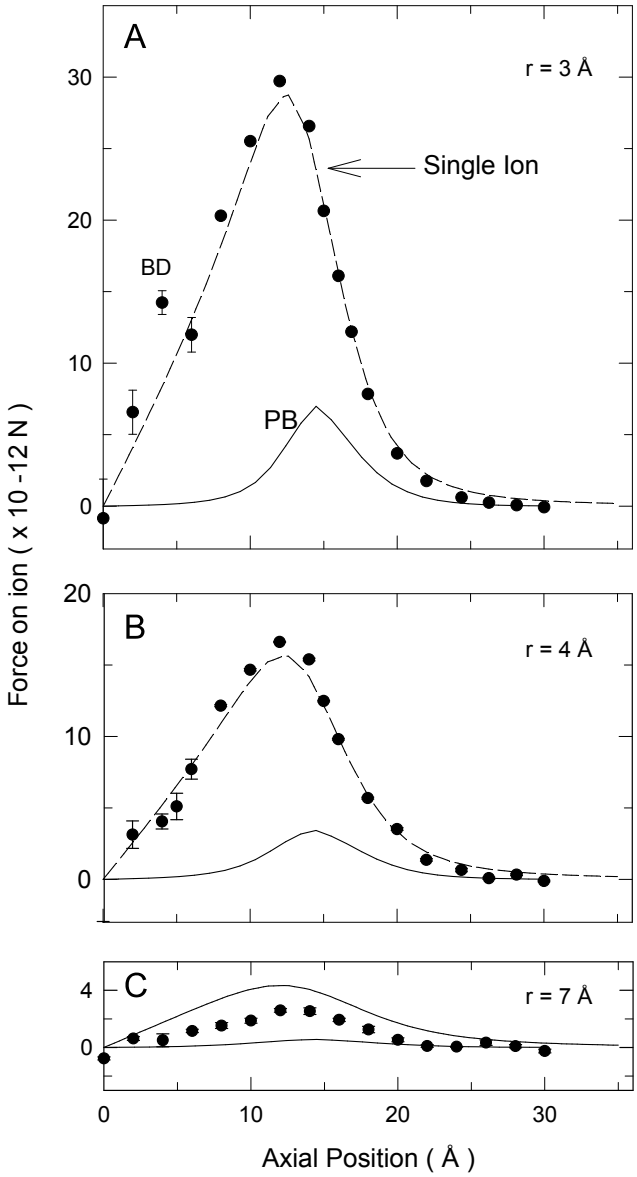

Figure 5.5: Test of the PB theory for the cylindrical channel shown in Fig. 5.4. The z-component of the force acting on a fixed cation at various positions along the channel axis is calculated using the PB theory (solid line) and the BD simulations (filled circles fitted with the dotted line). The radius of the channel is (A) 3 Å, (B) 4 Å, and (C) 7 Å. The height of the reservoirs is adjusted to keep the concentration fixed at 300 mM in all cases. The force on a single ion ($c_0 = 0$, dashed line) is also shown, for reference purposes.

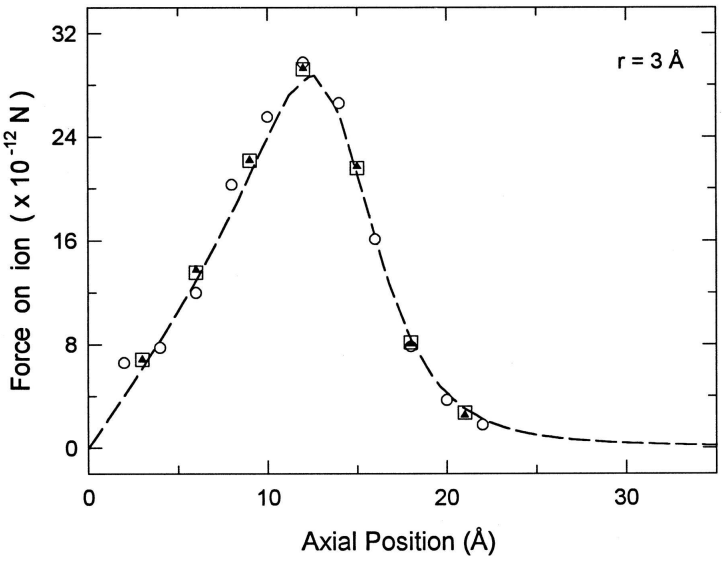

Figure 5.6: Effect of changing the activation distance of the hard wall potential in BD simulations. The force on a cation in a $r = 3$ Å channel is plotted as in Fig. 4 A but for three distance parameters, 1 Å (circles) to 0.5 Å (squares) and 0.1 Å (triangles). The ion-ion interaction from Eq. 3.13 is employed in the simulations. All the BD results follow the single ion results shown by the dashed line. The error bars are not shown to avoid cluttering.

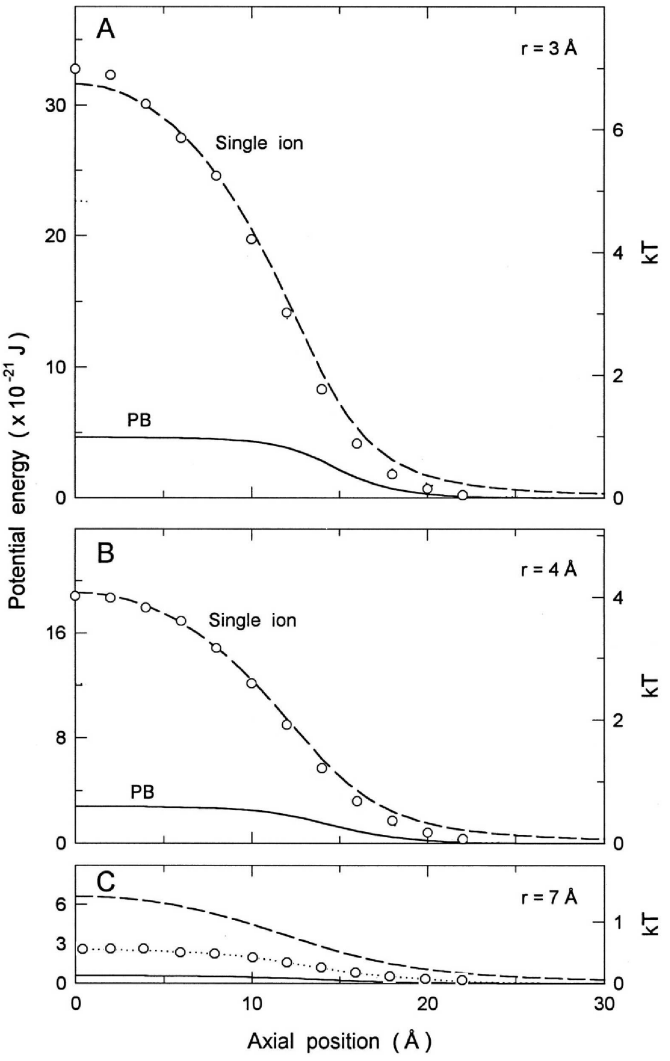

Figure 5.7: The potential energy profiles in PB (solid line) and BD (open circles) obtained by integrating the force curves in Fig. 5.5. The dotted line is a fit to the BD results in (C).

a narrow cylinder is further hindered in BD while no such hindrance occurs in PB theory. To quantify this statement, we compare the cation (Fig. 5.8 A) and anion (Fig. 5.8 B) concentrations predicted by PB (solid line) and BD (bars) theories for a $r = 3$ Å channel when the test ion is located near the pore mouth ($z = 12.5$ Å). In PB calculations, both anions and cations uniformly occupy the channel at about the average concentration, except near the test ion when the former shoots to very large values and the latter dips to zero as expected. This difference in the anion and cation concentrations leads to a net screening charge of $-0.61e$ in the channel. In stark contrast, both anions and cations are completely excluded from the channel interior in BD. While there is some excess of counter ions near the channel entrance, these only amount to $-0.01e$, which is too small to provide any shielding as seen from the force at $z = 12.5$ Å in Fig. 5.5 A. A constant anion concentration of 300 mM throughout the channel would correspond to a total charge of $-0.21e$. Thus the amount of anion charge is increased several-fold compared to the background in PB, while it remains negligibly small in BD.

Rather than repeating the above study for each channel size, which is not very informative, we demonstrate the changes in concentration by plotting the total screening charge in the channel as a function of its radius (Fig. 5.9 A). This study is carried out for a cation fixed at $z = 12.5$ Å where the force on an ion is at a maximum. The total screening charge in PB remains nearly constant with the increasing radius, the slight increase being due to the approaching bulk conditions (note that the screening charge in the channel remains less than $-e$ because the channel volume is limited to $z = \pm 15$ Å). In BD, this charge is negligible at $r = 3$ Å but it steadily rises with r, converging to the PB value at about $r = 11$ Å or 2 Debye lengths. As shown in Fig. 5.9 B, the force on the test ion at $z = 12.5$ Å correlates very well with the screening charge results in (A). The force in BD initially coincides with that of a single ion at $r = 3$ Å (no shielding), and with increasing channel radius, it gradually converges to the PB values at around 2 Debye lengths. This study establishes the domain of validity of PB theory for channels as 2 Debye lengths, below which the underlying mean field approximation breaks down to an increasingly larger degree with decreasing radius.

So far we have considered only the central axis in comparisons, which may give the impression that an agreement between the PB and BD results can be obtained in the larger size channels (Fig. 5.5 D). However, the central axis is a rather special place where the forces from the boundary charges are at a minimum, and the shielding effects in BD are maximized due to the azimuthal symmetry. From the sphere results it is expected that as the ion is moved towards the boundary

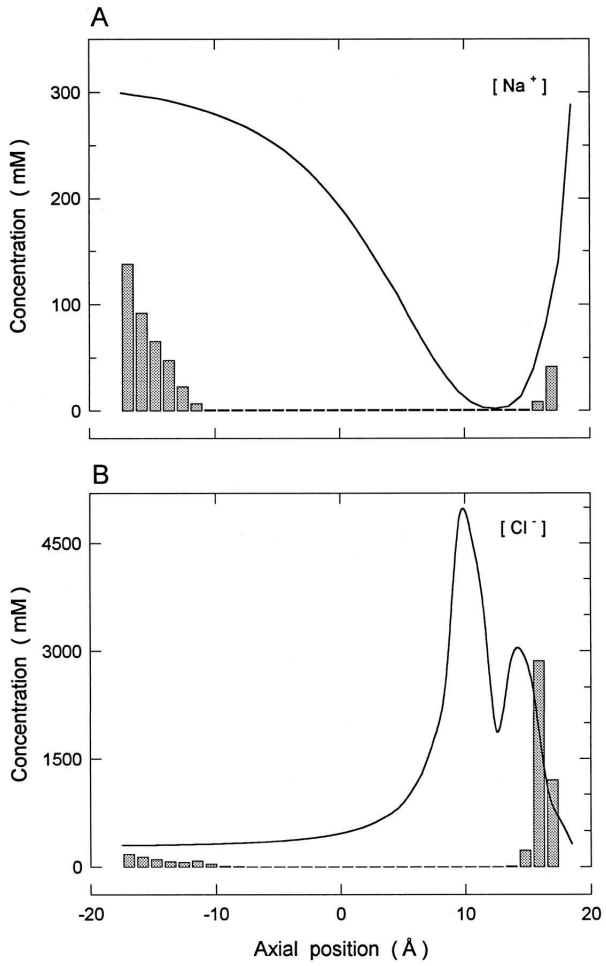

Figure 5.8: Variation of the average concentration along a $r = 3$ Å channel for cations (A), and anions (B) when a cation is fixed on the z axis at $z = 12.5$ Å (where the channel starts curving). In BD, the channel is divided into 32 layers and the average value of the concentration is calculated at each layer. The PB concentrations are indicated by the solid curve and the BD ones by the bar graph.

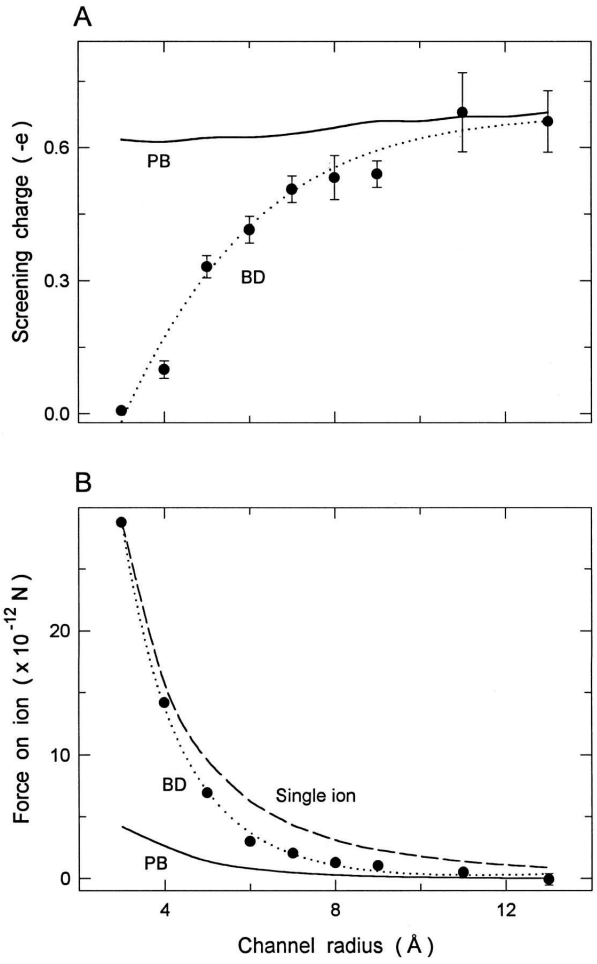

Figure 5.9: Pore size dependence of the screening charge and force on a cation held at $z = 12.5$ Å. (A) The net screening charge in the channel (from $z = -15$ to 15 Å) is plotted as a function of the channel radius. The PB results are shown by the solid line and the BD values by the filled circles fitted with the dotted line. (B) Force on the cation as the channel radius is increased. The PB (solid line), BD (filled circles fitted with a dotted line) and single ion results (dashed line) are indicated in the figure.

discrepancies between the two theories will resurface. This is quite obvious for the radial component of the force but not so for the z component. In Fig. 5.10, we present comparisons of the z-component of the force on a test ion similar to Fig. 5.5 D (reproduced at the top) but along a line that is offset from the z axis by 4 Å (Fig. 5.10 B) and 8 Å (Fig. 5.10 C). Shielding effects are again overestimated in PB theory compared to BD as the ion approaches the boundary. To see this more clearly, we show in Fig. 5.11 how the z-component of the force changes as the ion is moved radially from the centre to the boundary. Up to 3 Å from the centre the two theories agree, that is, shielding of the force in PB theory is reproduced in BD. But after that, shielding progressively weakens in BD in contrast to PB theory which provides a very good shielding right up to the boundary. Thus even in large channels, the predictions of the PB theory are bound to fail as one approaches the channel walls. Such discrepancies in large channels are relevant, for example, in calculating concentrations near a binding site, but not in ion transport as ions tend to stay near the channel axis where the radial force is minimum [48, 127].

The BD results so far clearly indicate that narrow channels with radii 3-4 Å are pretty inhospitable places for ions regardless of their background concentration. Therefore for ion permeation to take place, it is essential to reduce the energy barrier of a bare channel by placing fixed charges of opposite sign on the protein wall. To test the PB theory in this more realistic case, we place a set of negative charges in the walls near each end of a $r = 3$ Å channel. Eight monopoles with charges $-0.09e$ are spread evenly around the channel circumference at $z = 12.5$ Å and $z = -12.5$ Å, where the channel starts curving. The PB, BD and single ion results for the z-component of the force on a test cation (as in Fig. 5.5 A) are compared in Fig. 5.12 A. The fixed negative charges on the channel wall reduce the presence of counter ions in the channel and the associated shielding, hence lead to much larger forces in PB theory compared to Fig. 5.5 A, in better agreement with the BD results. The four-fold discrepancy observed in the bare channel (Fig. 5.5 A) is now reduced to about a factor of 2. As the test ion is moved away from the channel, shielding becomes more and more effective and the force in BD goes gradually from the single ion curve towards the PB result. In Fig. 5.12 B, we show the potential energy profiles obtained from the force curves in Fig. 5.12 A. Besides the usual discrepancy between PB and BD theories, perhaps a paradoxical result is that shielding actually increases the energy barrier in BD compared to that of a single ion. The reason for this ironic result can be seen from Fig. 5.12 A; shielding operates when the ion is outside the channel where the force is attractive but not inside when it is repulsive.

As a final study in cylindrical channels, we consider the possibility that the

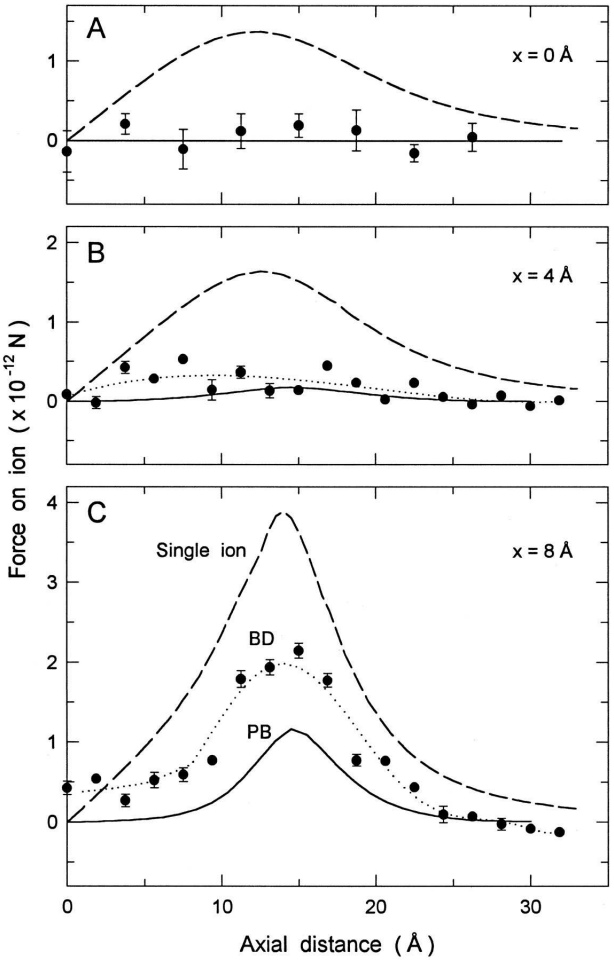

Figure 5.10: Comparison of the z-component of the force on a test ion in a $r = 11$ Å channel when it is offset from the central axis by $r = 4$ Å (middle) and $r = 8$ Å (bottom).

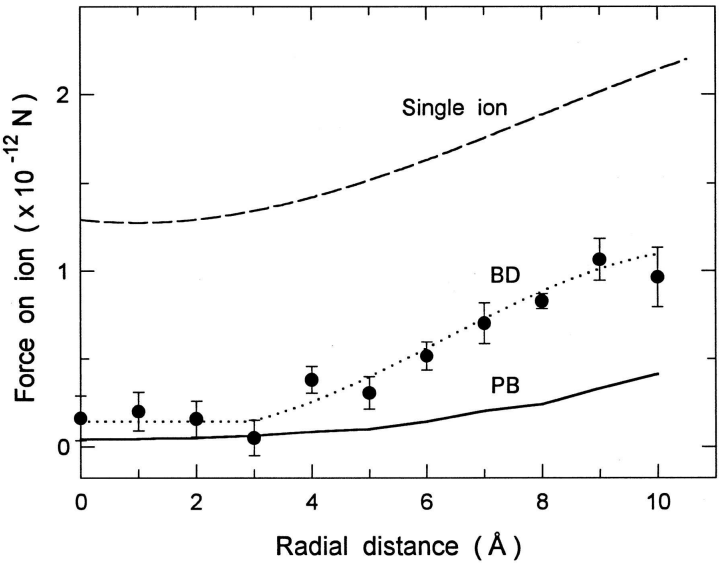

Figure 5.11: Comparison of the z-component of the force on a test ion in a $r = 11$ Å channel as it is moved radially from the centre to the channel boundary at $z = 8.75$ Å.

dielectric constant inside the channel may be smaller than 80, especially in narrow channels. This can be implemented in a straightforward manner in the PB algorithm where a 3-dimensional grid is used, but it is not so easy in the BD simulations where a boundary element method is used in solving Poisson's equation. (Note that in the studies in later chapters the finite difference technique was included in the BD routines such that it could be used during simulations.) This problem has been tackled in previous BD simulations [40, 42], by using the reduced value of the dielectric constant, ϵ_c, in both the channel and reservoir, and including the neglected Born energy difference between the channel-reservoir configurations with ϵ_c-80 and ϵ_c-ϵ_c as a short range energy barrier at the channel entrances. We refer to the above references for details of this implementation in the BD program. The Born energy difference for a 3 Å channel is calculated using the PB program at zero concentration, which gives a barrier height of 3.5 kT for $\epsilon_c = 40$ and 11.8 kT for $\epsilon_c = 20$. In PB calculations the change in ϵ is implemented in 5 equal steps from the channel entrance at $z = 17.5$ Å to $z = 12.5$ Å, and similarly at the other end. The potential energy profiles for $\epsilon_c = 20$ and 40 are compared in Fig. 5.13. The barrier height for a single ion increases roughly as $1/\epsilon_c$, and a similar trend is seen in BD. At lower ϵ_c, BD results deviate more from those of single ion because of the appearance of shielding at the mouth region. We attribute this to the stronger

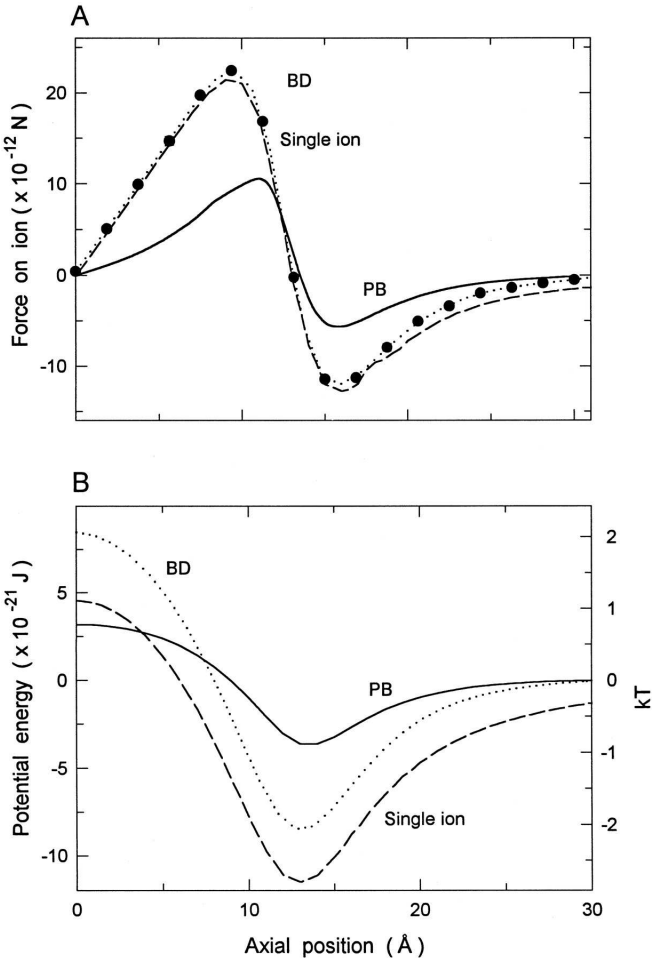

Figure 5.12: Effect of placing fixed charges in the channel wall in a $r = 3$ Å channel. (A) Force on a cation as in Fig. 5.5 A but with fixed charges. (B) Potential energy profiles as in Fig. 5.7 A but with fixed charges.

Coulomb attraction between the test ion and counter ions, which increases as $1/\epsilon_c$. The corresponding increase in barrier height is much faster in PB theory so that the discrepancy with BD gets smaller with decreasing ϵ_c (but stays several-fold in any case). This faster increase of barrier height in PB is related to the loss of shielding inside the channel with reduction in ϵ, which affects the PB results but not BD. Nevertheless, the overall conclusion remains the same as before; greater shielding in PB results in much lower energy barriers compared to BD.

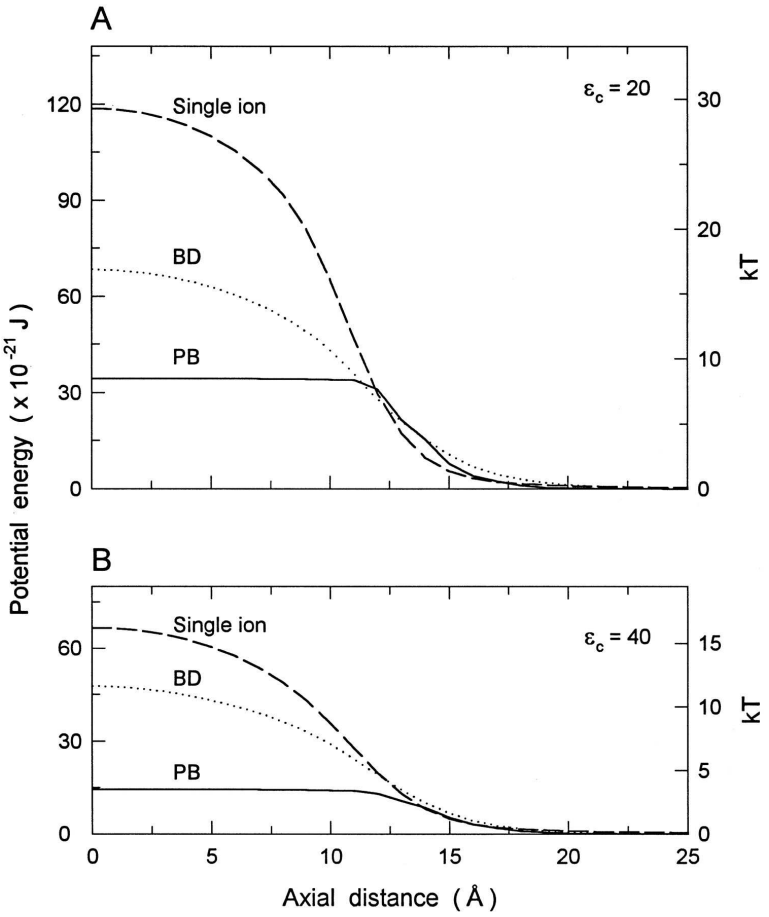

Figure 5.13: Effect of changing the dielectric constant in the channel, ϵ_c, on the potential profile of a test ion in a $r = 3$ Å channel without fixed charges. (A) shows $\epsilon_c = 20$ and (B) $\epsilon_c = 40$.

5.6.3 Catenary model

The above study in cylindrical channels gives a good idea about the expected working range of the PB theory. To demonstrate the robustness of those conclusions, we repeat the force and potential energy calculations in a more realistic channel geometry with vestibules. This 'catenary shaped channel' is generated by rotating the closed curve shown in Fig. 5.14 about the axis of symmetry. The vestibule of this channel is similar in shape to that visible in the electron microscope pictures of the acetylcholine receptor channel [202], making this a better approximation of a real biological ion channel. The vestibules are generated by a hyperbolic cosine function, $z = a\cosh(x/a)$, where $a = 4.87$ Å. The entrance to the vestibule has a fixed radius of 13 Å. Two such identical vestibules are connected to a cylindrical transmembrane segment of radius 4 Å and length 10 Å. It is assumed for convenience that the vestibules have the same shape and size, although the electron microscope images show the extracellular vestibule to be larger than the intracellular vestibule.

We show in Fig. 5.15 A the z-component of the force as the test ion is moved along the central axis of the channel. The concentration is maintained at 300 mM in both the PB calculations and the BD simulations. As before, PB calculations are shown by the solid line, the BD results are indicated by the filled circles which are fitted by the dotted line, and the dashed line shows the force on a single ion. The BD calculations of force closely track the single ion results in the narrow parts of the channel (up to $z = 10$ Å), and reinforce the earlier conclusion on impossibility of shielding in narrow parts of the channel. There is a large discrepancy between the PB and BD results in this region as in Figs. 5.5 A-B. As the ion is moved further along the z axis, the channel expands and shielding becomes more and more effective in BD. This is reflected in the force values in BD gradually moving from the single ion curve to the PB results in the $z = 10$-30 Å range. The potential energy profiles obtained from the force curves in Fig. 5.15 A are shown in Fig. 5.15 B. Shielding is seen to have reduced the energy barrier of a single ion by 40% in BD, however, the barrier in BD is still three times larger than the PB result. Thus in a channel with vestibules, shielding definitely plays some role but its effect is nowhere near the PB predictions, where shielding demolishes the barrier presented to a single ion for all practical purposes.

5.7 Conclusions

These comparisons of PB theory with BD simulations in various configurations clearly demonstrate the range of validity of the former. When the distance of an

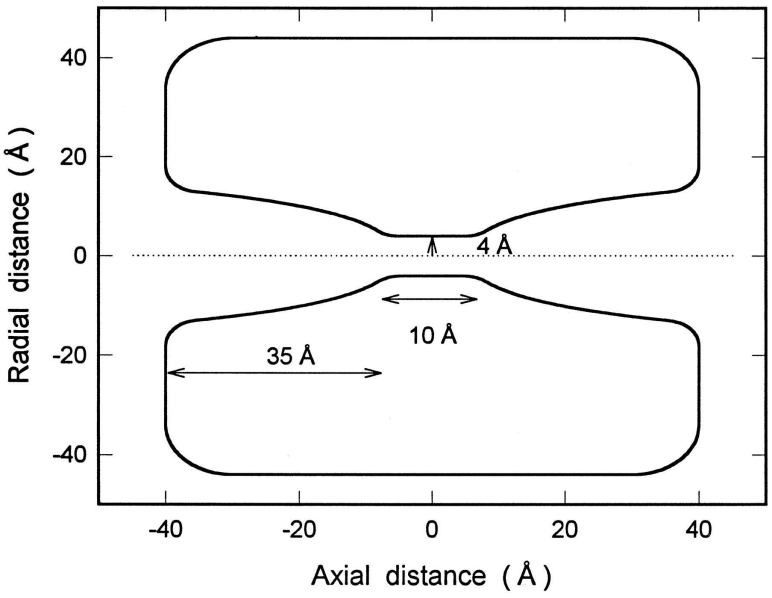

Figure 5.14: Diagram showing the cross section of the catenary geometry that approximates the shape of the acetylcholine receptor channel. A three dimensional channel is generated by rotating the curves about the central axis by 180°. Vestibules at each side of the membrane are constructed using a hyperbolic cosine function, $y = a\cosh(x/a)$ where $a = 4.87$ Å. The radius at the entrance of the vestibule is 13 Å and at the cylindrical transmembrane segment 4 Å. Cylindrical reservoirs (not shown), 30 Å in radius and 22 Å in height, are attached to the vestibules.

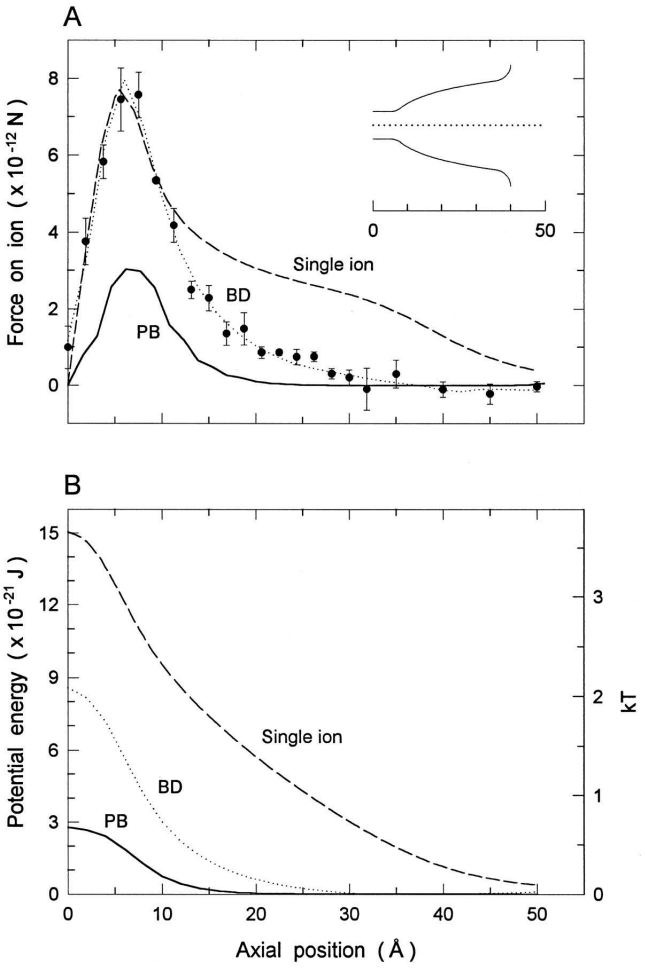

Figure 5.15: (A) The z-component of the force on a cation for a 300 mM electrolyte in a catenary channel is plotted against its axial position. The force obtained from the PB theory is shown by the solid curve and the BD results are indicated by filled circles with error bars fitted with the dotted line. The dashed line indicates the force in the case of a single ion ($c_0 = 0$). (B) The potential energy profiles obtained from the force curves in (A).

ion from the channel wall is less than 1 Debye length, the PB calculations largely overestimate the shielding effects and cannot be expected to give reliable values of the force on and potential energy of an ion. The convergence of the PB and BD results occurs when the ion's distance from the channel wall is about 2 Debye lengths, depending on the quantity and the geometry considered. Since the radii of membrane channels are typically smaller than the Debye length, PB theory cannot be used to obtain reliable estimates of electrostatic forces and potential energies of ions in the channel environment.

Our BD results demonstrate that if the radial profile of a channel is less than the Debye length throughout, it is unlikely to contain any counter ions. This conclusion is especially reinforced in realistic channel configurations where fixed charges of opposite sign, that are necessary for ion permeation, make it virtually impossible for any counter ion to enter the channel (cf. Fig. 5.12). For such channels, it is clearly better to use Poisson's equation rather than PB, as no shielding due to ionic atmosphere is possible. This conclusion appears ironic in the historical context of the field because PB theory was advanced as an improvement of Poisson's equation in ion channels. Channels whose radial profiles exhibit large variations are more difficult to reconcile with the existing continuum theories because each is valid in a limited range. For such channels, BD simulations certainly offer a more reliable method for calculations of forces and potentials. Nevertheless, if one insists on using a continuum description, one could presumably extrapolate from Poisson's to the PB equation as the channel widens by using the BD results as a guide.